STATUS AND PERSPECTIVES OF THE FRENCH CRG-IF INTERFACE BEAMLINE BM32

REPORT FOR THE BEAMLINE REVIEW PANEL OF MAY 2015

APRIL 2015

G. Renaud, J.-S. Micha, O. Robach, F. Rieutord, M. De Santis, O. Ulrich

Contents

Overview : history, role and impact of the beamline

The French CRG Interface (IF) Beam Line (BM 32) is dedicated to study the physics and chemistry of surfaces, interfaces, thin films and nanostructures and to study the mechanical properties at the micron scale. It was one of the first beamlines available to users, in 1994. It first held three monochromatic-beam experimental stations that were used alternatively, one equipped with a **multipurpose goniometer (GMT)**, one dedicated to X-ray absorption spectroscopy (XAS) experiments, and one devoted to surface X-ray diffraction in ultra-high vacuum (UHV) called SUV (Surfaces under Vacuum). In 2000, the XAS station moved to a new, dedicated beamline BM30B (CRG-FAME), and SUV evolved toward **INS (In situ Nanostructures on Surfaces)**, more oriented toward studying nanostructures. In 2006, the beamline optics was completely refurbished with two vertically focusing mirrors in addition to a two crystals sagitally focusing monochromator. A white beam microfocus configuration, producing a sub-micrometric beam in the GMT hutch, was added. In parallel, a **micro-diffraction** setup was developed.

The goniometer of the **GMT** station has three main characteristics, which makes it unique for some investigations. The goniometer is very accessible and versatile, so that many different scattering experiments can be performed, bulk or surface sensitive, with the sample surface either horizontal or vertical. Different sample environments such as a cryostat and a small vacuum chamber are available. Several others have already been used: magnet and cold finger, Langmuir trough, dilution fridge etc... The most specific feature is the possibility to deviate the beam downwards for studying liquid surfaces, and the availability of well adapted cells for these measurements. Although such equipment is now available on other stations, in particular on the Troïka Beamline, the advantages of the IF beamline are the very clean X-ray beam with low background, and the possibility to work at much higher energies (up to 30 keV), which is necessary for studies of interfaces between dense materials (liquid/liquid or liquid/solid). Because of its very versatile design, the GMT instrument is a user-oriented facility that fits the needs of a wide community. The research on the GMT diffractometer has been balanced between studies of « soft » and « hard » condensed matter.

A new instrument (**μ-Laue**) for Laue microdiffraction was added in 2006, to be used in alternance with the GMT goniometer in the first hutch. This setup is similar to the ones developed at APS by G.E. Ice, and at ALS by N. Tamura. A white (5-30 keV) microbeam (0.5x0.5 μm2) arrives on the surface of the polycrystalline sample, under an angle of 40°. Each illuminated crystallite produces a Laue pattern, which is collected onto a 2D detector located near 2θ=90°, and then analyzed for local orientation and deviatoric strain. Sample scanning then provides 2D maps of orientation and deviatoric strain. By monochromatizing the incident microbeam, using the beamline monochromator, it is then possible to measure the photon energy of one or several diffraction spots of a Laue pattern previously acquired in white beam mode, to retrieve the hydrostatic part of the local strain. This (comparatively) time-consuming measurement is usually performed only for a few points on the map. Historically, the driving force behind the construction of the setup was the need by the CEA labs using the GMT goniometer to perform texture and strain analysis in thin-film microelectronics structures (< 1 μm thick). The problem was to fill an "analysis" gap for films in which there were too few grains for powder analysis, but too many grains for single crystal analysis with monochromatic macro-beam. The reflection geometry, and the absence of sample rotation associated to white beam were found to be particularly well adapted for these samples. The technique is of course not limited to thin films, and allows to study the near surface region of bulk polycrystalline materials. This brought several new users from Materials Science on the beamline. The possibility to obtain the 2D strain distribution, with a submicron space resolution (at least in 2D), in fine-grained polycrystals, attracted specialists of Mechanics trying to elucidate the Hall-Petch effect, which delays toward higher stress the start of the plastic regime in materials. Another strong area of activity is the in situ study of poly or single-crystalline objects of micrometer dimensions, while they are submitted to mechanical testing, electrical testing, or thermal annealing. This to investigate how the small size of the objects and of their confinement inside foreign materials affects their functional properties. The technique was also recently applied to single 400nm-diameter epitaxial nanowires of III-V semiconductors, of interest for their optoelectronic properties. The small counting time needed (a few seconds) made it clear that for well-crystallized materials, studying crystallites of 100 nm or even smaller should be feasible. More macroscopic studies involve monitoring of the build-up and relaxation of stress

around grain boundaries during plastic deformation, for comparison with plasticity models, or monitoring the distribution of stress between the two phases of a shape memory alloy while exploring the super-elastic regime.

Finally, The **INS** station is based on a UHV diffractometer devoted to Surface X-Ray Diffraction (SXRD), Grazing Incidence X-ray Scattering at wide (GIXS) and Small (GISAXS) angles and X-ray reflectivity and possibly Surface X-ray Absorption Spectroscopy (S-XAS) on surfaces and interfaces, and during thin film and nanoparticle growth. The main advantages with respect to other existing stations are the possibility to perform *in situ* deposition with up to seven sources in the X-ray chamber, as well as a very good RHEED system and Auger analysis under grazing incidence, which can be operated simultaneously with x-ray measurements during deposition or annealing. In addition to physical evaporation, an injector has been recently added opening the world of chemical vapor deposition (CVD) under ultra-high vacuum, also called Chemical Beam Epitaxy (CBE).

With these three instruments, the beamline has a large impact in the French research community in nanoscience. In addition, both instruments serve each year as a support for practicals and tutorials dedicated to students during their Master at the local Grenoble University, and for HERCULES (the Higher European Research Course for Users of Large Experimental Facilities) students. The local team is then involved in the corresponding teaching. Note also that courses on surface X-ray diffraction and GISAXS were organized within the CNRS training framework, on the INS instrument.

Organization, committees and funding

The IF CRG beamline is part of a program established in 1991 by the two French research agencies: CNRS (Centre National de la Recherche Scientifique) and CEA (Commissariat à l'Energie Atomique). Two CRG beamlines - IF and D2AM – have been operational since 1994. A third beamline has a split radiation fan with one branch –FIP- operational since 1999, and the second branch equipped with the FAME beamline. A CRG/French Council with representatives of the two agencies is responsible for financial, personnel and scientific policy of the entire program. The program is executed locally by a "structure d'exploitation" regrouping the three Department Head of "Institut Néel (CNRS)", "Service de Physique des Matériaux et Microstructure" (INAC CEA-Grenoble) and "Institut de Biologie Structurale" (CEA-CNRS lab.), all established at Grenoble. The Grenoble University is also participating through a Contract for supplying student training every academic year. The personnel working on the beam lines are employed by these local laboratories. As a consequence the concept of in-house research is slightly different from the one at ESRF. The beam line and instrument scientists perform research programs of their own laboratory. The facilities of the three labs (infrastructure, workshop, design, secretary...) are available.

About 20% of the total available beam time is reserved for upgrade, maintenance and in-house research. One third of the remaining beam time is due to the European community, and is allocated by European committees through the usual application for beam time at the ESRF. The 2/3 of remaining beam time is open to the entire French community, and is allocated on the basis of merit of experiment proposals by the SOLEIL committees, twice a year, as for the ESRF beamtime. The available user beam time is calculated applying the rules observed at ESRF: time is reserved for in-house research, buffer between experiments and maintenance. In-house research is reviewed as well by the Committee.

Funding of the equipment has been initially provided by CNRS, CEA, Ministry of Research, Grenoble University, Région Rhônes Alpes and Conseil Régional. The construction cost of the beamline was 17.8 MF (Millions of French Francs), excluding salaries of the staff members, which are paid by CNRS or CEA. CNRS and CEA share the operational cost on a 60-40 basis. In 2014, for instance, the IF beam line has a budget of 205 k€ (recurrent cost including reimbursement to ESRF, and investment). It decomposes into 75 k€ of recurrent cost refunded to ESRF. Hence, only 130 k€ are left to run the beamline, including recurrent costs and small developments. All non-recurrent operation has to be funded by external contracts which are actively searched for by the local team, on the basis of their own research. Indeed, no funding is available at the French level for large upgrades. Typical funding by external contracts varies between a few tens and a few hundreds of k€.

A refurbishment project has been conducted in 2006 together with the build-up of the white-beam microdiffraction setup. The overall cost of the project (900k€) was shared between the CEA (200k€) and the CNRS (200k€), with a strong contribution from the applied research division of the CEA through the basic technological research (RTB) program (500k€). These contributions allowed a renewal of the beamline optical elements and the design of a micro-diffraction setup prototype.

Then the development of the microdiffraction instrument was further carried out (new detectors, new optics, postdoc) thanks to a grant (580k€) from the French National Research Agency (ANR). (MiDiFabl project within the PNano program (2007-2010)).

The gas distribution system to perform UHV-CVD with silane, germane and ethylene in the INS instrument has been funded by the Grenoble Nanoscience Foundation for (250 k€) and by the CEA-INAC (100 k€). The Nanoscience Foundation also granted a bursary for an 18 month postdoc starting in April 2010.

The upgrade of the INS instruments has been funded by a contract asked directly to the French Ministry and called "Equipements d'Excellence" (EquipeX). It provided a total investment fund of 1190 k€ plus an 18 month CCD contract for a research engineer.

Beamline Optics

The beamline optics was totally upgraded in 2006 and has two operation modes. A normal mode that delivers monochromatic (6.5-50keV) 150x250 (VxH) µm2 beam on GMT or INS stations and a pink micro-focus mode (2-30keV) that delivers a 0.5x0.5 µm2 beam on GMT. In this mode, the optics could also deliver a monochromatic microbeam (10-30keV). The beamline was designed by the BM32 team.

The configuration for the optics is of a classical layout where entrance slits are followed by a 3 optical element group (first mirror, monochromator and second mirror) in charge of X-ray white beam processing, and finally exit slits. To achieve a good harmonic rejection, both mirrors work at variable incidence, therefore adjusting cut-off energy to working energy. Good energy resolution is reached thanks to the first mirror that collimates the beam for the monochromator. The second mirror vertically focuses the beam either on the sample (normal mode) or on a micrometric 2-directions slit system located at the end of the optical hutch (pink micro-focus mode). The INS diffractometer needs a fixed beam vertical position. Therefore, the monochromator crystal gap is adapted to compensate for the vertical offset given by the variable angle of the mirrors.

The first mirror M1 is made of a single crystalline 1.3 m long Si bar, coated with 500Å Ir exhibiting a 3Å roughness, a slope error of 1.5 µrad rms on the full length, and only 1 µrad rms on the 300 mm central area. This mirror can be bent up to 5 km radius in order to vertically collimate the divergent beam from our bending magnet onto the first crystal of the monochromator. The cooling system consists in water circulation in copper blades, dipping in liquid InGaN ternary alloy placed in two channels dug on both sides of the Si bar, thus avoiding transmission of vibrations to the mirror. The maximal allowed thermal power for this mirror is 580W, corresponding to a ring current of 500mA, thus anticipating future ESRF upgrades.

The second mirror M2 is identical to the first, except for the absence of the cooling system and a higher maximum curvature (radius down to 2.5km) to allow vertical focusing on the micrometric slit.

The monochromator is a double crystal Si(111) type with the whole optical block under vacuum. The rotation stage is equipped with a high resolution encoder to achieve 0.35 µrad resolution. It is mounted on a translation stage to follow the beam reflected from the first mirror when the incidence angle is adjusted to select the cut-off energy. The rotation stage carries the first and second crystal assembly.

The first crystal assembly is a 10mm thick Si crystal with an optimized shape allowing a drastic reduction of the thermal bump [1]. It is glued on a copper plate cooled by water circulation. The roll of this plate can be dynamically adjusted by a piezo actuator to achieve automatic stabilisation of horizontal position of the beam against thermal drifts arising from ring current decrease.

The second crystal assembly is the standard Si ribs crystal mounted on an ESRF-CNRS bender type and is used for the sagittal focusing. The bender assembly is carried by three rotations (weak links): two for crystal roll and yaw and one for the two crystals parallelism (pitch). This latter movement will be finely adjusted by a piezo actuator to achieve automatic intensity maximization, thus compensating drifts as in [2]. Moreover, the bender is carried by two crossed translations: one adjusting the gap between the crystals and the second adjusting the shift between crystals along beam propagation axis.

In pink microbeam mode, the mirrors M1 and M2 are working under a fixed 3mrad incidence angle (cut-off energy > 30 keV), the gap between the monochromator's crystals is opened to let the beam outgoing from the M1 mirror pass through the monochromator directly onto mirror M2 and the pink beam is vertically focused onto the micrometric slit. As the main scientific goals are to measure 2D-maps of grain orientation and deformation in thin polycrystalline materials with a lateral resolution of 0.5 µm, we have to take up 2 major challenges: achieve a pink microbeam of size 0.5x0.5µm^2 and have it stabilized to better than 0.2µm.

To deliver the pink microbeam, a classical Kirkpatrick-Baez (KB hereafter) achromatic microfocusing device is used, which is composed of 2 fixed-curvature elliptic perpendicular mirrors. The KB mirrors are Pt-coated and work under fixed incidence angle of 2.9mrad (cut-off energy > 30keV), the first KB mirror being 290 mm long and the second 140 mm. The KB works under real object / image condition by demagnifiying the micrometric slit. The demagnification factor is simply the ratio between object distance and image distance. Therefore, the KB is brought as far as possible from the micrometric slit and as close as possible to the sample, leading to demagnification ratio in the vertical plane of 145 and 45 in the horizontal plane. Moreover, beam spot size increases from beamline mirror polishing slope errors or from mirror imperfect bending need to be minimized. As a consequence, the slope errors of the mirrors M1 and M2 on their central 300mm are below 1µrad, and the KB mirror slope errors are lower than 0.2µrad on full length.

For controlling and tuning the optics, specific software have been written, either at low level to support special device controllers, or at high level to have a user friendly and easily adjustable beamline. A feedback system was developed for automated tuning of the second crystal of the monochromator to maximize the flux and compensate the long term drifts.

[1] J.S. Micha et al, Nucl. Instrum. Meth. A **A 710**, 155-160 (2013)
[2] O. Proux et al, J. Synch. Rad. **13** (2006) 59-68

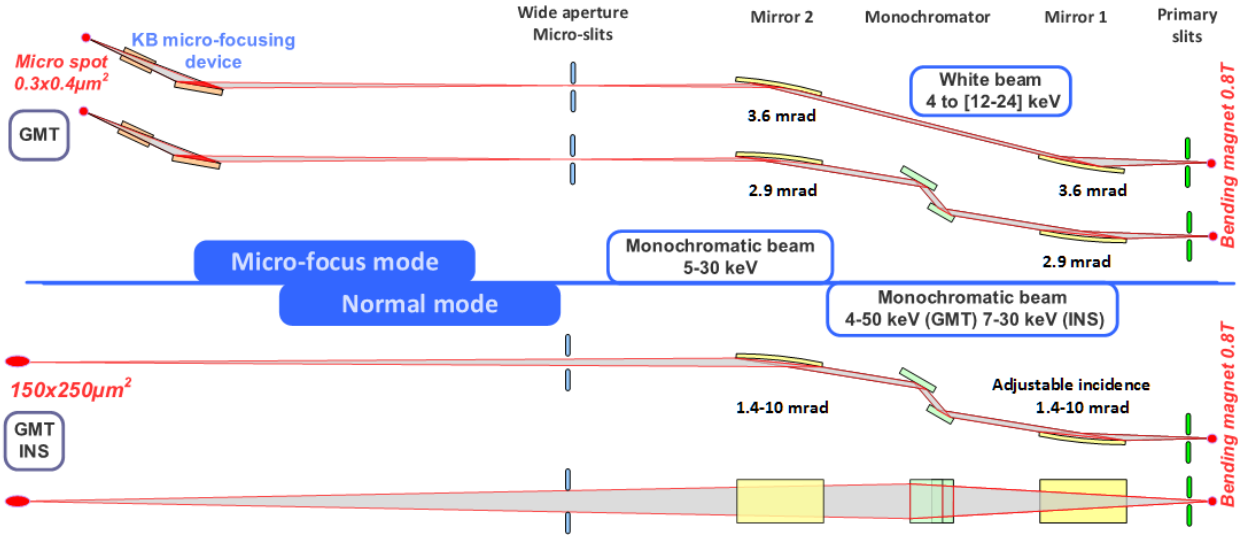

Figure 1: Schematic representation of the two configurations of the optical elements, mirrors and monochromator, providing either a sub-millimetric monochromatic beam of high energy resolution (the normal mode) or a sub-micronic beam that may be either white or monochromatic in the so-called micro-focus mode.

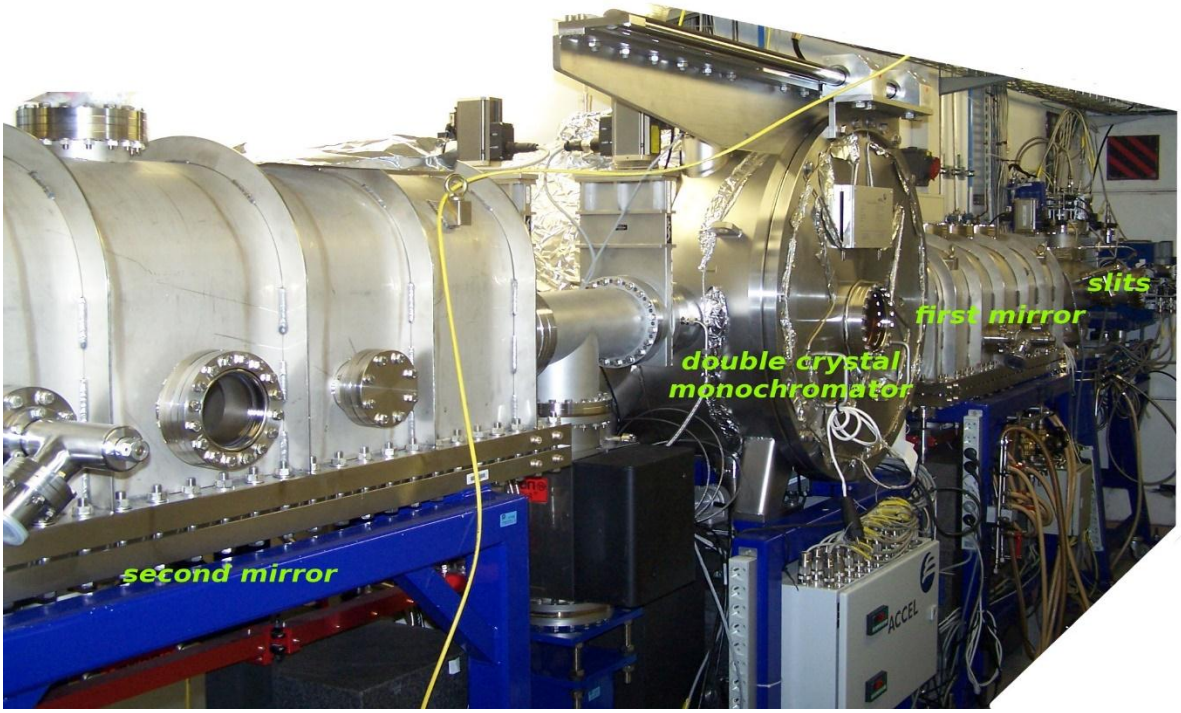

Figure 2: Photograph of the vacuum chambers of the optical hutch hosting the main optical elements, slits, mirrors and monochromator.

List of beamline staff, functions and scientific interest

The functions, scientific interest and involvement in the beamline activity of the beamline staff are briefly described below. Most of the researchers perform their own research using the beamline. The percentages indicate the fraction of their time devoted to "duty" tasks such as administration, engineering, development, local contact …, i.e. all tasks performed to run, use and develop the beamline, excepted personal research.

J.-S. Micha UMR CNRS-CEA-Grenoble, Research-Engineer/Local contact on GMT and µLaue 80%
- X-ray optics elements design: monochromator crystals and optics mirrors
- Involvement in development of the µLaue setup
- Software developer and administrator of LaueTools suite

G. Renaud, CEA-Grenoble, Researcher/Local contact on INS 50%
-Scientist in charge of BM32 beamline, of INS instrument and INS2 project
-*In situ* GIXS/GIXD/GISAXS/GI-MAD/A-GISAXS studies in UHV during growth
-*In situ* growth of nanowires by UHV-CVD, graphene and of nanoparticles organized on it.

F. Rieutord CEA-Grenoble, Researcher, In charge of GMT instrument 20%
- Fundamental studies of technological processes: direct bonding and wafer splitting. Adhesion and wetting at the nanoscale.
- Implantation and fracture. Crack development and propagation.
- Strain and stress measurements in technological samples (sSOI, interconnects, …)

O. Robach CEA-Grenoble, Researcher/Local contact on GMT and µLaue 30%
- Development of methods / tools for measuring local strains, orientation gradients, and microstructure on the micron scale, based on the µLaue technique.
- Development of "add-ons" of the µLaue technique (DAXM for 3D resolution, Rainbow for spot energy)
- Software developer of LaueTools suite
- Orientation gradients and stress in polycrystals at the micron scale in technological and model samples (growth, implantation, in situ mechanical testing)

M. De Santis, CNRS Institut Néel/ Researcher/Local contact on INS 25%
- Structure and magnetic properties of ultrathin films and surface alloys.
- Template mediated growth of nanostructures.
- Self-organisation of molecules at the surface.

O.Ulrich CEA-Grenoble INAC, Engineer 80%
- Beamline operation manager, in charge of technical aspects on BM32, including computing control command for the three instruments and detectors, as well as financial aspects and day-to-day interaction with the different ESRF services.
- Involvement in developing µLaue experiment to improve features and performances of data collection.
-Also strong technical involvement in the INS2 project.

O. Geaymond CNRS, Engineer assistant. Responsible for technical tasks on the BL, mostly on INS. 80%

F. Boudaa CEA, Research Engineer on an 18 month contract ending in july 2015, connected to the INS2 project 80%

The instruments

The Laue Microdiffraction setup (µLaue)

O. Robach, J.-S. Micha, O. Ulrich and F. Rieutord
CEA-Grenoble, Institut Nanosciences et Cryogénie, SP2M/NRS, 17 rue des Martyrs, 38054 Grenoble Cedex 9

The strong demand for structural characterization of objects with ever decreasing sizes has driven the development of new methods to determine not only the average internal structure but also the local structure at submicron scale. Probing the local strain, shape (size, orientation) and composition of micro and nano materials is the main objective of our Laue micro-diffraction setup. This dedicated setup is unique in Europe.

Two fixed-curvature elliptical KB mirrors are used to achieve a sub-micronic (hxv) =0.4x0.3 µm^2 white beam with a X-ray energy range of 5 to 22 keV (adjustable).

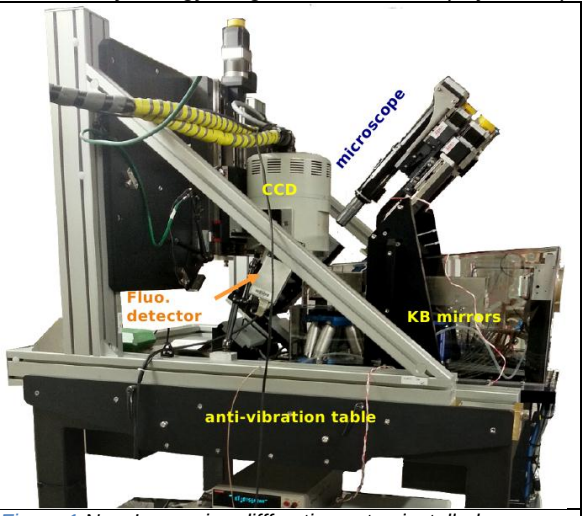

Figure 1 New Laue microdifffraction setup installed on BM32 in 2012 featuring fixed curvature KB mirrors, a motorized CCD camera translation stage, an active vibration damping table, and an in-house developed automatic feedback on the tilt angle. In situ experiments can be performed applying electrical current, thermal or mechanical loads.

A typical Laue pattern on a thick grain (>5µm) requires less than 0.5s counting time. Larger counting times are needed for low Z materials, smaller grains (< 0.5 µm), and grains with large orientation gradients (> 10 mrad/µm).

Selected regions of interest on the sample surface can be finely aligned on the x-ray beam by means of an optical microscope featuring a 50X objective and a 12X zoom, low depth of focus (< 1 µm) and high lateral resolution (0.3µm). In addition, x-ray fluorescence mapping can be used for locating micro-markers on the sample when the microscope is retracted.

The spot positions in the Laue pattern can be monitored as a function of time to detect *in situ* phase transitions, crystal deformation or reorientation. The mapping of the spots positions as a function of beam position on sample helps to localize regions where stresses or defects concentrate, e.g. after sample elaboration or after applying a load.

At higher level of analysis, each single Laue pattern once indexed fully determines the grain orientation (3 Euler angles) and the deviatoric shape of the unit cell (i.e. b/a, c/a, α,β,γ). Large orientation maps (figure 3) built from a raster sample scan then provide e.g. the local texture and the relative strain levels of between grains of different orientations. Such maps also allow

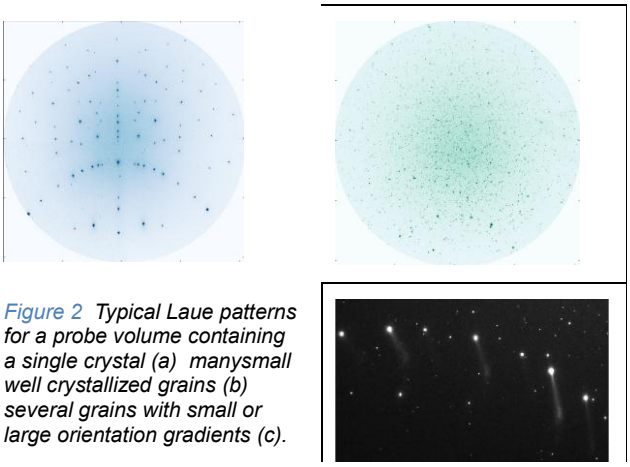

Figure 2 Typical Laue patterns for a probe volume containing a single crystal (a) manysmall well crystallized grains (b) several grains with small or large orientation gradients (c).

selecting particular grains for fine intra-grain mapping of orientation and strain gradients. Complementary methods for spot energy measurements (monochromator, energy dispersive detector, transmission Diamond monochromator) may then be used for local full strain tensor or line profile analysis.

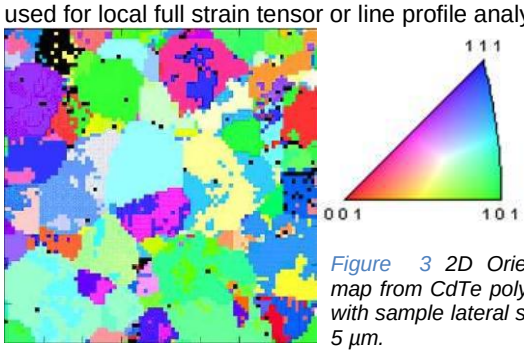

Figure 3 2D Orientation map from CdTe polycrystal with sample lateral steps of 5 µm.

A home-developed open source software suite, *LaueTools*, facilitates the data analysis by means of Graphical User Interfaces and scripts. During the experimental run, its online treatment tools help to choose the best data collection strategy. After the experiment its fast parallel computing modules allow the automatic analysis of several thousands of images.

Applications of this instrument are mostly in Material Science : energy-related materials (Solid-oxide fuel cells, nuclear fuels, photovoltaic cells), complex integrated circuits from the micro-electronics industry (2D and 3D interconnects), structural materials (superalloys for turbine blades, shape memory alloys for medical applications, stainless steel for piping in nuclear plants), biology-related materials (nacre, asbestos toxicity). More fundamental studies include *in situ* mechanical testing on model macro, micro or nano objects (FIB-machined metallic micro-pillars, nanowires, whiskers, bi-crystals, tri-crystals), in view of improving the description of the mechanical properties of polycrystals or micro and nano objects.

Selected publication(s): O. Robach, J.-S. Micha, O. Ulrich, O. Geaymond, O. sicardy, L. Haertwig, F. Rieutord, Acta Cryst. **A 69**, 164-170 (2013); O. Robach, J.-S. Micha, O. Ulrich and P. Gergaud, J. Appl. Cryst.. **44** p 688–696 (2011) ; O. Ulrich, X. Biquard, P. Bleuet, O. Geaymond, P. Gergaud, J. S. Micha, O. Robach, and F. Rieutord, Rev. Sci. Instrum. **82**, 033908 (2011)

Grant(s): ANR AMOS, ANR MicroStress

Contacts : robach@cea.fr, micha@esrf.fr

The instruments

The In situ Nanostructures and Surfaces (INS) endstation

G. Renaud[a], O. Ulrich[a], P. Jeantet[b], D. Grand[b], O. Geaymond[b], M. De Santis[b] and F. Boudaa[a]
[a&b]Université Grenoble Alpes (UGA)
[a]CEA-Grenoble, Institut Nanosciences et Cryogénie, SP2M/NRS
[b]CNRS-Institut Néel

The INS station is devoted to studies of surfaces, interfaces, nanostructures and thin films in Ultra High Vacuum, in particular during their growth, by means of three techniques using hard X-rays: Grazing Incidence X-ray Scattering (GIXS, which here is generic for SXRD, GID, GIXRD etc…), Grazing Incidence Small Angle X-Ray Scattering (GISAXS), and X-ray Reflectivity (XR). In the recent years, a gas injector allowing for growth of Si and Ge using UHV-CVD has been added to the existing MBE (up to seven sources) possibilities. The diffractometer and UHV/MBE/CVD chamber of the INS instrument are being replaced (spring 2015) by new ones with extended possibilities.

The INS instrument consists of a large and well-equipped UHV chamber mounted on a 4-circle diffractometer of z-axis type for X-ray studies, coupled to UHV introduction and preparation chambers located in the X-ray hutch. The diffractometer supports a large UHV chamber, with allowance for a rotation of the whole chamber defining the incidence angle (α) of the X-ray beam with respect to the vertical sample surface. A goniometric head allows alignment (two perpendicular tilts (χ_1 and χ_2), three translations (X,Y,Z) of the sample inside vacuum. The rotary motion (ω) of the sample is obtained through the rotation of the whole goniometric head thanks to a differentially pumped rotary feedthrough. The sample surface is vertical. Two circles of the diffractometer are devoted to the two detector rotations defining the Bragg angle projections parallel and perpendicular to the surface (δ and β respectively). The x-ray UHV chamber has large Be windows giving access to large perpendicular momentum transfers (up to 45° input and exit angles). It is equipped with several sources for *in situ* epitaxial deposition and with standard UHV preparation and analysis tools (high temperature furnace, Reflection High Energy Electron Diffraction (RHEED), Auger Electron Spectroscopy (AES), Residual Gas Analysis (RGA), Ion Sputtering (IS), quartz micro-balance for calibration of deposition). Simultaneous real-time analysis with x-ray diffraction, RHEED and Auger spectroscopy can be performed during (co)deposition and/or annealing of ultra-thin films. The main characteristics of the setup are summarized below (see Figs. 1 & 2):

* The shared beam time with the other station makes it possible to investigate systems that require significant preparation time before performing an X-ray experiment (typically the UHV chamber can be made available a week before an experiment).
* The base vacuum is very low ~3 x 10^{-11} mbar.
* RHEED, (A)GISAXS, (A)GIXS(D), XR (and even SEXAFS) experiments on the same sample.
* Co-deposition: deposition of up to 7 materials.
* High signal to noise ratio, allowing for example the study of molecules, which would be destroyed by stronger X-ray sources.
* Fast sample introduction system.
*High temperature (remotely controlled) furnace (up to 2000°C).
* The beam energy can be changed easily and continuously. (Multiple) Anomalous scattering is very reliable.
* Sample cooling down to -100°C, optional.

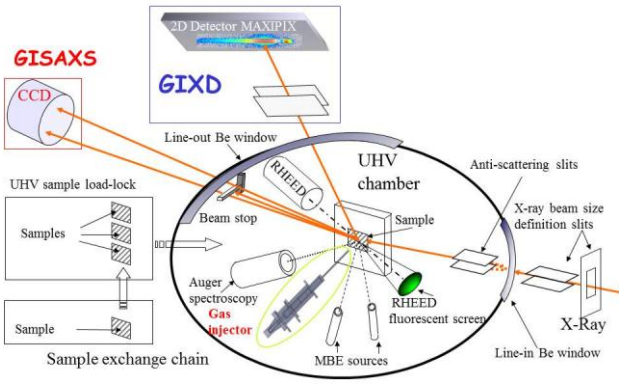

Fig. 1 Sketch of the INS setup

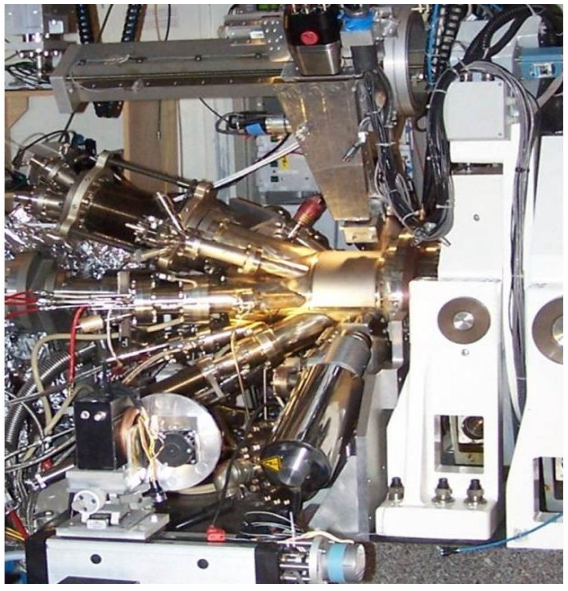

Fig. 2: Photograph of the X-ray station of the (former) INS set-up viewed from detector side. The beam comes in through a small Be window and exits through a large Be exit window (in light gray). Also visible on the photograph are the RHEED gun (bottom center), the Auger Spectroscopy CMA (upper left), a silicon evaporation cell (SUSI 63) middle left as well as other evaporation sources; the diffractometer delta and omega circles (in white on the right) and the detector flight tube with a 1D Vantec detector at the end.

First upgrade for better GIXD, GISAXS and UHV-CVD

In 2010, significant improvements have been done to the setup. In order to obtain a better resolution in GISAXS and GIXD the experimental hutch has been much enlarged toward the end of the beamline. The increase of the possible sample-detector distance up to 3 meters allows performing GISAXS and diffraction with a much higher resolution, together with the use of bulky

1D or 2D detectors on the diffractometer. A 5x1 ESRF Maxipix detector is now routinely used.

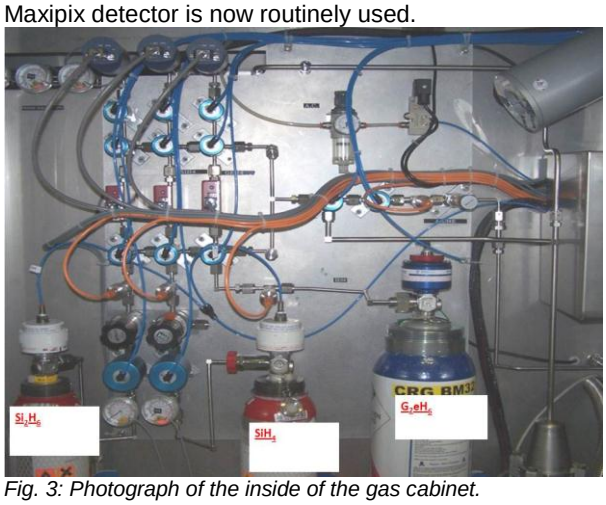

Fig. 3: Photograph of the inside of the gas cabinet.

In 2011, the experimental hutch and instrumental setup have been further adapted to implement a gas injector in the chamber. This injector from RIBER can be feed with three different gas lines. A gas distribution system has been realized that allows delivering well controlled fluxes (and pressures) of pyrophoric and toxic gases such as silane, disilane and digermane. In order to comply with ESRF high standard safety requirements, the upper pressure in the chamber has been limited to 10^{-4} mbar, and the gas flow to 1 sccm. The hutch is equipped with three gas detectors plus flame detectors plus special gas extraction. All the gas system is remotely controlled, operation sequences are automatic (bottle replacement, line purge, injections …) and interfaced with SPEC.

The INS-2 project: a complete refurbishment

In 2013, we obtained a so-called EquipeX contract from the French ministry in order to completely upgrade this instrument, whose core was already 20-years old, and which had been continuously evolving since then (in particular to perform GISAXS in addition to GIXD, adding internal slits and beam stops in UHV) with additions that were not fully optimized.

The principles behind the project were: -1- Keep all the existing UHV tools (RHEED, AES, Sources …); -2- make a more versatile, better adapted MBE/CVD/UHV chamber, capable of handling simultaneously as many tools as possible, while optimizing the internal tools such as slits and beam stops for GISAXS; -3- Ease the use of the three techniques (GIXS, GISAXS and extended reflectivity) in one experiment; -4- increase the speed of data acquisition in order to investigate processes such as growth at the second timescale as opposed to many tens of seconds before. -5- Allow for fast (<1 s) motion between different points of reciprocal space; -6- Ease the mounting and maintenance of the system; -7- Keep the existing satisfactory sample mounting (1" molyblocks) and heating systems, as well as the Riber modutracks introduction chambers.

Basically, the system (Figs. 4 and 5) consists in a new, faster and larger diffractometer, coupled to a new, larger UHV chamber equipped with beryllium windows (Fig. 6). The sample holder is a long rod in UHV ended by the sample heater at one end, and by a CF63 mounting flange at the other end. This flange is connected to a differentially pumped rotary feedthrough, itself connected to a large and heavy duty hexapod in air on the one end, and to a large bellows

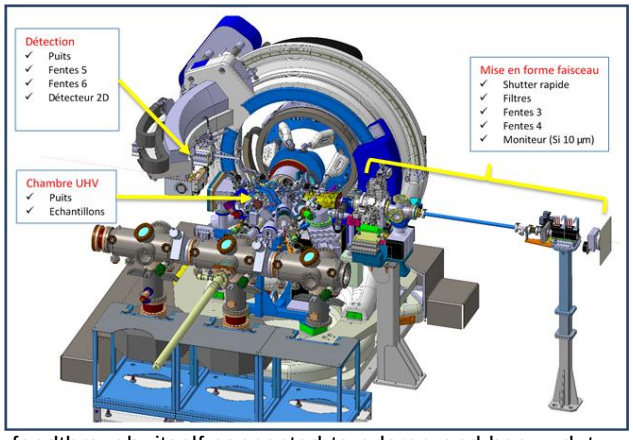

Fig. 4: 3D CAD overview of the full INS2 instrument

connected to the main chamber, on the other end. The hexapod provides 6-degrees of freedom for sample alignment, the corresponding motions being accommodated by the bellows. The hexapod allows for two perpendicular ±5° χ_1 and χ_2 rotations of 0.001° accuracy and three X,Y,Z translations of µm accuracy. All the other rotary motions have 0.005° absolute accuracy, lower than 0.001° resolution; axes parallel or perpendicular within 0.001°, and a sphere of confusion of 60 µm for the sample motions and 100 µm for the detector ones. The ω (±200°) sample rotation and the δ detector (-15°, +126°) rotations can reach speeds of 20°/s, and the β rotation (-1, 45°) reaches 10°/s. The α rotation defining the incident angle can be moved between -1 and 20°, without any disconnection of the chamber from the Modutrack introduction system, thanks to a long bellows in between.

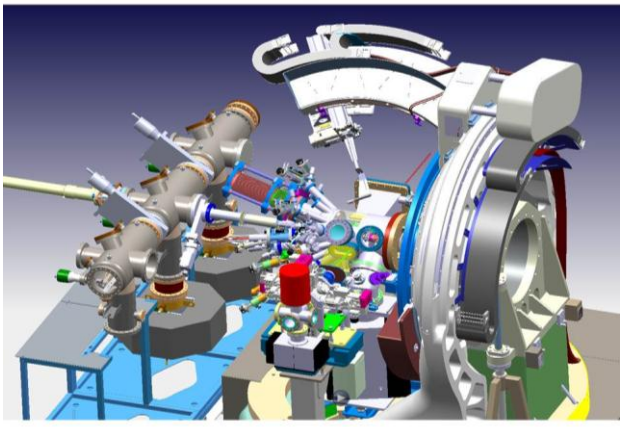

Fig. 5: 3D CAD representation of the INS2 instrument

The chamber is represented in Fig. 6.

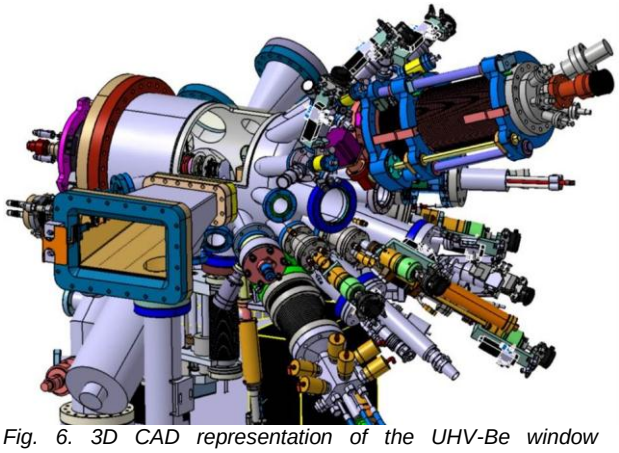

Fig. 6. 3D CAD representation of the UHV-Be window chamber equipped with its tools and with the large exit rectangular Be window.

In order to better define the incident beam, and remove any unwanted background scattering around it, the UHV system is limited on the X-ray entry side by a fixed, single-crystalline Be windows that should not yield small angel scattering. This is followed by in UHV anti-scattering slits, themselves followed by in UHV single crystalline Si diode monitor, and next by a differentially pumped tube placed inside a large bellows that allows for the α chamber rotation (-1 to 20°) (see Fig. 7).

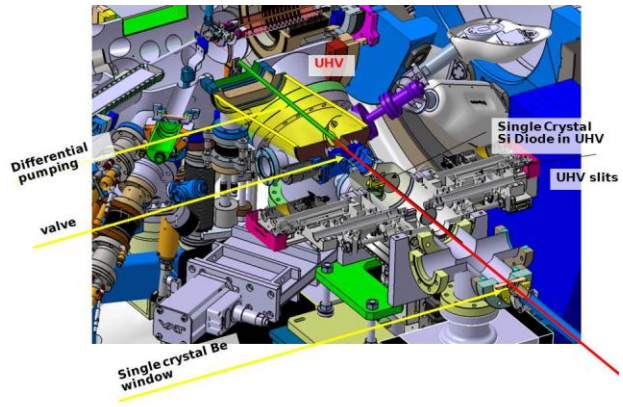

Fig. 7. 3D cut CAD view of the inside of the UHV chamber of the side of the incoming beam.

The ω-circle supporting the hexapod is mounted on a large vertical axis (Fig. 5) that allows to remove it from the inside of the δ circle in order to easily access to the chamber via its large flange for instrument mounting and maintenance.

On the exit side, a large, rectangular flange mounted on the chamber let the beam travel toward a large, rectangular Be window place 500 mm away from the sample. A T-shape beam stop is placed in UHV just before this exit Be windows (plus another one just after), allowing to stop the direct and reflected beams before they are scattered by the exit window. The low-angles lost in δ (from -1 to 12 degrees) on the hemispherical Be windows is recovered on the negative δ side through the large rectangular Be window.

The detector arm (see Figs. 4 and 5) holds a fully motorized slit placed just before the detector, which may be either a Maxipix 5x1 or a DECTRIS Eiger 1M R pixel detector, and a retractable fixed opening detector slit is placed as close as possible to the Be windows of the main chamber at large δ angles, and moved away for δ smaller than 12°.

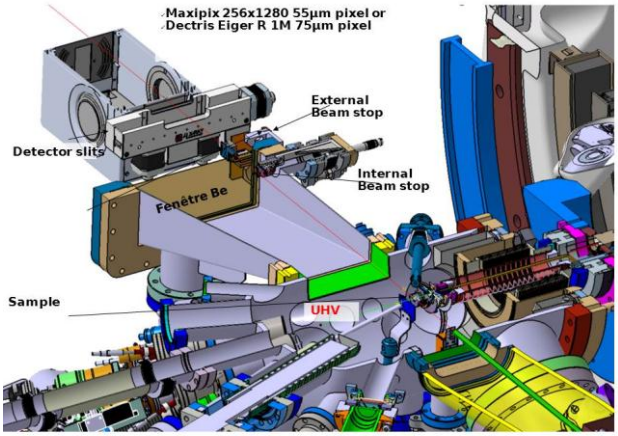

Fig. 8. 3D cut CAD view of the inside of the UHV chamber on the side of the exit beam.

Publications: *"The In situ growth of Nanostructures on Surfaces (INS) end station of the ESRF BM32 beamline: a combined UHV-CVD and MBE reactor for in situ x-ray scattering investigations of growing nanoparticles and semiconductor nanowires"*
V. Cantelli, O. Geaymond, O. Ulrich, T. Zhou, N. Blanc, and G. Renaud J. Sync. Rad., accepted, (2015) and F. Boudaa et al, in preparation

Grants: French Nanoscience Foundation, French EquipEX CRG/F

Collaborations:

Patent(s)

Contact: : gilles.renaud@cea.fr

The instruments

The Multitechnique goniometer (GMT)

F. Rieutord[a], , *J.-S. Micha*[b]
[a]CEA-INAC-SP2M [b]CEA-INAC-SPrAM

The GMT is a general purpose 2+2 axis surface diffractometer, well suited to most grazing incidence scattering techniques (GIXS, XRR, GISAXS) . It is normally dedicated to samples elaborated ex-situ but it can also accommodate a wide range of sample environments due to the large open space available around the goniometer center. It has been used during the last years for solid/solid, solid/liquid and solid/air surface and interface studies, mostly using X-ray energies between 20 and 30 keV.

The multitechnique goniometer (GMT) is a standard 2+2 goniometer devoted to surface scattering studies. It is normally used for surface studies of samples elaborated ex-situ.

As opposed to the UHV setup, the experiments taking place on GMT do not normally request lengthy surface preparations. Being located upstream with respect to the UHV station, it shares a hutch with the µLaue setup and both experiments alternatively use the beam while the INS setup is preparing its samples or baking out.

Yet, due to the large volume accessible around its center, the instrument can accommodate a large variety of sample environments, ranging from small enclosures (e.g. electrochemical cells) to a large UHV system with two chambers devoted to in-situ studies of catalytic processes. The goniometer can also handle vibration filtering tables for liquid surface studies, Helium cryostats, magnets, and a variety of furnaces. The first µLaue experiments were actually run using the goniometer as a support for both focusing and sample movement elements, while the 2D detector was mounted on the detector arm.

The instrument has been used in the last years mainly for the study of buried interfaces e.g. liquid/solid or solid/solid interfaces. We make use of the 20-30 keV energy range of our bending magnet to access the interfaces, crossing one of the phase over its whole width.

We have automated as much as possible sample changing. For solid/solid interfaces for example, samples are piled up and automatic alignment routines have been developed so as to be able to study series of about 20 samples. Routines for automatic data inversion (e.g. reflectivity data) have been developed in parallel.

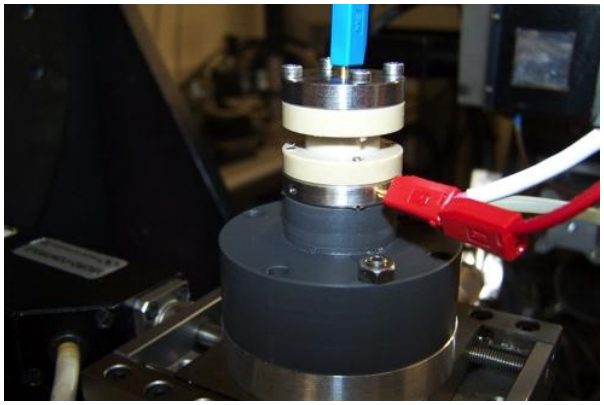

Figure 1 Small cell designed for Lithium batteries experiments. The cell replicates a button cell (coin cell) . The separation of the two electrodes (stainless stell contacts with electrode materials (Si , Li metal)) are separated by a PEEK cylindrical spacer thinned down to let the beam go through the electrolyte and probe the electrode/electrolyte interface (SEI formation layer). The crossed length for electrolyte is 15mm diameter.

The instrument has received little evolutions during the last 4 years. Its mechanics is still accurate enough and efforts have been put on developing or replacing the other beamline instruments. Only part of the electronics for motors has been upgraded with e.g. the installation of icepap controllers for detector slits motors.

More recently, we have started to use 2D pixel detectors for diffraction experiments. We use a 5-chip 256*1280 silicon pixel detector that can be mounted in both orientations regarding its long direction (generally along CTR direction, depending on sample orientation). The detector has been used for instance to record diffraction pattern from artificial gratings. Due to their small pixel size, low noise and high counting rates, these detectors are interesting and may speed up the acquisition of reciprocal space maps. However, the poor efficiency of these Si pixel detectors limits their usage for the medium high energy experiments but we expect this limitation to be removed with today's availability of CdTe pixel detectors. Tests have already been made and acquisition of a small size pixel detector is foreseen for the year to come.

Many of the experiment performed on GMT have a link with applied research subjects. We have worked on the physics of several steps of the SmartCut™ technology, especially implantation, bonding and fracture. Other subjects of technological interest have been addressed, like SEI (Solid Electrolyte Interphase) formation at the interface between electrode and electrolyte in Li batteries. Strain (GID,RSM) and size measurements (SAXS,GISAXS) on microelectronics system patterned using state-of-the-art lithography have also been recently performed.

Grants:	Collaborations:
Patent(s)	Contact: francois.rieutord@cea.fr

The instruments

Detectors on BM32

On BM32 we have a large choice of detectors to cover a wide range of techniques. These are commercially available detectors. Integration and development were necessary to interface some of them with our standard control system, which is the ESRF standard. These developments consist in electronics and software, in order to best match the experimental requirements of our 3 instruments.

For the optics, beam monitoring and data normalisation we are using standard silicon diodes with high accuracy electronic that transforms the analogue value into pulses integrated by the counting cards. We are also using a 4-channel picoammeter to monitor the beam, and a lock in amplifier to make a feedback on the second cristal of the monochromator and keep the flux at its maximum value whatever the power load on the optics.

On the experiment side we have detectors, from the basic zero dimension detector, to two dimensions CCD and pixel detectors. Since the last BLRP, the main change is the purchase of a pixel detectors to replace the 0D and 1D gaseous detector on INS instrument.

0D detector for diffraction :

The standard photomultiplier with NaI scintillator is still in used on GMT diffractometer behind slits that defines the analysis direction. Coupled to these detectors we also have automatic filter system used to avoid detector saturation and to extend the dynamics of detection chain.

In experiments that require high energy resolution we have a Rontec Si drift detector. This detector has a typical energy resolution of 250 eV at counting rate up to 400 kcps with a 5mm2 detection area. It is mainly used on the microdiffraction experimental setup to monitor the fluorescence signal from the sample, either to build fluorescence maps or simply to locate on sample. We also acquired a second detector of this type, a Ketek XR-SDD read with a XIA electronics. The energy resolution is 125 eV at 5.6 keV and the throughput of 100kcp/s

2D detectors :

We have four CCD detectors with various input size, pixels number and size, sensitivity, readout speed. Detector choice is done by users and its local contact in order to best match the experiment requirements. The QuadRo detector is still on repair due to a default on cooling system. This had no consequence on experiments as we have a backup solution with the MARCCD.

All CCD detectors are fully supported in standard acquisition system. Some use ESRF software developments, others have required special developments by BM32 team because they are not supported at ESRF or very specific features or control modes are required. On the INS diffractometer the 0D, 1D and 2D can be used at same time, giving access to many X-ray measurement techniques.

A 1280x256 (5x1) Maxipix pixel detector is also used on INS and GMT instruments. With a 55 µm pixel size a 500 µm Si thickness, and a 100 Kcps/pixel this detector is used for diffraction at energies under 25 keV, which cover 95% of experiments on INS and 50% on GMT.

	Input size mm2	Pixel	Pixel size µm2	Readout time no binning s	Readout time binning 2x2 s	Dynamic bits	Dynamic range dB	Specific feature/comments	Instrument
MAR 165	Φ 165	2048x2048	80	2.5	-	16	77		µLaue
QuadRo 4096	Φ 165	4096x4096	40	8.8	2.2	16	78	Off line data correction	µLaue
VHR	Φ 81	2672x2672	30	1.2/2.4	0.3/0.6	12/16	70	Electronic shutter, Antiblooming x1000, pipeline readout mode, possibility to extend dynamic up to 20 bits	µLaue
ImageStar	67x67	3056x3056	22	2.5	0.6	16	82	Antiblooming x100	µlaue/GMT/ INS

Selected publication(s) -	
Grant(s) : ANR-AMOS ANR-MircoStress	Collaboration(s):
Patent(s) :	Contact : olivier.ulrich@cea.fr

Example of Scientific Research and Highlights

In the next pages a selection of scientific hightlights on the three instruments for the period 2010-2015 is presented:

µLaue

HL1: Tensile strained germanium nanowires for photonics (Research in Collaboration)

HL2: Investigation of diffusion processes during the phase transitions (Research from outside users)

HL3: Plasticity at micron scale (Research from outside users)

HL4: A new method for fast Laue reflection energy measurements and its application to a chemical gradient material (Research of beamline scientists + outside users)

GMT

HL5: Implantation induced strain (Research of beamline scientists)

HL6: Wafer bonding (Research of beamline scientists)

HL7: Osmotic pressure effect on supported membranes layers (Research from outside users)

INS

HL 8: Growth and structure of ultrathin CoO/PtFe bilayers showing robust perpendicular exchange coupling. (Research in Collaboration)

HL 9: Effect of CoO/Ni orthogonal exchange coupling on perpendicular anisotropy of Ni films on Pd(001). (Research in Collaboration)

HL10 Kinetics of dewetting of Germanium on Silicon dioxide (Research from outside users)

HL 11 In situ monitoring of strain relaxation during the deposition of the shell in GaN/AlxGa1-xN core-shell nanowires grown by PAMBE (Research from outside users)

HL 12 In situ X-ray scattering investigations of the UHV-CVD growth of Si, Ge and SiGe core-shell nanowires – growth, composition, strain & bending (Research of beamline scientists)

HL 13 Growth, strain and organisation of Graphene on Ir(111) (Research of beamline scientists)

HL1: Tensile strained germanium nanowires for photonics

K. Guilloy[a], N. Pauc[a], A. Gassenq[a], P. Gentile[a], S. Tardif[a], F. Rieutord[a], J. Escalante[a], I. Duchemin[a], Y.M. Niquet[a], V. Calvo[a], G. Osvaldo Dias[b], D. Rouchon[b], J. Widiez[b], J.M. Hartmann[b], D. Fowler[b], A. Chelnokov[b], V. Reboud[b]
[a]INAC-SP2M, [b]LETI

The Laue microdiffraction technique takes advantage of the high photon flux, wide energy range available at beam line BM32 to probe the local lattice orientation and strain tensor with sub-micrometer resolution. It is therefore highly suited to study novel micro- and nanostructures in which the strain is tailored to fit the needs for micro- and optoelectronics applications. A key milestone on the road to the next generation microelectronics is the development of an integrated, CMOS-compatible light source. A promising approach to achieve this feature is to strain a germanium crystal in such a way that its electronic bandgap switches from indirect to direct. We report here on the effect of [111] tensile strain in germanium nanowires on the control the electronic bandgap energy.

Strain for photonics

On-chip integrated photonics offers the promise of faster data transmission and new functionalities for microelectronics. Most of the required components (modulators, detectors…) already exist, yet an efficient integrated light source is still missing. The development of a group-IV based source (silicon, germanium) would offer the CMOS compatibility that the integration of existing III-V solutions currently lacks. The problem with silicon or germanium crystals is that since their electronic bandgap is indirect, they are poor light emitters. All is not lost though, as in germanium the direct bandgap is only 0.14 eV above the fundamental bandgap and this difference can be further reduced by heavy n-type doping and/or tensile strain. In the latter case, single crystals of reduced dimensions are expected to be mechanically stronger than their bulk counterparts, due to their reduced number of defects allowing larger strain amplitudes. Several approaches are being considered to introduce large amplitude strain in Ge on Si: adding a stressor layer on top of the Ge film, applying an external mechanical stress, or using micropatterning to geometrically concentrate the stress from a pre-loaded layer in a narrow region. The typical stress directions are <100> or (001) for uniaxial or biaxial stress. In these conditions, the strain thresholds for changing the bandgap type have been predicted to be about 2 % and 4.6 %, respectively. However, in the case of <111> uniaxial stress, the picture is not as clear: strain thresholds between 1 % and 4.2 % have been predicted for the same stress configuration but not yet experimentally confirmed.

Suspended [111]-stressed Ge nanowires

Germanium nanowires are an ideal system to investigate the influence of the strain on the electronic properties: they are uniaxial, high-quality single crystals. The nanowires that were investigated were grown along [111] and featured a built-in axial p-i-n junction located at the center of the nanowire, allowing for a direct probing of the electronic properties. Stress was introduced by releasing pre-streched Si_3N_4 arms on which the extremities of the wires were anchored. Photocurrent spectroscopy was used to measure the bandgap energy shift for various arms lengths (Fig. 1a) while the deviatoric strain components were measured using Laue microdiffraction in the same samples (Fig. 1b). We could calculate the corresponding full strain tensor by assuming uniaxial stress along [111], the outer surface of the nanowire being free from external stress. Strains along the wires axis ranging from 0 to 1.5% were measured, scaling linearly with the stretching arm length (with a small offset due to the underetching of the Si layer under the arms).The dependence of the redshift of the bandgap energy on the strain amplitude was consistent with previously published theoretical calculations for the transition of light holes at the Γ point in [111]-strained Ge (Fig. 1c).

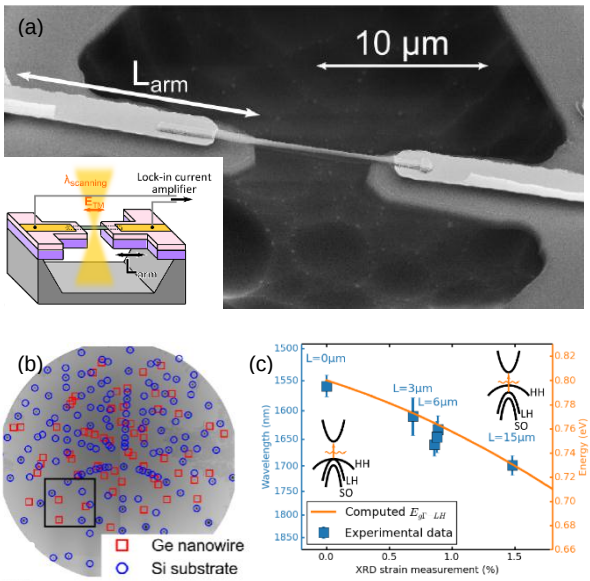

Figure 2 (a) SEM micrograph of a suspended Ge nanowire under uniaxial stress from the Si3N4 arms. (inset) Photocurrent spectroscopy measurement setup, optical selection rules for an incident light with the electric field along the wire axis state that only the light holes transitions can be observed. (b) Laue microdiffraction pattern, showing the Ge nanowire and the underlying Si substrate. (c) Bandgap energy and corresponding wavelength *vs* [111]-strain. The theoretical model of Γ-light holes transitions shows a good agreement with the experimental data.

In conclusion, the combination of synchrotron white beam microdiffraction and photocurrent spectroscopy allowed for the precise experimental determination of the relationship between the strain along [111] and the redshift of the bandgap energy in Ge, consistent with the predictions of the deformation theory. Future studies may now turn to other strain orientations (either uniaxial or biaxial) in different types of suspended nanostructures. Complementary x-ray diffraction techniques may also be used to measure experimentally the last parameter of the strain tensor, *e.g.* at the neighboring monochromatic ID01 beam line or using the 'diamond' monochromator technique being developed at BM32.

Publications: K. Guilloy *et al*., Nano Letters (2015). DOI : 101021/nl5048219

Grants:

Collaborations: CEA-LETI Grenoble

Patent(s)

Contact: kevin.guilloy@cea.fr, samuel.tardif@cea.fr

HL2 : investigation of diffusion processes during the phase transitions

M. N. Schneider[a], C. Stiewe[b], T. Schröder[c], P. Urban[a], O. Oeckler[a]
[a]Univ. LMU München,[b]German aerospace Centre Köln, [c]Univ. IMKM Leipzig Germany

Micro-focused white-beam (Laue) diffraction partially excludes space-averaging effects typical for conventional X-ray diffraction experiments, and large areas of reciprocal space are recorded in a single diffraction pattern. It is ideally suited for the *in situ* temperature-dependent investigation of diffusion phenomena. Laue diffraction patterns of various GeTe-rich $(GeTe)_nSb_2Te_3$ crystals grown by chemical transport reactions.

Metastable modifications from stable phases are highly used in modern data storage media such as Blu-Ray Discs or non-volatile PC-RAM. They can alter crystal metrics and defects nature and distribution (Fig. 1).

Laue diffraction patterns of quenched $(GeTe)_{15}Sb_2Te_3$ crystals (Fig. 2) do not show strongly broadened Bragg reflections at room temperature, in contrast to samples

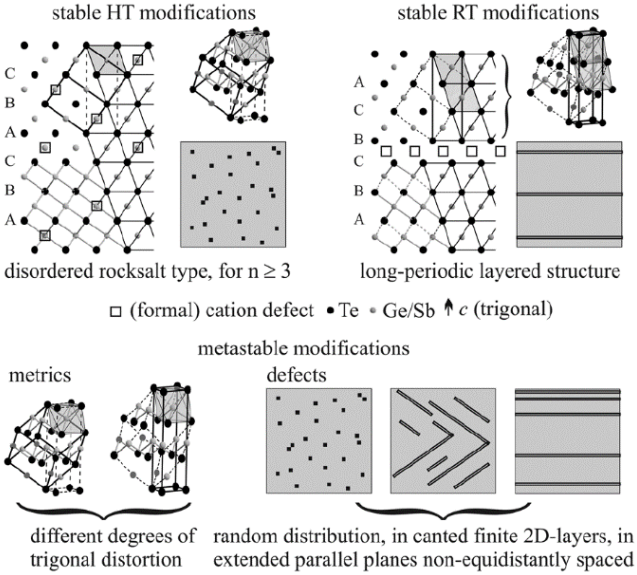

Figure 1 Structures of different modifications of GeTenSb2Te3 pahses with schematic representations of cation defect distributions.

with lower GeTe content. The diffraction patterns exhibit groups of reflections which result from the superposition of the intensities from individual domains with unit cells clearly deviating from pseudo-cubic metrics. Reflections belonging to individual domains can be indexed based on a h*R* cell with a = 4.22 Å and c = 10.57 Å. The ratio a/c = 0.399 lies between that of α-GeTe (a/c = 0.389) and that of a cubic cell in h*R* setting (a/c = 0.408). Whereas no diffuse scattering is observed between groups of reflections, there are weak diffuse streaks that interconnect the reflections of one group. These are due to domain-wall scattering (cf. Fig. 2). Upon heating the sample above 330 °C, additional Bragg reflections of the rocksalt-type high temperature phase appear in between the reflections of each group and gain intensity as the rhombohedral distortion of the individual domains decreases. At 400 °C only reflections which can be indexed with a c*F* cell with a = 6.00 Å are observed (cf. Fig. 3). In contrast to samples with lower GeTe contents, $(GeTe)_{15}Sb_2Te_3$ does not show nanostructures with pronounced short-range correlated cation defects.

At all temperatures, there was no diffuse scattering indicative of extended planar faults. Intrinsic cation defects can be assumed to concentrate at domain boundaries. However, slightly below the transition temperature to the cubic high-temperature modification, trigonal and cubic domains coexist. Although the $(GeTe)_{15}Sb_2Te_3$ crystal can be viewed as a multiply twinned Sb_2Te_3-doped variant of GeTe, the phase transition is different from the continuous, displacive rhombohedral to cubic transition of GeTe at ≈ 432 °C as it requires diffusion of defects from domains boundaries to form the disordered rocksalt type. Upon cooling the crystal below 330 °C, the sharp reflections of the high-temperature modification significantly broaden and the diffraction patterns resemble to those observed for $(GeTe)_{12}Sb_2Te_3$ at room temperature. This indicates that a nanotwinned transformation twin is

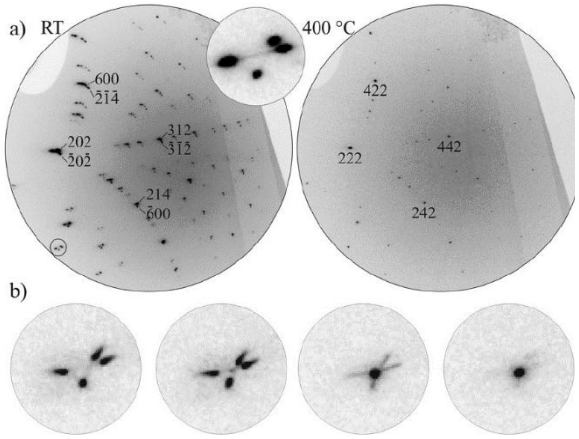

Figure 2 a) Laue diffraction patterns of $(GeTe)_{15}Sb_2Te_3$ collected at room temperature and at 415 °C, the inset shows an enlarged group of reflections from different domains (exemplarily indices of some reflections are given); b) changing intensity distribution of the reflection group indicated in a) between 330 and 340 °C (left to right) during heating.

formed, whereas before heating a growth twin was present.

As a conclusion, our investigation clearly demonstrates that x-ray techniques providing average structure; e.g. powder diffraction, are not sufficient to understand the relevant temperature dependent structure–property relationships of these materials because the diffusion processes and thus the changes of the real structure are predominantly reflected as diffuse scattering. The ability of Laue microdiffraction technique to isolate single domain scattering signal is then an asset and enables to localize and study crystal defects at small scale.

Publications: M. N. Schneider, X. Biquard, C. Stiewe, T. Schröder, P. Urban and O. Oeckler
Chemical Communications **48** (16) 2192-2194 (2012)

Patent(s)

Contact: oliver.oeckler@gmx.de

HL 3: Plasticity at the Micron Scale

C. Kirchlechner[a,b], C. Motz[c], P.J. Imrich[b], N. Malyar[a],, G. Dehm[a]
[a]MPI für Eisenforschung Düsseldorf Germany, [b]Montan Univ. Leoben Austria, [c]Univ. des Saarlandes, Sarrebrücken Germany

The plastic deformation at the microstructural length scale is not thoroughly understood. Main questions are (i) the size dependent flow stress of single crystals, (ii) the accumulation and self-ordering of dislocations during fatigue and (iii) the dislocation-interface interaction. Polychromatic x-ray microdiffraction is an outstanding tool to investigate the number and type of stored geometrical necessary dislocations (GNDs) *in situ* and therefore, a unique tool to interlink the mechanical response with the underlying and evolving microstructure.

The flow stress of a material, being the stress where a permanent change in sample shape occurs, inherently depends on the chemical composition and the microstructure of the material, including also the density and type of lattice defects. From a classical point of view, the flow stress should not depend on the geometrical sample dimensions. This assumption, valid over centuries and used as a fundamental base of design in mechanical engineering, was proven to be incorrect less than a decade ago. Uchic et al [1] have reported on the tremendous increase of the flow stress when sample sizes are reduced and reach micron or even sub-micron dimensions. This size effect is not only interesting from a scientific point of view, but also a challenge for future developments. The on-going trend in miniaturization – for instance in microelectronics – requires a thorough understanding of the material properties at this length scale.

Microsized single crystalline copper pillar specimens (7x7x21µm³) which were synthesized by focused ion beam (FIB) milling have been tested *in situ* at the µLaue station of BM32. The experiments used the Synchrotron Straining Device (SSD) with a load resolution of 0.01mN (figure 1). Both, compression and tensile experiments have been performed. Based on the experiments the impact of instrumental constraints and imperfections on the dislocation structure during deformation have been evaluated. Furthermore, the unexpected activation of low-ranked slip systems was proven in a second study [3].

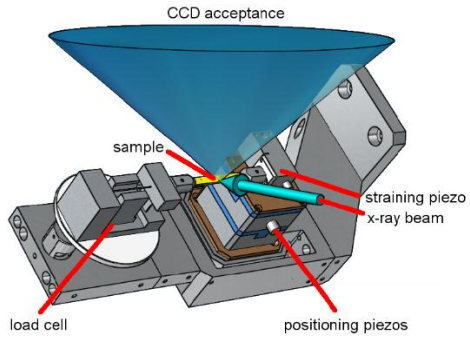

Figure 1 Versatile straining device developed at Univ. Leoben and later at MPI-E Düsseldorf used for in situ mechanical tests on microsized specimens. Various static or cyclic loads can be achieved: tensile, compression, bending and torsion. The setup can fit easily others synchrotron beamline environments and SEM characterization equipments performed in labs.

Micro-bending beams were cyclically loaded in both – positive as well as negative direction to mimic cyclic loading present in real micro-electro-mechanical-systems (MEMS). The Laue diffraction spot thereby showed full reversibility in some cases and continuous damage accumulation in others. Main reason for the two different behaviors is the geometric arrangement of internal interfaces like grain-boundaries which causes a certain dislocation pile-up in the first, and dislocation cross-slip in the second case.

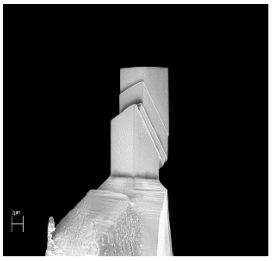

Figure 3 Post mortem Scanning Electron Microscopy (SEM) image of a single crsytalline Cu pillar deformed at BM32 with slip steps steps following a single {111} crystallographic plane.

The interaction mechanisms between dislocation and grain boundary are not well understood at the mesoscale. Cu bi-crystals had been deformed at BM32 and the accumulation of dislocations in both crystals, as well as the change of grain boundary character due to storage of dislocations in the boundary had been measured *in situ*. It was proven that some grain boundary characters allow for slip transfer or act as sink for dislocations, while others are a strong barrier for dislocation motion.

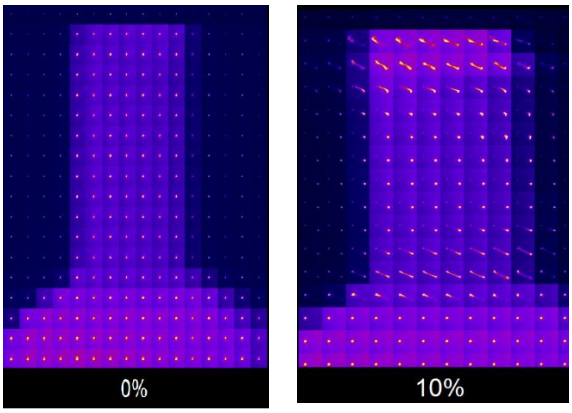

Figure 3: Cu Pillar at initlal state and after 10% deformation under compression performed in situ. Circular spots indicate low GND densities, whereas elongated ones indicate storage of GNDs

[1] Uchic MD, Dimiduk DM, Florando JN, Nix WD. Sample dimensions influence strength and crystal plasticity. Science 2004;305:986.

Publications: [1] C. Kirchlechner, J. Keckes, J.S. Micha, G. Dehm, Advanced Engineering Materials, 13 (2011) 837-844.
[2] C. Kirchlechner, J. Keckes, C. Motz, W. Grosinger, M.W. Kapp, J.S. Micha, O. Ulrich, G. Dehm, Acta Materialia, 59 (2011) 5618-5626.
[3] C. Kirchlechner, P.J. Imrich, W. Grosinger, M.W. Kapp, J. Keckes, J.S. Micha, O. Ulrich, O. Thomas, S. Labat, C. Motz, G. Dehm, Acta Materialia, 60 (2012) 1252-1258

Patent(s)

Contact: kirchlechner@mpie.de

HL 4: Measuring "length" lattice parameters in Laue microdiffraction: the Rainbow method and its application to a chemical-gradient material

O. Robach[a], J.-S. Micha[b], O. Ulrich[a], O. Geaymond[c], O. sicardy[d], J. Haertwig[e], F. Rieutord[a], M. Fonović[f], A. Leineweber[f], E.A. Jägle[g], E.J. Mittemeijer[f,h].

[a]CEA-INAC-SP2M, [b]CEA-INAC-SPrAM, [c]CNRS-Inst. Néel, [d]CEA-LITEN, [e]ESRF, [f]MPI for Intelligent Systems, Stuttgart, [g]MPI für Eisenforschung Düsseldorf, [h]Institute for Materials Science, Stuttgart, Germany

A new method was developed for measuring the energy of a Laue spot while remaining in the white-beam mode. It was first validated on several Ge single crystals with various orientations, then applied to lattice-parameter depth-profiling in a surface-nitrided Ni-5%Ti sample, to correlate depth-variations of the N-concentration and the unit cell volume.

Laue microdiffraction allows the mapping of the crystalline microstructure in polycrystals. A Laue pattern measures the angular coordinates of the q diffraction vectors, but not their length. It therefore provides the deviatoric shape of the unit cell, but not its volume. For a fixed (non-rotating) sample, the only way to obtain the volume is to measure the energy of a Laue spot.

A new variant of Laue microdiffraction was developed for this aim on BM32. The technique consists in inserting a single-crystalline diamond plate in the x-ray beam path. When the energy of a diamond diffraction line coincides with that of a Laue spot, its intensity is attenuated. By scanning the diamond angle, the spot energy profile can then be measured in an "inverted" way, with an energy resolution in the 10^{-4} range. The profile provide the average energy and the energy width of the spot.

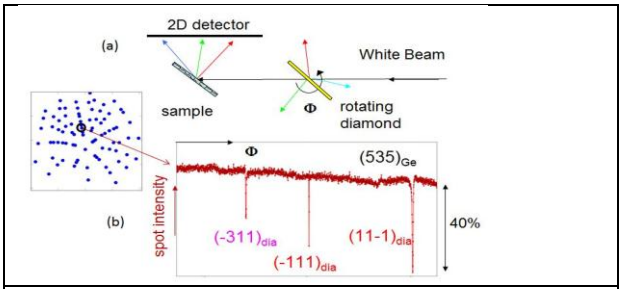

Figure 1 : a) experimental setup for measuring Laue spot energies using a rotating diamond plate. b) intensity of a Ge (535) spot cut by three Bragg lines (-311), (-111) and (11-1) of the diamond during its rotation. Spot energy and crystal orientation-strain are determined at the same time for the same probed sample volume. In practice only a few diamond lines provide large attenuation (>25%). The calibration of the rotating diamond geometry is refined using 50 dips measured on a Ge single crystal over a 2.5 degree angular range.

Nitridation is used industrially for surface hardening. The Ni-few%Ti alloy is used as a model material for nitridation studies, as it accepts a large (few %) concentration of N while retaining a homogeneous austenitic structure. At 5% Ti however the nitrided layer splits into two sublayers with widely different peak positions on the powder diffraction spectra : a strongly expanded (few %) surface N1 phase (6-7 µm thick) and a less-expanded deeper N2 phase (15-20 µm thick) already observed for lower Ti content.

The goal of the Laue microdiffraction study was to obtain a depth profile of the N-induced lattice-expansion, inside a single big grain reaching up to the surface, in a cross section of the nitrided material.

A line scan perpendicular to the layers revealed strong orientation gradients in the nitrided layers, with only 6-10 broad (40-pixels-wide) spots remaining in the N1 layer, while the un-nitrided alloy showed more than 50 sharp (1-2 pixels-wide) spots, i.e. good crystalline quality. The large biaxial strains in the nitride are therefore accompanied by significant bending and torsion of the lattice, i.e. the material is very far from a "perfect epitaxy" model where stress is just a linear function of strain.

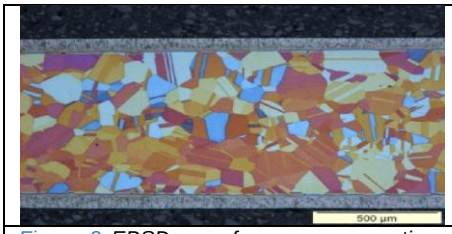

Figure 2 EBSD map from a cross section of polycrystaline nitrided $Ni_{0.95}Ti_{0.05}$ alloy. Profiles of N concentration and strain have been taken along the vertical direction.

The depth profile of the "mean" lattice parameter (the cubic root of the unit cell volume) was measured up to the beginning of the N1 layer. By comparing it to the N-concentration profile the coefficient for Vegard's law could be obtained.

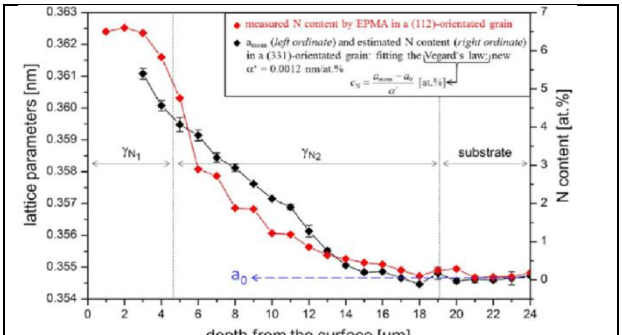

Figure 2 (left ordinate –black curve) Lattice parameter in nitride Ni-5%Ti alloy derived from Laue energy measurements as a function of the depth from the surface. (right ordinate) N concentration deduced from Laue (black) the Vegard's law and from rescaled data from atomic probe microscopy (red). gN1 and gN2 are the two phases evidenced in powder diffraction.

Publications: O. Robach et al, Acta Cryst. **A 69**, 164-170 (2013), M. Fonovic et al, submitted to Metall. Mater. Trans. A (2015)	
Grants:	Collaborations: MPI Stuttgart, ESRF, CEA-LITEN
Patent(s)	Contact: robach@cea.fr

HL 5: Implantation induced strain

F. Rieutord[a], *Frederic Mazen*[c], *Shay Reboh*[c], *J.-S. Micha*[b]
[a]CEA-INAC-SP2M [b]CEA-INAC-SPrAM [c]CEA-LETI

Implantation is a widespread technique to force incorporation of a foreign material into a bulk or layer film, independently of solubility or phase stability issues. Yet, the implantation has many physical effects, the first of which being a strain induced by the incorporation of additional foreign atoms, a first basic effect being a volume change. A detailed characterization of the strain state post implantation can be obtained using X-ray scattering [1], that can be related to simulations or energetics of the system as a function of atom location. The thermal evolution of this strain state upon annealing is important as this is very often a required second-step, both when implantation is used to incorporate dopant atoms, but also when implantation is used to create a weak layer at a given distance from the top entrance surface (as in our application related to the SmartCut™ technology).

Strain versus dose behavior in implanted materials

The SmartCut™ process is based on the implantation of light ions into a substrate to induce a weakened layer at some controlled depth below the surface of a crystal. The characterization of the stress and strain state of this layer is essential to understand the mechanisms that will ultimately lead to fracture. X-ray scattering is an ideal probe to measure strain and compute stress in crystalline materials. For implantation in silicon crystal as of the SmartCut™ technology, we have recorded the scattered intensity along the normal to the surface, close to the 004 Bragg peak. Typical curves are shown Fig.1. The full analysis of this curve gives the strain profile as a function of z.

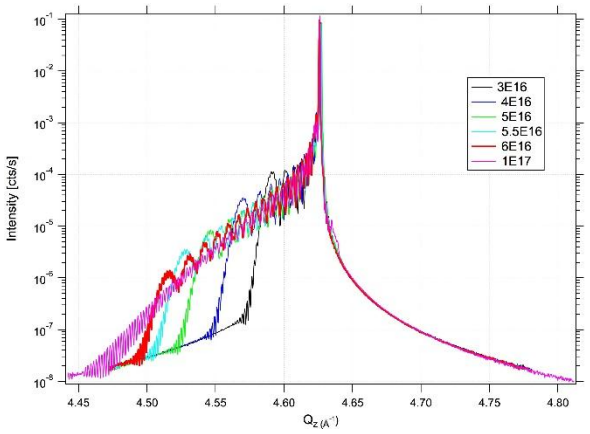

Fig.1 Example of scattering intensity curve around the Si 004 Bragg peak. Two fringe periods are visible related respectively to the width of the implanted layer and to the distance between the implanted layer and the surface. Curves have been taken for different implanted doses (H+).

We have used this technique to measure the strain for various materials (Si, Ge, InP, etc..) and various types of implantation conditions (H, He, temperature, dose, dose rate,..). In silicon, at small implantation doses, the strain profile results were shown to be consistent with ab-initio volume change calculations [1] when considering hydrogen in the so-called Bond-Center (BC) location. This can be also related to IR absorption spectroscopy data.

When investigating the effect of implantation dose, we mentioned previously that we found the same unexpected behavior already observed in many other instances, i.e. an increase of the strain to dose sensitivity (Fig.2). To investigate the reasons for this behavior, we combined the X-ray strain measurements to direct stress measurements using radii of curvature. We could demonstrate that this behavior is due to a change in elastic parameters of the implanted layer [3], which could be quantitatively measured (Fig.3).

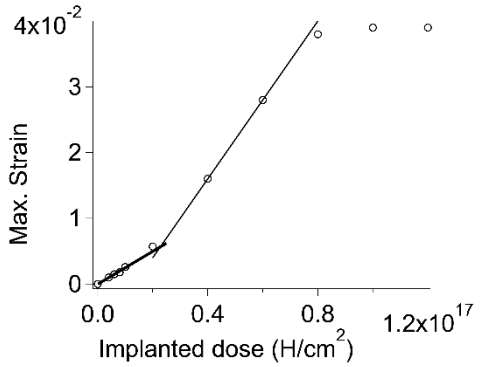

Fig.2 Strain versus implanted dose for hydrogen implanted in silicon. The curve shows a supralinear behavior at doses larger than typically 2 10^{16} H^+/cm^2 while a saturation would rather be expected.

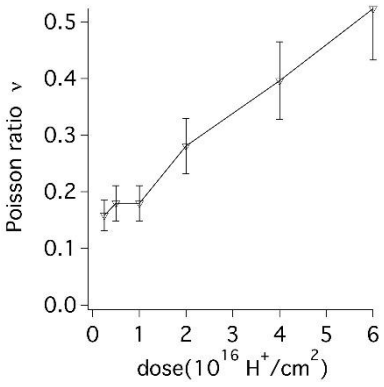

Fig.3. Evolution of the Poisson ratio ν for implanted silicon, as a function of implantation dose, as deduced from stress and strain measurements. The coefficient at low dose is consistent with pristine silicon values while it tends to 0.5 for very high doses, a value expected for incompressible solid with reduced shear resistance.

Grants:	Collaborations: CEA-Cadarache, CEA-Saclay
Patent(s)	Contact: francois.rieutord@cea.fr

HL 6: Wafer bonding

F. Rieutord[a], Damien Massy[a], Samuel Tardif[a], Caroline Rauer[b], Hubert Moriceau[b]

[a] CEA-INAC-SP2M [b] CEA-LETI

Medium to high energy X-rays available at ESRF are well suited for the non-destructive study of buried interfaces as e.g. wafer bonding solid/solid interfaces. Direct bonding is a key technology for assembling materials with several uses in the field of microelectronics. For example it is used in the manufacture of silicon-on-insulator substrates by assembling oxidized silicon wafers in the BSOI, BESOI or SmartCut™ technologies [1]. In addition to being industrially important, direct wafer bonding interfaces are also good test vehicles for studying solid-solid contact at the nanoscale. We show below what is the influence of the lateral asperity length scale on the contact closure.

Understanding the contact between solid surfaces is a long standing problem which has a strong impact on the physics of many processes such as adhesion, friction, lubrication and wear. Experimentally, the investigation of solid/solid interfaces remains challenging today, due to the lack of experimental techniques able to provide sub-nanometer scale information on interfaces buried between millimeters of materials. The general situation when contacting two rough solid surfaces is the presence of a gap of reduced density between the solids, due to the incomplete match of the two asperity systems. The mechanical behavior of contacts under load is generally modeled by the compression of these asperity systems. The macroscopic contact physics (e.g. Amontons/Coulomb laws for friction) can be derived from the mechanical behavior of individual asperities and their statistical distribution. When using flat solids with polished surfaces, roughness and gap widths are generally in the nanometer range. In this range, in addition to external loads, the attractive forces between solid bodies (e.g. van der Waals) contribute to closing the interface gap.

We have shown using interfacial high energy X-ray synchrotron reflectivity that the essential features of the residual gap between contacting surfaces can be measured. The presence of this nano-gap is general to the contact of solids. When one considers the sealing of standard silicon oxide interfaces, the hydrophilicity of the surfaces plays a large role. We have shown that in wafer bonding and upon temperature, wafer bonding essentially proceeds via a ziplock mechanism, where the few contact points present at low temperature progressively spread to the whole interface. The adsorbed water management plays a key role in this process [2]. Water fills the interface gap contributing to increase room temperature bonding energy. During the annealing step however, its effect may be deleterious as excess water may prevent full surface contacting or may react with silicon to produce trapped hydrogen gas.

Collapse instability in hydrophobic silicon bonding [3]

When bonding hydrophobic silicon (i.e. silicon surfaces that have been de-oxidized and hydrogen-passivated) no significant amount of water is present and the interfacial gap between asperities is essentially empty. This is clearly visible on the electron density profile where the mid-interface electron density is close to zero, in agreement with the presence in this situation of a small number of contact points.

This general situation of a large fraction of empty gap between few contacting asperities can however be removed in some peculiar situations where attractive forces take over repulsive contributions, depending on both height and wavelength of asperity distributions (roughness). In this case, the two surfaces “collapse” on one another resulting in full contact.

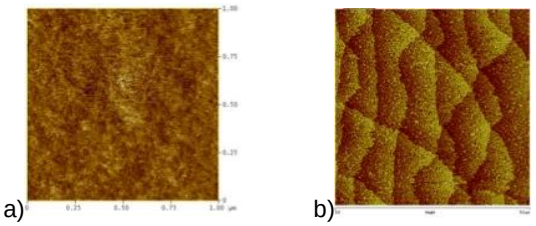

Fig.1. Two AFM images of hydrophobic (i.e. hydrogen passivated) silicon surfaces with different wavelength for the roughness obtained through different surface preparations. This lateral wavelength is a key parameter for interface sealing. The vertical roughness amplitudes are similar (0.2nm rms) in both cases.

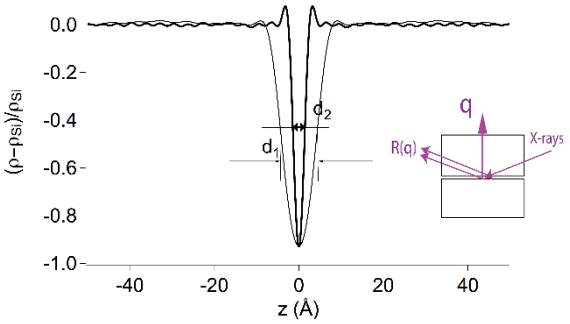

Fig.2: Interfacial reflection geometry and interface electron density profiles as measured using high energy X-ray reflectivity. Bonding were obtained using 1a and 1b surface preparations. Gap widths d_1 and d_2 correspond to asperity driven (a) and full surface contact (b), respectively.

A criterion for this instability has been established in the standard case of van der Waals attractive forces and elastic asperity compression repulsive forces (Hertz model): $L = K/A\ \sigma^4$ where L and σ are lateral and vertical amplitudes of roughness, K is a reduced elastic parameter and A is the Hamaker constant. It has been confirmed experimentally (Fig.1 and 2) in the case of silicon direct bonding, using high-energy X-ray synchrotron reflectivity and adhesion energy measurements. The possibility to achieve fully closed interfaces at room temperature opens interesting perspectives to build stronger assemblies with smaller thermal budget

Publications: [1] Moriceau, H., Fournel, F. and F. Rieutord. in *Silicon-on-Insulator (SOI) Technology Manufacture and Applications*, ed. by Woodhead Publishing Cambridge (2014) [2] Ventosa, C. et al. , Electronic and Solid State Letters 12 (2009): H373. [3] F.Rieutord et al EPL 107 (2014) 34003.

Grants: CEA-SOITEC partnership

Collaborations: CEA-LETI SOITEC

Patent(s)

Contact: francois.rieutord@cea.fr

HL 7: Osmotic pressure effect on supported membranes bilayer

T. Charitat[a], A. hemmerle[a], G. Fragneto[b], J. Daillant[c]
[a]Institut Charles Sadron Strasbourg, [b]Institut Laue Langevin Grenoble, [b]CEA-Saclay & SOLEIL

Understanding interactions between membranes requires measurements on well-controlled systems close to natural conditions, in which fluctuations play an important role. By grazing incidence X-ray scattering experiments, the interaction potential between two lipid bilayers, one adsorbed on a solid surface and the other floating close by has been investigated. In this highly hydrated model system interactions are two orders of magnitude softer than those in multilayer stacks. Our data are consistent with the Poisson–Boltzmann theory, in the regime where repulsion is dominated by the entropy of counter ions. Due to very weak entropic repulsion potentials, it was allowed to discriminate between the various models proposed in the literature. The interaction potential between supported bilayers can be tuned at will by applying osmotic pressure, providing a way to manipulate these model membranes, thus considerably enlarging the range of biological or physical problems that can be addressed.

Interactions of lipid membranes are not only crucial for membrane fusion and trafficking, endo- and exocytosis [1], they are also fascinating from the fundamental and physical aspects. Membranes indeed exhibit extremely complex interactions with their environment where molecular scale enthalpic (hydration, van der Waals, electrostatic...[1,2]) and fluctuation related entropic contributions are inextricably involved. Determining the interaction potential between bilayers is challenging and first studies were performed on multilamellar stack

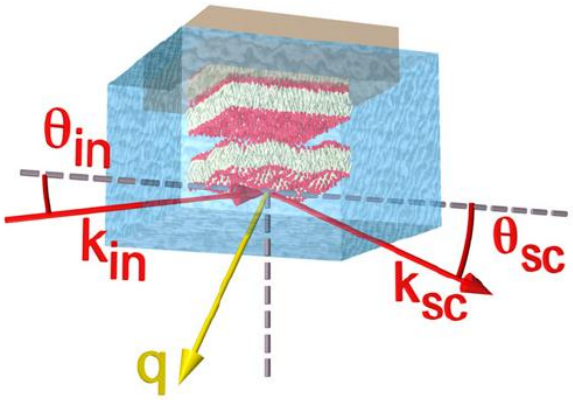

Figure. 1. Schematic view of the experimental setup for specular and off specular reflectivity. The grazing and scattered wavevectors (respectively angles of incidence) are $\mathbf{k}_{in}$ *and* $\mathbf{k}_{sc}$ *(respectively* θ_{in} *and* θ_{sc}*); q is the wavevector transfer.*

where static defects can dramatically affect bilayer interactions. Combining analysis of specular and off-specular reflectivity have led to a refined characterization of membrane elastic parameters and interaction potential on Double supported Bilayer (DB) [3].

X-ray scattering experiments were carried out to measure the elastic parameters of a supported bilayer for water thicknesses comparable to those one can find in multilamellar systems. An osmotic pressure with an hydrosoluble polymer (PVP), to double supported bilayers of DSPC in both gel and fluid phases was applied in situ (Figure 1(a)). To investigate the contribution of the electrostatic interaction due to the dissociation charges of membranes various concentrations of salt were added to the systems, and resulting curvature of the interaction potential was measured by a coupled analysis of specular and off-specular reflectivities (fig. 2).

Adding polymer (PVP) in bulk solution clearly shows that we can apply an osmotic pressure to a supported DB. Results compare well to those obtained in multilamellar systems where the interaction potential is

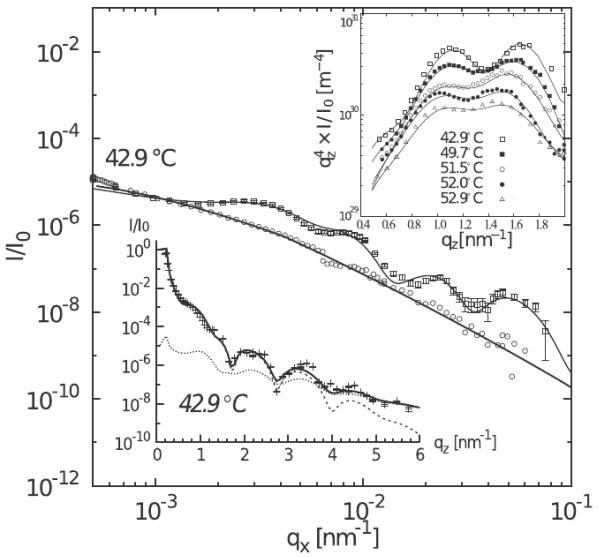

Figure 2. Off-specular reflectivity from Si substrate and an OTS bilayer at T=42.9 °C (open squares) as a function of in-plane q component, qx. (Upper inset) Off-specular reflectivity as a function of normal component, qz for several T. (Lower inset) Specular experimental and modelled reflectivities (see [1])

dominated by the hydration term. Analysis of experiments with added salt requires to take into account the electrostatic potential described by the Debye-Hückel model (typically with charateristic length λ_D=0.3 nm) in addition to soft-confinement one. Thanks to a fine sensitivity to very small amount of charge surface, electrostatic interactions between bilayers for various Debye lengths have been obtained and quantified [4].

[1] Sackmann, E. Physical Basis of Self-Organization and Function of Membranes: Physics of Vesicles, Handbook of Biological Physics, Elsevier Science B.V., 213 (1995).
[2] Lipowsky, R., Handbook of Biological Physics, Elsevier Science B.V., 521 (1995).
*[3] L. Malaquin, T. Charitat, J. Daillant, European Physical Journal E, **31**, 285 (2010)*
[4] A. Memmerle, L. malaquin, T. charitat, S. Lecuyer, G. Fragneto, J. Daillant, Proc ; Nat. Acad. Sc. USA, 109 19938 (2012).

Publications *A. Memmerle, L. malaquin, T. charitat, S. Lecuyer, G. Fragneto, J. Daillant, Proc ; Nat. Acad. Sc. USA, 109 19938 (2012). L. Malaquin, T. Charitat, J. Daillant, European Physical Journal E, **31**, 285 (2010)*	
Patent(s)	Contact: charitat@ics.u-strasbg.fr

HL 8: Growth and structure of ultrathin CoO/PtFe bilayers showing robust perpendicular exchange coupling.

M. De Santis[a], A. D. Lamirand[a], H. C. N. Tolentino[a], M. M. Soares[a], A. Y. Ramos[a], S Grenier[a],J. C. Cezar[b], A. de Siervo[c], and M. Jamet[d].
[a]Institut Néel, CNRS and UJF, BP166, 38042 Grenoble, France; [b]Laboratório Nacional de Luz Síncrotron-LNLS, CP6192,13083-970 Campinas, Brazil ; [c]Instituto de Física Gleb Wataghin, Universida de Estadual de Campinas-UNICAMP, 13083-970 Campinas, Brazil ; [d]Institut Nanosciences et Cryogenie-INAC, CEA, 38042 Grenoble, France.

The structure of epitaxial CoO/PtFe/Pt(001) layers was studied *in-situ* by GIXRD. PtFe grows (001) oriented, while the oxide forms a distorted CoO(111) layer due to the epitaxial strain. The magnetic properties of the systems were studied *ex-situ* by XMCD and XMLD at LNLS (Brazil). X-ray absorption spectroscopy provided a full description of the spin orientations in the CoO/PtFe double layer. The exchange bias shift is preserved up to the bulk Néel antiferromagnetic ordering temperature of T_N = 293 K, a unique example that is likely related to the original strain-induced distortion and strengthened interaction between the two well-ordered spin layers.

There are several issues with building a reliable, efficient exchange-bias magnetic bilayer with a thickness of only a few nanometers. Essentially, they rely on the growth of an antiferromagnetic ultrathin layer (AFM) on a ferromagnetic (FM) ultrathin layer while enhancing, or maintaining as much as possible, the magnetic properties of the respective bulk materials. The AFM is aimed at inducing the magnetic exchange field necessary to pin the FM spins toward one preferred direction, the so-called “exchange bias effect” widely used in spintronics devices like spin valves. Ideally, the growth should be epitaxial so as to use the strain between the two layers as a parameter for tuning the magnetic properties. The FM/AFM exchange coupling relies on a variety of microscopic and atomic parameters, such as crystallographic order, surface morphology, strain effects, spin orientation, and competing anisotropies. Usually it establishs at a temperature quite lower than T_N.

Using in situ x-ray surface scattering in the growth chamber of BM32/INS, we have followed these structural parameters while growing atomic layer by atomic layer a promising couple: a 1.2 nm thick FM FePt alloy, followed by a 3 nm thick AFM CoO layer, on a Pt substrate. FePt was chosen for its perpendicular magnetic anisotropy (PMA), PMA is promising for low power consumption and high-performance memories. PMA means that the spins of the Fe atoms are all aligned along one intrinsic preferred direction, which is perpendicular to the surface of the layer. Mixing Pt and Fe takes advantages of the crystal fields and the spin-orbit coupling effects that results in the PMA. The PtFe layer is terminated by a Pt layer to reduce the oxidation of the Fe atoms as one grows the CoO layer on top of it. Temperature and time of deposition are the controlled key parameters for the growth while quality and structural features were monitored with the x-rays. A detailed crystallographic characterization determined the lattice parameters, the thicknesses and proved the epitaxial growth. We also found a specific distortion induced on the AFM layer by the strain, interestingly, it is a distortion that resembles the one existing in the bulk material, where it is related to the AFM ordering.

The magnetic properties were then determined ex situ at the PGM beam line at the Laboratório Nacional de Luz Sincrotron (LNLS, Brazil) using x-ray absorption spectroscopy with polarized x-rays. The angular dependence of the absorption of linearly polarized x-rays showed us that the CoO AFM spins are all aligned in the plane of the layer. With x-ray circular magnetic dichroims (XMCD), we measured the Fe perpendicular magnetization against an applied magnetic field as well as a small contribution from perpendicular non-compensated Co spins. By monitoring the direction and the amplitude of the magnetic signals against field and temperature, we found that the 1.2 nm thick FM layer follows the magnetic field with an exchange-bias shift in one direction, a clear sign that the Fe spins are influenced by the Co spins. We then raised the temperature to the bulk T_N (293 K) where the CoO layer loses its AFM ordering to find that our layer sustains an EB shift up to its bulk T_N even down to a thickness near 3 nm, demonstrating a robust perpendicular exchange coupling. This is a unique example where the EB effect remains effective up to the bulk T_N for an ultrathin CoO layer, a result that can be understood by the structural distortion that originates from the strain. Our study illustrates the power of in situ structural characterization for growth control, and the understanding of the magnetic properties under the light of these crystallographic information

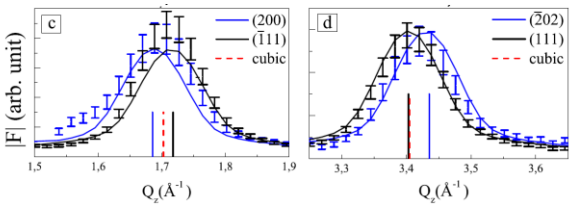

Fig. 1 X-ray scattering through CoO rods: Scattered marks correspond to experimental data and plain lines are obtained by the structural refinement procedure. Vertical lines indicate the two peaks in monoclinic (plain blue and black) and in cubic (dashed red) cells.

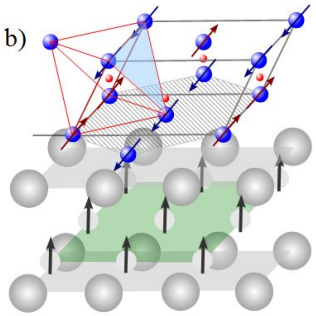

Fig. 2. Scheme of the interface between FePt (small Fe and large Pt grey spheres) and CoO (blue Co and red O spheres). The Fe spins are perpendicular to the surface, while the AFM spins lie mainly in the surface plane.

Publications: 1) A D Lamirand, M M Soares, M De Santis, A Y Ramos, S Grenier and H C N Tolentino: Strain driven monoclinic distortion of ultrathin CoO films in the exchange-coupled CoO/FePt/Pt(0 0 1) system, J. Phys.: Condens. Matter **27** 085001 (2015). 2) A. D. Lamirand, M. M. Soares, A. Y. Ramos, H. C. N. Tolentino, M. De Santis, J. C. Cezar, A. de Siervo, and M. Jamet, Robust perpendicular exchange coupling in an ultrathin CoO/PtFe double layer: Strain and spin orientation. Phys. Rev. B, Rap. Com., **88**, 140401 (2013)

HL 9: Effect of CoO/Ni orthogonal exchange coupling on perpendicular anisotropy of Ni films on Pd(001).

M. Przybylski[1,2], P. Kuswik[1,3], L. Gastelois[1,4], H. Tolentino[5], M. De Santis[5], A. Lamirand[5], A. Y. Ramos[5], M. Soares[6].
[1]Max-Planck-Institut f¨ur Mikrostrukturphysik, 06120 Halle, Germany, [2]AGH University of Science and Technology, 30-059 Krakow, Poland, [3]Institute of Molecular Physics, Polish Academy of Sciences, 60-179 Poznan, Poland, [4]Centro de Desenvolvimento da Tecnologia Nuclear, 31270-901 Belo Horizonte, MG, Brazil, [5]CNRS, Institut Neel, 38042 Grenoble, France, [6]European Synchrotron Radiation Facility, 38043 Grenoble, France.

The CoO/Ni/Pd(001) system was grown on INS/BM32 and its structure was studied *in-situ* by GIXRD. This interface allows to study the effect of orthogonal exchange coupling on the perpendicular anisotropy of Ni films. *Ex-situ* measurements of its magnetic properties have shown that the thickness range in which Ni films show a perpendicular easy magnetization axis is extended by growing CoO on top of them, however, only at temperatures below T_N of CoO. The perpendicular orientation of Ni spins and the in-plane orientation of CoO spins are confirmed by the magneto-optic Kerr effect/x-ray magnetic circular dichroism and x-ray magnetic linear dichroism, respectively. Additionally, a perpendicular exchange bias shows up at low temperature.

Perpendicular magnetization is strongly required in particular for giant magnetoresistance (GMR) and/or tunnelling magnetoresistance (TMR) based devices for magnetic recording and magnetic random access memory (MRAM). Magnetization of one of the ferromagnetic (FM) layers in such devices usually is pinned to the antiferromagnetic (AFM) underlayer, whereas the second one can be freely magnetized in two opposite directions (resulting in different resistivity, depending on whether the magnetizations of both FM layers are oriented parallel or antiparallel). The pinning is realized by employing the exchange bias effect, which is due to the coupling between FM and AFM spins at the interfaces. In this experiment FM/AFM coupling was exploited, not only to pin the magnetization but also to enhance perpendicular anisotropy of the FM layer. The exchange bias effect in FM/AFM interfaces has attracted much interest for decades. However, the microscopic mechanism responsible for this phenomenon has not yet been fully understood. The reason is that it is difficult to detect directly (and locally) the AFM spin configuration. The existing models explain the exchange bias effect for systems with an uncompensated AFM surface and with collinear FM/AFM exchange coupling at the interface. However, theoretical calculations for compensated interfaces show that the AFM and FM spins may be coupled perpendicularly and that they generate an effective uniaxial anisotropy. An in plane spin reorientation transition, driven by perpendicular coupling, has been theoretically predicted for temperatures close to the Néel temperature of the AFM layer and has been observed experimentally, for instance for Fe/NiO bilayers grown on Ag(001)-stepped surface. Here our goal was to verify whether perpendicular FM/AFM coupling is possible in a plane perpendicular to the sample plane, i.e., whether the anisotropy axis of the uniaxial coupling-driven anisotropy can be oriented perpendicular to the sample plane. This could result in a perpendicular easy magnetization axis for FM films that otherwise, without such a coupling, would be magnetized in the sample plane or in an increase of thickness up to which perpendicular magnetization is sustained in FM films with initial perpendicular easy axis.

For this purpose we have elaborated and studied *in-situ* the structure of a FM/AFM interface using the INS/BM32 experimental set-up. A 23 ML thick Ni film was grown on Pd(001) substrate. The layer exhibits a (001) epitaxy with a slight tetragonal distortion (c/a=0.97). Such thickness is well above the thickness at which magnetization rotates from perpendicular towards in-plane orientation at room temperature (SRT). On top of it, 3ML of CoO were grown showing (001) crystallographic orientation and a slight tetragonal distortion. The lattice constant values a=418 pm and c=431 pm were obtained, resulting in a c/a of 1.03. This result is quite important because it is known that for CoO(001) a c/a>1 results in a cobalt spin orientation in the surface plain. Surface X-ray diffraction analysis showed a negligible Ni oxidation, which does not extend beyond the first monolayer at the interface. No other structural modifications of the Ni film were observed, and in particular no changes in the tetragonal distortion. Magnetic properties were probed ex-situ at Halle by magneto-optical Kerr effect measurements. The film exhibits in-plane magnetization at room temperature. However, the easy axis reorient perpendicular to the surface below 250 K. Such a reorientation is not observed for Ni films of the same thickness but not covered with CoO. The conclusion is that below the Néel temperature the exchange coupling, which has to be in a spin-flop configuration, is responsible for the spin reorientation transition. The ability to manipulate the SRT trough the coupling with an AFM layer has an evident interest in spintronic.

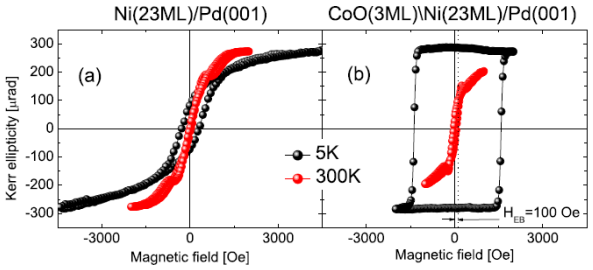

Fig. 1 Polar hysteresis loops at 5 K and at RT for 23 ML of Ni on Pd(001): (a) before and (b) after covering with 3 ML of CoO(001). The rectangular loop and increased Kerr ellipticity in remanence correspond to the perpendicular anisotropy of Ni at 5 K after covering with CoO, whereas the large H_c and the measurable H_{EB} refer to the exchange coupling between AFM CoO and FM Ni.

Publications: P. Kuswik, P. L. Gastelois, M. M. Soares, H. C. N. Tolentino, M. De Santis, A. Y. Ramos, A. D. Lamirand, M. Przybylski, and J. Kirschner, Effect of CoO/Ni orthogonal exchange coupling on perpendicular anisotropy of Ni films on Pd(001), Phys. Rev. B 91, 134413 (2015).

HL10 Kinetics of dewetting of Germanium on Silicon dioxide

Frédéric Leroy, Thibault Passanante, Fabien Cheynis, Pierre Müller
CINaM-CNRS, UMR 7325, Campus de Luminy, Marseille, France

When metastable thin films are annealed at sufficiently high temperature, they may agglomerate to form an assembly of 3D nanostructures. Several *ex situ* analysis of the morphology of dewetted Si/SiO_2 (Silicon On Insulator, SOI) and Ge/SiO_2 (Germanium On Insulator, GeOI) thin films have been performed. However there is a lack of *in situ* study and the complex kinetic evolution of the dewetted area is not known in particular for Ge/SiO_2. Our main goal was to measure by GISAXS, *in situ* and in real time the dynamics of dewetting of Ge/SiO_2 at different temperatures and film thicknesses.

All samples have been obtained from (001) GeOI wafers, fabricated by the SmartCut™ process at CEA-LETI. The initial thickness of the Ge film is about 40 nm. To control the film thickness we have performed ion bombardment at RT. The film thickness could be monitored *in situ* by measuring the periodicity of the Pendelossung fringes of the (02L) truncation rod. Typical thicknesses from 6 nm to 40 nm have been achieved. After ion bombardment, the sample is annealed at 600°C during 1 hour to heal the defects and reach a perfect crystalline state as controlled by the width of the Ge diffraction peak. The evolution of the morphology of the Ge film during dewetting has been studied *in situ* by GISAXS. A typical sequence of 3 GISAXS patterns (X-ray incident beam along [110]) is reported in Fig 1.

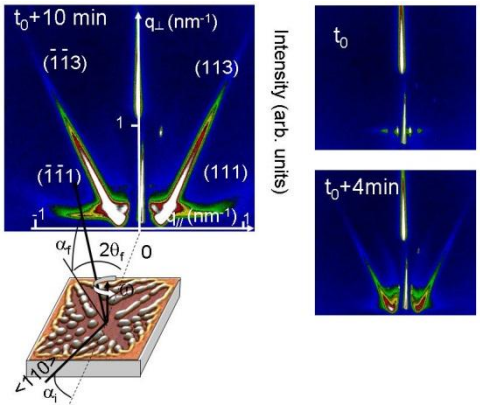

Fig.1 Left: GISAXS principle and experimental patterns from the dewetting of a 32 nm thick Ge/SiO_2 thin film at 870°C. Right (top): Initial GISAXS pattern at t_0, t_0+4min (right bottom) and t_0+10min (left, complete dewetting). We clearly observe the diffuse scattering rods arising from (113) and (111) facets. The signal is rapidly increasing during the dewetting process.

Before dewetting the diffuse scattering pattern is characteristic of a flat surface. Then the dewetting process gives birth to scattering rods at precise angles with respect to the normal to the surface. This indicates that the germanium film agglomerates into oriented and faceted Ge nanostructures. A complete analysis of several GISAXS patterns obtained for various azimuth shows that the main facets are (113), (111), (15 3 23) and (311). All these facets belong to the Ge equilibrium shape. We know from LEEM experiments that, as for Si/SiO_2, the Ge dewetting mechanism proceeds *via* void nucleation then growth with shedding of 3D Ge nanostructures that keep constant size and shape during dewetting. Thus the diffuse scattering rods intensity arising from a facet is proportional to the number of Ge nanostructures at the surface. Therefore the GISAXS intensity versus time allows us obtaining the evolution of the fraction of the dewetted area.
Figure 2 shows the diffuse scattering intensity coming from the (113) facets versus dewetting time. The normalized intensity evolution has been obtained for several Ge thicknesses.

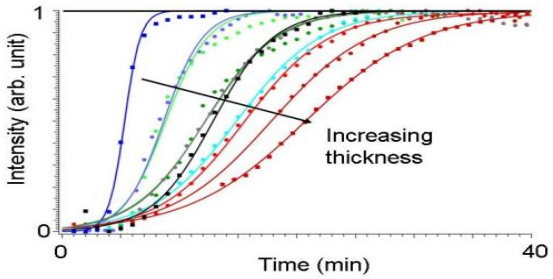

Fig. 2: GISAXS normalized intensity extracted from the diffuse scattering intensity arising from (113) facets. The intensity increases as function of time as dewetting proceeds. The S shape of the intensity profile gives access to the dewetting kinetics for different film thicknesses (6 nm – 41 nm).

Since the dewetting proceeds *via* simultaneous nucleation of many dewetted zones, the total dewetted area increases first quadratically (constant dewetting fronts velocity). Then, at late stages, the total dewetted area increases more slowly due to the coalescence of neighboured dewetting areas until complete dewetting and saturation of the GISAXS intensity. All intensity curves have thus a *S* shape, which was analysed analytically by describing the fractional dewetted area within the framework of the so-called Kolmogorov-Johnson-Mehl-Avrami model (KJMA model).

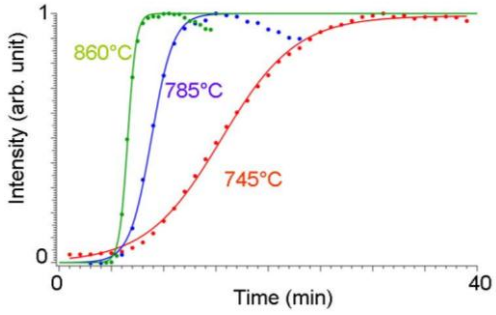

Fig.3 Graph of the evolution of the normalized GISAXS intensity of (113) facets. The normalized intensity is equal to the dewetted area fraction. Three different temperatures are plotted (745°C, 785°C and 860°C).

Figure 3 shows the GISAXS intensity arising from (113) facets versus time recorded at three different temperatures. For the highest temperatures the stationary state is followed by a weak intensity decrease that originates from a slow shape evolution towards equilibrium of the formed nanostructures after dewetting that does not occur at lower temperatures. The intensity curves have been fitted assuming a simultaneous nucleation of the dewetting zones. From this analysis we can estimate, by an Arrhenius plot, the activation energy of the dewetting process: 1.9 eV.

Publications: *Agglomeration dynamics of germanium islands on a silicon oxide substrate: A grazing incidence small-angle x-ray scattering study* F. Cheynis, F. Leroy, T. Passanante *et al.* Appl. Phys. Lett. **102** (16), 161603 (2013)

Grants:

Collaborations:

Patent(s)

Contact: : leroy@cinam.univ-mrs.fr

HL 11 In situ monitoring of strain relaxation during the deposition of the shell in GaN/AlxGa1-xN core-shell nanowires grown by PAMBE

K. Hestroffer, H. Renevier, C. Leclere, B. Daudin
CEA Grenoble, Institut Nanosciences et Cryogénie, SP2M/NRS

Using the INS instrument of the beamline IF, our first objective was to understand the process of nucleation of GaN nanowires grown by Plasma Assisted Molecular Beam Epitaxy. The questions we aimed at answering were related to the very first stages of the GaN nanowires growth. What happens on the Si surface when exposed to Ga and N simultaneously? When exposed to N only? When exposed to Ga only? What conditions make the start of nucleation possible? How is it related to the Ga flux involved?
Our second aim was to monitor *in situ* the evolution of strains involved when depositing an AlN shell around these GaN nanowires.

Nucleation

Although it wasn't included in the proposal we submitted, this part of the work we performed was the most successful one. As a matter of fact, we discovered that when exposed to the slightness beam of active nitrogen, the Silicon surface is nitridated. This nitridation consists in the formation of a crystalline structure detectable by its corresponding peak in the reciprocal space (Fig. 1). Interestingly, the intensity of such peak increases and very quickly (less than 1 minute after the start of the nitridation process) saturates. Then, when further exposed to N (up to 10 minutes), the intensity of the peak remains constant. Such a surface was afterwards simultaneously exposed to Ga and N. We noticed that a *sine qua non* condition for the GaN to start growing (i. e. for the peak related to crystalline GaN to appear) is the decrease of the intensity of the peak related to nitridated Silicon (Fig.2

This decrease was first understood as the destruction of the crystalline layer but later on, rather interpreted as an amorphisation of the layer. Interestingly, no matter how important the Ga flux is, the SiN peak always takes more or less the same time to disappear. An other interesting result is the fact that even when attempting to protect the silicon surface by leaving it under a constant Ga flux prior to the turning on the plasma cell, the nitridation happens anyway.

On the other hand, when playing with AlN, the behaviour is totally different. AlN is often used as a buffer layer to improve the nanowires orientation. It is usually grown by alternatively supplying Al and N. In this case, it was interesting to observe that although the surface is covered with aluminium, the SiN related peak appears and almost instantly its intensity fades. Once the thin AlN buffer was grown (corresponding to about 40s of deposited Aluminium), it was also observed that the GaN nanowires start growing much faster than on bare Silicon (about 5 minutes on AlN VS 2h00 on bare Silicon in this case)

Strains in core-shell nanowires

The requirements for a successful measurement of non –biased strains in core-shell nanowires are the following: straitness of the GaN cores, homogeneity of the shell thickness from nanowire to nanowires and symmetry of the shell on a given nanowire. Such features were supposed to be obtained by performing Selective Area Growth, which is being able to properly control the density of nanowires and therefore better managing their final morphology. However, prior to the experiment, it was not possible to perform such growth and therefore to determine the appropriate growth conditions. As a consequence, we decided to attempt growing a core-shell sample on bare Silicon. It can be seen from the pictures below (Fig. 3) that the nanowires are too dense and the shell totally inhomogeneous along the nanowire length. The measured strains are therefore difficult to interpret.

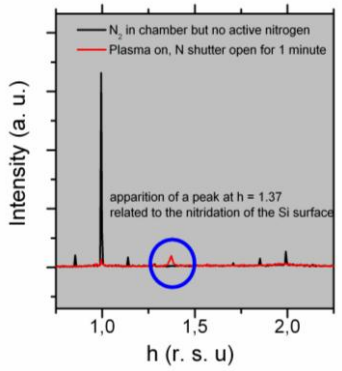

Fig. 1. h-scan around $(1\ 0\ 0)_{Si}^{hex}$ *before (black line) and after (red line) turning on the plasma. Without the presence of active nitrogen, one can see the typical Si 7x7 reconstruction. With the introduction of active nitrogen, the 7x7 has disappeared and a peak at h = 1.37 has shown up. This peak is related to the formation of crystalline* Si_xN

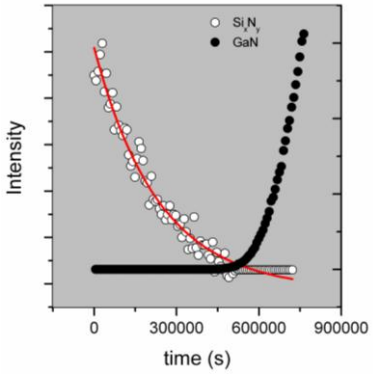

Fig. 2. Evolution in time of the peak related to crystalline Si_xN_y $(1.37\ 0\ 0)_{Si}^{hex}$ *and of the peak related to GaN* $(3.62\ 0\ 0)_{Si}^{hex}$ *while depositing Ga and active N.*
Fig. 3. Scaning Electron Micrographs of the GaN/AlN core

shell nanowires grown during the experiment

Publications: *In situ study of self-assembled GaN nanowires nucleation on Si(111) by plasma-assisted molecular beam epitaxy* K. Hestroffer, C. Leclere, V. Cantelli, C. Bougerol, H. Renevier and B. Daudin, Appl. Phys. Lett. **100** (21) 212107 (2012)	
Grants:	Collaborations:
Patent(s)	Contact: : bruno.daudin@cea.fr

HL 12 *In situ* X-ray scattering investigations of the UHV-CVD growth of Si, Ge and SiGe core-shell nanowires – growth, composition, strain & bending

T. Zhou[a], O. Geaymond[b], O. Ulrich[a] and G. Renaud[a]
[a&b]Université Grenoble Alpes (UGA)
[a]CEA-Grenoble, Institut Nanosciences et Cryogénie, SP2M/NRS
[b]CNRS-Institut Néel

Physical (MBE) and chemical (CVD) evaporations are combined in the INS chamber to grow Ge and Si nanowires (NWs) by the Vapor-Liquid-Solid (VLS) process, in which a supersaturated drop of liquid metal-semi-conductor eutectic leads to the catalytic precipitation of the semiconductor. We discovered a large supercooling effect for liquid AuSi on the Si(111) surface, when it is (6x6) reconstructed thanks to gold atoms that form pentagons, which stabilize the liquid by enhancing the amount of icosahedral atomic order. State of the art pure Ge, Si as well as core-shell and axial GeSi heterostructures are grown in the setup and analyzed *in situ* with X-rays scattering at small and wide angles during their growth. The incubation time between the exposure to gas and the onset of NW precipitation has been studied as a function of temperature, flux and size, and qualitatively interpreted. The strain and intermixing were analyzed in core-shell nanowires grown under different conditions by use of GI-MAD. More recently, oriented MBE deposition of Ge and Au on one side of Si NWs was used to bend them *in situ*, due to surface and interfacial (misfit) stress. The bending profile was recovered by diffraction for different deposits. A comparison with an *ad hoc* mechanical theory allows deducing the surface and interface stress during growth.

In situ studies of Si and Ge nanowire growth

The observations performed combining GISAXS and GIXD during the growth of Si NWs are summarized in Fig. 1.

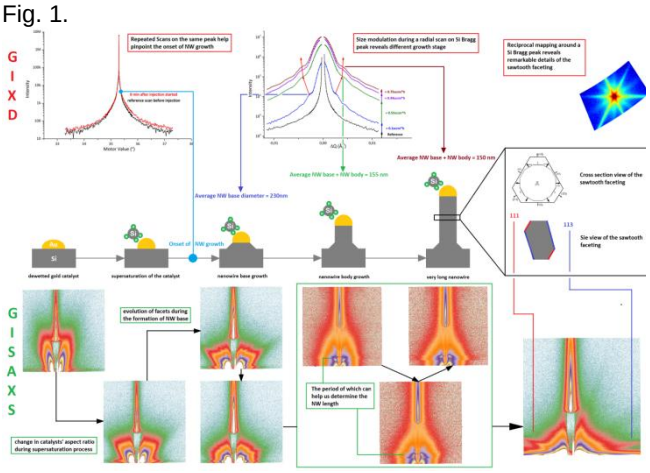

Figure 1 : GIXD and GISAXS measurements of the VLS growth of Si NWs on Si(111) substrate by UHV-CVD.

With GISAXS, we first observed a sudden change in the aspect ratio (contact angle) of the liquid catalyst as soon as the precursor gas was introduced into the growth chamber. This is related to the increase of Si percentage in the liquid alloy during the supersaturation process, which might be partially or solely responsible for the so called incubation time which manifests itself as a characteristic delay between the beginning of the injection and the onset of the NW growth. In our case, the incubation time, which varies from tens of seconds to several minutes depending on the growth condition, was measured by conducting the same diffraction scan on a Si Bragg peak or by a time scan at the foot of a peak.

Under appropriate growth conditions, the size distribution of the NWs could be narrow enough to give rise to an observable NW size modulation during GIXD measurements. The result is a gradually decreasing value in direct space from 230nm to 150nm, which can be explained by the initial growth of the larger NW base and the subsequent growth of the smaller NW body.

Once the NW growth begins, the NW length can be tracked by analysing modulations in GISAXS measurements. Finally, the well-known sawtooth faceting was observed by both GISAXS and GIXD.

Much as expected, changing the flow rate seems to affect only the growth speed while changing the growth temperature also affects the mean NW size as a result of increasing level of catalyst agglomeration at higher temperatures. Similar results were obtained during the growth of Ge NWs.

Growth of GeSi heterostructured NWs

We next moved to growing heterostructure nanowires (Fig. 2).

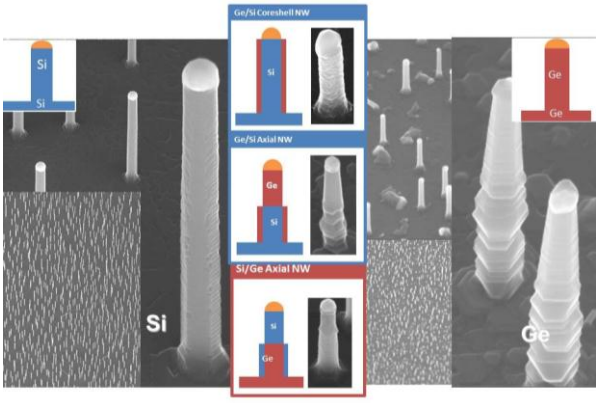

Figure 2 : SEM images of typical Si, Ge and SiGe heterostructured NWs grown in the INS setup.

Our primary focus was the Ge/Si coreshell NW due to its high yield, homogeneity, its possession of larger strain compared to axial heterostructures and feasibility of carrying out *in situ* experiments. The objective was to measure the strain relaxation during growth of the Ge shell deposited on the sidewall of the Si NWs. However, due to our large beam size (300µm*400µm), we also expect signals from other objects such as the Si/Ge islands formed on the sample surface as illustrated in Figure 3 (top left).

Our way to filter the unwanted signals involves the growth of a reference sample (Figure 3 top right) which has everything but the coreshell NWs. We did it by depositing only 1ML of gold, enough to form the wetting layer, but insufficient for the formation of AuSi catalyst islands which are mandatory for the growth of NWs. Immediately after the first injection, we observe on the NW sample, a signal having an atomic spacing in between that of bulk Si and bulk Ge (Figure 3 bottom left) whereas on the reference sample nothing was observed. This indicates that the signal must come from the NW sidewall and hence is the object what we intend to study. Further study reveals that these SiGe alloy islands on the NW sidewall have an average atomic spacing that is 3.1% larger than that of bulk Si, and has an average size of around 37 nm. To understand the composition of the mixed signal, we performed GI-MAD measurements. The result as well as our interpretation are shown in Fig. 4. The calculated Ge composition Ge% sits right on the green dashed line (Figure 4 left)

which corresponds to a fully relaxed alloy while its value suggests a gradually increasing Ge% from 40% at the Ge/Si interface to 100% at the NW sidewall surface (**Erreur ! Source du renvoi introuvable.** 4 right).

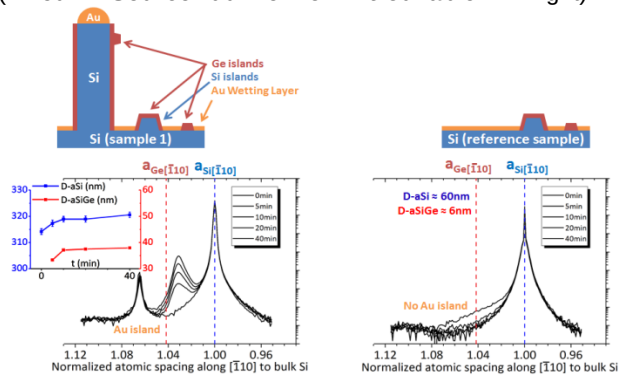

Figure 3 : Top left : illustration of the nano-objects found at the sample surface which includes the SiGe coreshell NW as well as some Si/Ge islands. Top right : only the unwanted islands can be found on the reference sample surface. Bottom left : Measured intensity of a radial scan along the [-110]$_b$ direction at different growth stage. The three peaks from left to right are Au peak, mixed SiGe peak and Si Bragg peak. Inset: rocking scans on both the Si peak (blue) and on the mixed SiGe peak (red) reveal the size of the nano-objects. Bottom right: The same measurement on the reference sample.

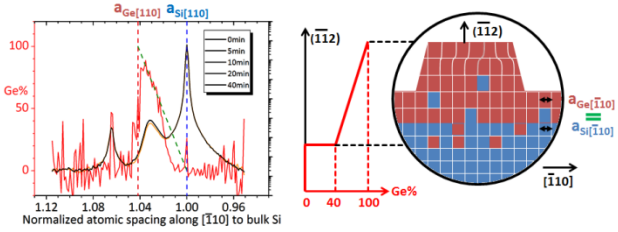

Figure 4 : (left) Calculated Ge concentration with anomalous scattering measurements after 20min of injection. (right) Graphical illustration of our interpretation of the data.

In situ bending of NWs

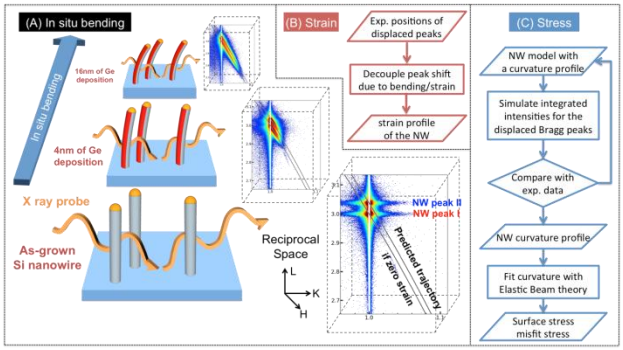

Figure 5: (A) Schematics of the bending experiment and process flow chart of the analysis routine used for retrieving (B) strain and (C) stress information from the diffraction data.

The *in situ* bending of Si NWs was induced by depositing with MBE a second material on one side of the NWs. The strain profile along the longitudinal direction of the NWs was obtained by analyzing the position shift of the displaced Bragg peaks whereas the total stress applied on the NWs was deduced by fitting the NW curvature, retrieved from integrated intensities of the displaced Bragg peaks, with a formula based on classic beam theory.
Among all the materials studied, Ge deposition on Si NWs is probably the most intriguing case. With the analysis method described briefly in Fig. 5, we were able to reconstruct the bended shape of the NWs (Figure 6A), and to retrieve the related strain and stress (Figure 6B) information. The reconstructed shape agrees well with our *ex situ* Electron Microscopy observations (Figure 7). Our findings indicate that the bending induced by Ge deposition on Si NWs sidewall at 220°C is mainly driven by the misfit stress, which scales almost linearly with Ge film thickness. The result is distinctively different when conducted at RT: the bending is found to be driven by the surface stress, which evolves from tensile eventually to compressive in the later stage of Ge. Our experimental and analysis method is applicable to all kinds of single crystal system, being it a massive amount of objects (thin film on wafer, NW arrays) or a single object (microcantilever, unique NW), depending on the focused size of the beam spot.

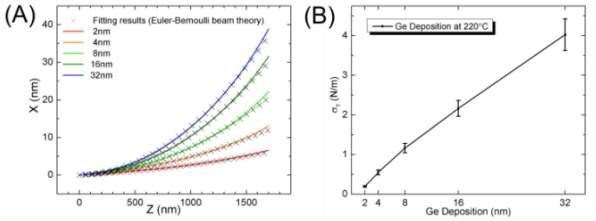

Figure 6: (A) Reconstructed NW shape based on integrated intensities of the displaced Bragg peaks: deflection of the neutral surface X as a function of Z in the principle plane of bending for Si NW with 2, 4, 8, 16, 32nm of Ge deposition. The black crosses are best-fit results using Euler-Bernoulli beam theory for a tapered NW. (B) The extracted total stress as a function of Ge deposition at 220°C.

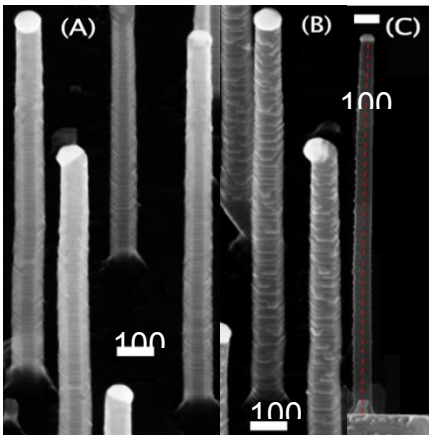

Figure 7: 45° perspective view of the Si NWs after 32nm of Ge deposition at 220°C. (A) The periodic sawtooth faceting was preserved on the three facets that were kept from Ge deposition whereas (B) Intensive surface roughening was observed on those three that were exposed to Ge deposition. (C) Side view of a Si NW after 32nm of Ge deposition. The viewing direction is perpendicular to the principal plane of bending. Red dashed line denotes deflection of the neutral surface as retrieved from experimental integrated intensities.

Publications: "Substrate-enhanced supercooling in AuSi eutectic droplets" T.U. Schulli, R. Daudin, G. Renaus, A. Vaysset, O. Geaym!ond and A. Pasturel, Nature 464, 1174 (2010). T. Zhou, PhD-thesis, in press

Collaborations:
Patent(s)
Contact: : gilles.renaud@cea.fr

HL 13 Growth, strain and organisation of Graphene on Ir(111)

F. Jean[a,b], J. Coraux[b], N. Blanc[a,b] and G. Renaud[a]
[a&b]Université Grenoble Alpes (UGA)
[a]CEA-Grenoble, Institut Nanosciences et Cryogénie, SP2M/NRS
[b]CNRS-Institut Néel

Within the framework of the ANR project NMGEN (NanoMagnétisme sur Graphène Epitaxié sur Métaux), several experiments were carried out in the INS ultra high vacuum (UHV) setup. They were performed under two guidelines, a better understanding of the structure of graphene on iridium and the growth and study of nanoparticles (NPs) on top. Graphene on Ir(111) is grown *in-situ* in the UHV setup by a chemical vapor deposition process (CVD) of ethylene on the surface of an iridium single crystal. The substrate is cleaned previously by a combination of ion bombardment and annealing at high temperature under oxygen.

Graphite's negative thermal expansion coefficient (TEC) below 500 K has been known for a long time. Graphene, a single layer of graphite, has been predicted to exhibit negative TEC as well, below 300 K, with a unique dependence of its lattice parameter with temperature due to the out-of-plane vibration modes, which its membrane-like topography allows. This prediction was tested on both suspended graphene, in electromechanical resonators, and on supported graphene, for graphene exfoliated from graphite and transferred to SiO_2/Si. The loose contact between graphene and SiO_2 presumably explains why graphene does not follow the TEC of the support. Which TEC graphene exhibits under the influence of a support with which it forms a good contact is of fundamental interest and an open question in any future application operating at variable temperature. The answer to this question is indeed, as we shall see, related to the formation of defects and strain, which are both known to modify the properties of graphene.

The evolution of the graphene lattice parameter was studied *in operando* using the RHEED (reflection high energy electron diffraction) technique available in the INS UHV chamber, either during the *in situ* growth of graphene, or during annealing under oxygen, or ion bombardment of a full one monolayer thick graphene sheet. On the first hand, during the growth at high temperature, it has been observed that the graphene shift between different commensurate phases, as the flakes become larger and larger. On the other hand, strains up to 2.2% in the graphene were uncovered during the ion bombardment when the density of defects is high (less than 1nm between defects). These results have been published in the Physical Review Letters.

We have performed a series of in situ temperature-dependent high resolution surface X-ray diffraction experiments, from 10 to 1300 K, with high quality graphene. Graphene is known to have a weak interaction with this substrate. We found that graphene on its substrate exhibits no negative thermal expansion coefficient in the broad temperature range that we explored (Figure 1). The weak graphene-metal interaction indeed forces graphene's lattice parameter to follow the temperature dependance of the metal lattice parameter.

The lattice properties of the two materials are however distinctive, and this shows up as graphene unlocks from the metal lattice at a certain threshold, corresponding to a situation when the in-plane compressive (upon cooling down) elastic energy overcomes the sum of the binding and bending energies of graphene on iridium. Graphene forms linear delaminations: several micrometer-long and few nanometer-high wrinkles that are readily revealed in microscopy experiments.

The transition between the two regimes – graphene locked and unlocked on its substrate – gives rise to a hysteretic change of graphene's lattice parameter. Remarkably, after having unlocked from the substrate, graphene re-locks on it, adopting another, well-defined epitaxial relationship. At high temperature, this relationship approaches a coincidence of 21 carbon

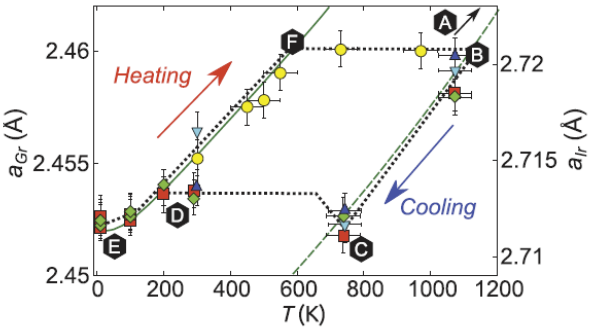

Figure1 : Graphene lattice parameter a_{Gr} (left axis), as a function of temperature. The solid green curve is the evolution of the bulk Ir lattice parameter (right axis) with temperature. The growth is referred to as point A, and measurements began at the lower temperature on point B at 1073 K

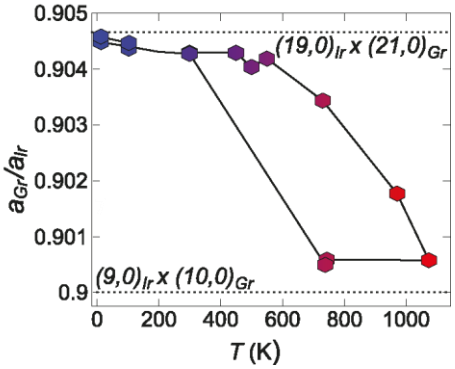

atoms with 19 Ir atoms, which is of high order, while at low temperature, the relationship is lower order, with 10 carbon atoms matching 9 Ir atoms (Figure 2).

Fig. 2: Ratio of the graphene to iridium lattice parameters as a function of temperature. Dotted lines highlight low- and high-order lattice coincidences (commensurabilities).

Publications: N. Blanc, J. Coraux, C. Vo-Van, A. T. N'Diaye, O. Geaymond, and G. Renaud, Phys. Rev. B 86, 235439 (2012); N. Blanc, F. Jean, A. V. Krasheninnikov, G. Renaud, and J. Coraux, Phys. Rev. Lett., 111, 085501 (2013). F. Jean, T. Zhou, N. Blanc, J. Coraux and G. Renaud, Phys. Rev. B 88, 165406 (2013)

Grants: French ANR NMGEM

Collaborations:

Patent(s)

Contact: : gilles.renaud@cea.fr

Perspectives for the Laue Microdiffraction setup (µLaue)

O. Robach, J.-S. Micha, O. Ulrich and F. Rieutord

The Laue microdiffraction setup uses more than one third of the beamtime on BM32. Until now there is no comparable instrument in Europe. Lateral spatial resolution and beam stability are already very satisfactory. Ergonomicity and user friendliness can still be improved for better data quality and throughput. The development of complementary experimental and analysis techniques will be pursued towards a better data quality, a higher accuracy in the determination of structural and physical quantities and 3D spatial resolution.

Upgrade of the KB mirrors :

After a few weeks of operation with the new KB mirrors in 2012, a diffuse halo appeared around the white x-ray microbeam, most likely due to the (visible) beam-induced carbon deposition on the mirror. A progressive degradation of the horizontal beam size (200=> 700 nm) was also observed, possibly due to the inhomogeneous illumination of the horizontally focussing mirror, causing a non-uniform carbon thickness. A horizontal beam size of 300 nm was recovered by using only one half of the mirror, to match the actual beam size before the KB. Possible methods for removing the carbon are currently being explored. The first method to be tested will be an in situ cleaning of the mirrors using the x-ray beam and an hydrogen+argon mix.

Diamond transmission filter

The current setup for the Rainbow method, build with second-hand parts, needs to be replaced. A new easily retractable setup with dedicated elements is under construction. The goal is to gain time on the recalibration of the abacus giving the attenuated energies versus rotation angle for all the diamond Bragg reflections. New macros to move the diamond to a certain energy for a certain reflection, and new online analysis tools will also be developed. Theoretical work is also needed to model the energy spectrum transmitted by the diamond, in amplitude and polarization, for better prediction of the dip depth. The aim is to optimize the diamond orientation in terms of statistics and energy resolution, for a given local crystal orientation on the sample.

DAXM :

3D depth resolution using wire-scanning was already extensively tested using two different scanning angles and one to four wires. The code for geometry calibration and reconstruction of depth-resolved Laue patterns including is operational for "thin" samples. Code development is still needed for thick samples (> wire diameter). Better accuracy in the absolute depth-position of the diffraction source will be attempted using wire scanning on the fluorescence of a very thin (1 µm) Ge film. A new motorized wire setup is in the design phase, with optimized scanning angle and best use of available motor range. It will include a manual stage for adapting the wire height to the sample thickness.

DIC and Laue-DIC:

A complete setup for in situ optical image correlation

will be mounted on the microdiffraction setup (with a microscope and commercial software). This will allow the monitoring of the (mostly plastic) total strain field during mechanical testing, for comparison with the orientation gradients and stress fields collected with Laue microdiffraction, and adaptation of the micro-Laue grid between successive deformation steps. The DIC method is also useful for differential analysis on Laue patterns, providing improved accuracy in the monitoring of spot displacements. The corresponding code still needs developments before being accessible to external users.

LaueTools Suite

The development of data analysis tools will be pursued in view of increased speed, better ergonomicity, additionnal functionnalities, and easier installation. The main GUI is already very user friendly with appropriate documentation. New GUI's need to be built for fast online data analysis, in time to adapt the data collection strategy, and help during data collection with the complementary techniques(Rainbow method, DAXM).

User training on data analysis

When the instrument started operating, the european user community for Laue microdiffraction was very small, and needed developing. Many presentations at schools and conferences were given by staff and users to highlight the large variety of possible uses of the technique, from the simplest to the most complex. Now the user community needs to be stabilized, which implies helping new users with the data analysis. Two one-day courses on the analysis software were already organized, and will be repeated in the future.

Scientific directions

Laue microdiffraction's strong point is in the orientation (angular) space, in contrast to powder diffraction whose strong point is in the radial (length) space. Both methods become more comparable when applying the Rainbow method. Spot description in orientation space still needs better understanding and physical models (e.g. using disclinations instead of dislocations). Most intra-grain elastic strain maps are impossible to understand without the associated lattice orientation map. This fact is still overlooked by many authors. This is where the technique has a very high potential for a much better understanding of stress fields.

Grants:	Collaborations: ENSAM Paris (ANR MicroStress)
Patent(s)	Contact: odile.robach@cea.fr, micha@esrf.fr

Foreseen research directions using GMT

F. Rieutord[a], *J.-S. Micha*[b]

[a]CEA-INAC-SP2M [b]CEA-INAC-SPrAM

Being a general purpose diffractometer, the research areas covered by the multitechnique goniometer are by essence very diverse. Based on the trends observed during the last four years, we give here a few lines along which the instrument may develop. This will still include high energy studies of buried interfaces and thin films. An important source of experiments come from technological materials - ranging from micro-electronics related subject area to new energy technologies - that often needs to be studied in-situ or operando

The multitechnique goniometer has been extensively used for a variety of scattering studies, mainly concentrated on the interface studies. Due to the high flux available at high energy on our beamline (Ec≠20keV) (especially compared to national synchrotron beamlines), we tried to emphasize specifically on experiments requiring this type of energy range.

Not surprising, studies of liquid/solid interfaces or solid/solid interfaces (bonding) represent a significant part of GMT activity. This development will be continued, as the possibility for medium to high energy X-rays to penetrate fair lengths of materials, is clearly an asset of X-ray techniques over other structure determination techniques (e.g. electron based). The ability to study in-situ materials, in operando with no or little sample preparation is specially important for technological samples which have to be characterized in conditions as close as possible to their conditions of use.

When strain and stress measurements are concerned, this possibility is even more important. Stress and strain depend on boundary conditions which must not be changed by sample preparation. The possibility of measuring strain fields using a monochromatic beam will complement other measurements using microbeams as performed e.g. using white beam MicroLaue (BM32) or other mapping techniques (ex. Kmaps on ID01). Techniques like Huang scattering to measure strain around defects or cavities in crystalline materials will be investigated. Reduction of Thermal Diffuse Scattering when performing reciprocal space maps is also something we are considering for experiments aiming at revealing low levels of diffuse scattering by defects. This can be done using a lightweight simple cooler.

Finally, installation of a compact multifunctional tensile test machine that could be used both with microLaue and on the goniometer in monochromatic mode will be done. Several users have already designed and used such type of equipment on the beamline and we will try to build / acquire such general purpose testing machine to complement these often specific equipments.

Soft condensed matter processes or electrochemical processes involving liquids at electrodes are also difficult to study using other techniques due to the high vapor pressure of the liquids or electrolytes. Several experiments and programs (e.g. FP7 European programs) have started around the study of new innovative energy storage systems (e.g. Li batteries) and will certainly be carried on during the next years.

The demand to characterize thin deposits of material is very strong, especially from our colleagues from applied research.

The availability of new 2D detectors on the beamline (specially pixel detector) should foster the development of new techniques for polycrystalline thin film studies. Strategies to maintain angular resolution (e.g. beam microfocussing to limit footprint length, knife edge above sample...) will have to be developed. Installing a KB in front of the sample will be studied to improve 2D detection strategies.

This type of studies using monochromatic beams would complement very well the local measurements performed using the Laue microdiffraction setup.

Reciprocal space maps using these 2D detectors (e.g. on implanted samples) should also be developed to perform the so-called 3D scattering. We anticipate that significant software development will be needed to tackle the large amount of data produced by this type of studies.

The goniometer is also rather old now (>20y). Although the base mechanics (circles) remains very good and precise, several parts of it could be improved. For example, an increased stiffness of the goniometer head would be desirable, together with sample changer capabilities in order to better automate some experiments. The horizontal sample geometry could be improved (access to higher angle) if extra movement stages were present.

The high demand for scattering studies on technological samples, together with the mid-term need for renewed instruments may call for the building of a new instrument dedicated to these new technology materials and to the techniques covered at the moment by the GMT goniometer. In any case we will continue developing subjects in close connection with demands from the society.

Subject of industrial interest will be continued, in cooperation with other programs from ESRF, CNRS or CEA aiming at promoting synchrotron radiation use for industrial purposes (ex: IRT program).

Grants:	Collaborations:
Patent(s)	Contact: francois.rieutord@cea.fr

Future perspectives and possible plans for upgrades of the BM32 beamline, seen in the perspective of the Upgrade Program

The optics of the BM32 beamline was upgraded in 2006, with optical elements of the highest quality (roughness, slope error…) available at that time. The choice and quality of the optical elements was such that the 1:1 focusing of the X-ray source in the normal mode configuration of the BL optics (see Fig. 1 of optics description, p 10) provided a doubly focused beam (250 μm H x 150 μm V FWHM) only slightly larger in both directions than the source size (200 μm H x 90 μm V FWHM) at that time. These imperfections of the 1:1 focusing arise because of the optical aberrations and imperfections of the two mirrors and the two monochromator crystals. Since then, the vertical emittance of the ESRF X-ray source has steadily decreased, yielding source sizes of 184 H x 30 V μm^2 (see Table 1) today. However, the vertical size of the focused beam has not evolved, staying around 150 μm.

Through the Upgrade II, the ESRF will completely change the lattice of the synchrotron ring in order to continue decreasing the vertical emittance, but also to decrease dramatically the horizontal emittance as well. The bending magnet beamline should be replaced by a short two-pole wiggler (with additional contributions from nearby dipoles), with a further decrease of the vertical size from 31 μm (V) down to 9.5 μm FHMM, and of the horizontal size from 184 μm (H) down to 54 μm FWHM (see Table 1). This translates in a corresponding gain in brilliance of ~3.3 in both directions, hence a total potential gain of 11. This potential gain in brilliance is complemented by a ~2 to 3-fold gain in flux (see Fig. 1). A 2-fold factor arises from the 2-pole wiggler, and some additional flux, mostly on the low-energy side, is provided by the neighboring dipole.

Hence, in principle, if we were able, by the horizon 2020, to design, fund and realize a "perfect" focusing optics, a gain of ~20 with respect to an ideal present situation could be gained, and even a gain of two orders of magnitude considering the aberrations of the present optics.

Realizing a much smaller size of the focused beam in both directions while keeping the (relatively) low divergence (~1 mrad H x 0.13 mrad V, FWHM) provided by the 1:1 focusing would allow very significant improvements of some of the experiments performed on the GMT, μdiffraction and INS instruments, both quantitative and qualitative.

Concerning the INS instrument, all measurements are performed under very grazing incidence, the sample surface being vertical. Presently, only a very small portion (typically 15 μm/250μm ~1/16) of the horizontal beam is intersected by the sample in this geometry. If we were able to focus the beam horizontally down to 54 μm, a ~5-fold factor could be gained on the intensities. Combined with the ~2.3-fold increase in flux, one order of magnitude would be gained (no gain is expected vertically) allowing e.g. kinetic studies of growth or ripening at a ten time shorter time scale. The much smaller vertical size would be of great help for GISAXS measurements. The background scattering from scattering elements (windows, monitors…) in the input beam would be decreased by two orders of magnitudes; while the much smaller beam size would allow reaching much smaller values of the momentum transfer. The small vertical beam would also allow investigating objects of ~10 μm size on a surface, *e.g.* patterned areas.

For GMT, that can be operated also with horizontal samples (e.g. for reflectivity experiments), the reduction in the vertical size would also be beneficial specially when using high energies. Due to the small value of grazing angles used when working around 30keV, a reduced source and image sizes would reduce the losses associated to the necessary collimations and hence increase significantly the total flux at sample position.

These few examples illustrate the clear conclusion that, with a perfect optics, the corresponding gain, in between one and two orders of magnitude, would not only allow new science (e.g. fast kinetic studies) to be performed, but also would provide more quantitative data in a given time, and hence a more efficient use of the beamtime.

Regarding the Laue microdiffraction station we expect at least of 2 fold increase of the incident flux on sample according to the estimation of the central part flux reported by J. Chavanne. High energy part of energy spectrum will not be used since mirrors - in both optics and experimental hutches (Kirckpatrick-Baez (KB) cut energies above 30keV. The predicted higher flux at low energy will benefit the measurements of 5-10 keV Laue spots that are attenuated by air absorption namely along the path from the sample to the detector. Moreover, the smaller horizontal source size would allow the design of new KBs system with a shorter second KB mirror (horizontal focusing) and a first mirror closer to the sample with the aim of decreasing the effects of the slope errors and carbon contamination on the beam size and wings. Finally due the primary small acceptance in the two directions performed by uptream primary slits small impact of the larger power density is expected.

There are a few drawbacks that would be anticipated, though, such as a i) small shift of the distribution of X-rays towards lower energies (see Fig.2), the maximum flux being around 14 keV as opposed to 19 before; ii) Possibly two images of the focused beam at different longitudinal positions along the beam because of the two (BM and wiggler) sources being separated longitudinally iii) a higher heat load on the optical elements (Table1); (iv) a much higher coherence of the X-ray beam that will reveal much more the imperfections of the optics.

The first two drawbacks will probably be overcome just by using slits around the focus point to remove the contribution from the low-field dipole. That way, the energy spectrum will remain unchanged, and only one focus point will be got. But the main difficulty will be to find an optical configuration, and its realization, that will provide a focused beam with a size comparable to the source size, *i.e.* with aberrations far smaller than the present one, by a factor of at least 4 horizontally and more than 10 vertically. We believe that this is a real challenge, because we want to keep at the same time as much as possible of the beam fan; i.e. refocus about 1 mrad horizontally and 0.13 mrad vertically. The first condition implies about 30 mm wide optical elements, and the second about 1m long mirrors as well as quite long monochromator single crystals. On the ESRF beamlines, optical elements have been designed with very low aberration, but over much smaller sizes (typically a few mm horizontally and 200 mm longitudinally) because of the much smaller divergences. Coupling of a large horizontal divergence with the narrow vertical sizes will bring specific problems to BM beamline optics. Aberrations associated to sagittal focusing will have to be tackled, especially when considering highly bent optics for high energy operation.

However, these smaller divergences may also allow using different focusing elements such as compound refractive lenses that could even be located in the front end using transfocators to change them as a function of energy. Today, the largest of these elements have diameters of only 2 m. We believe that a very significant R&D work has to be done to provide the required optics, which is impossible to realize with our own staff and funding. We will thus have to look for specific funding, which is a difficult task in the present funding situation for research in France, but this might ultimately be solved. From the technical point of view, a strong support from the ESRF seems to be a prerequisite for such a project.

	Horizontal source size (FWHM, µm)	**Vertical source size (FWHM, µm)**	**Power density at port end (W/mm^2)**
Present 0.85 T BM -9 mrad	184	31	2.34
New S28B Lattice wiggler - 7.85 mrad	54	9.5	4.65

Table 1: Sizes and power densities of the X-ray present and purported X-ray source (from J. Chavanne presentation on BM sources UPII of March 2015)

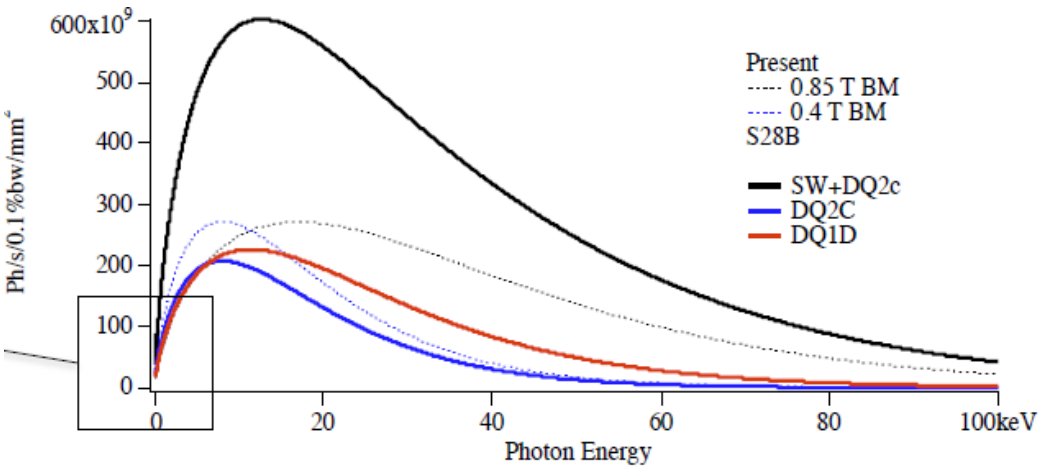

Fig. 1: On-axis photon density at front end (from J. Chavanne presentation on BM sources UPII of March 2015).

Annexes

Annex 1 Statistical information about the use of the beamline

The following statistics cover the period 2010-2015 of operation of the BM32 beamline. As a CRG beamline, two selection committees hereafter called ESRF and CRG committee allocate beamtime to European and French users (resp. one third and two thirds). Three instruments share the beamtime: INS, µLaue and GMT (the two latter are hosted in the same experimental hutch and have some common users).

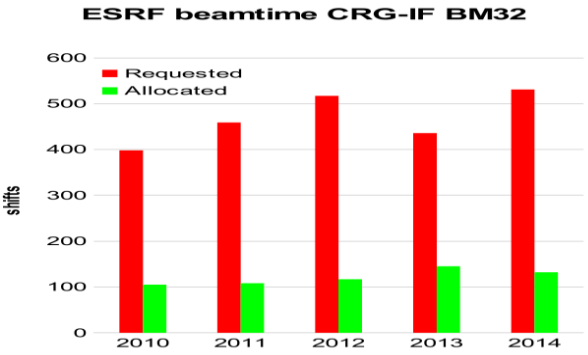

Figure 1: Evolution of the number of requested and allocated ESRF beamtime shifts over the period 2010-2014

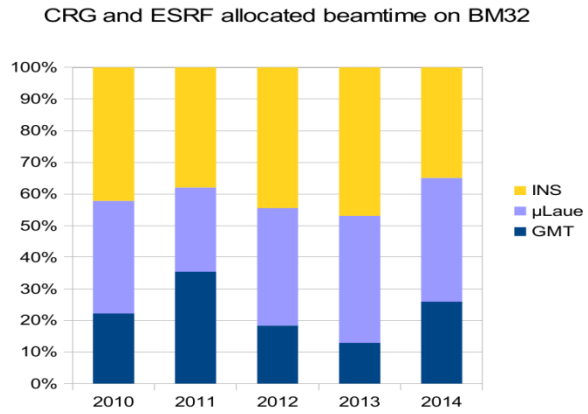

Figure 2: Distribution per instrument of the beamtime allocated by ESRF and French committees 2010-2014.

Beamtime overbooking: 280 shifts (resp. 140 shifts) are allocated for CRG (resp. ESRF) beamtime by program committees of the french synchrotron SOLEIL committee (resp. several ESRF committees) per full operational year. Over the 4 years period. at least 400 shifts per year are requested on BM32 and the mean overbooking ratio (requested/allocated number of shifts ratio) is 3.9 for ESRF beamtime (fig. 1). For the CRG beamtime the ratio is lower and equals 2.25. The instruments distribution of requested and allocated beamtime on CRG beamtime in figure 2 illustrates how the beamtime is shared among the instruments.

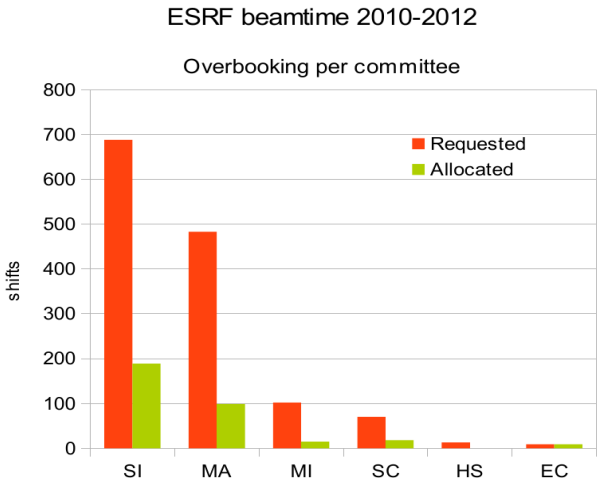

Figure 3: Requested vs allocated beamtime per ESRF committee of ESRF beamtime (2010-2012). Committees: (SI) Surfaces and interfaces, (MA) Applied Materials & Engineering, (MI) Methods and Instrumentation, (SC) Soft Condensed Matter & Biological Materials, (HS) Crystals & Ordered Systems, Structures, and (EC) Environment and Cultural Heritage Matters

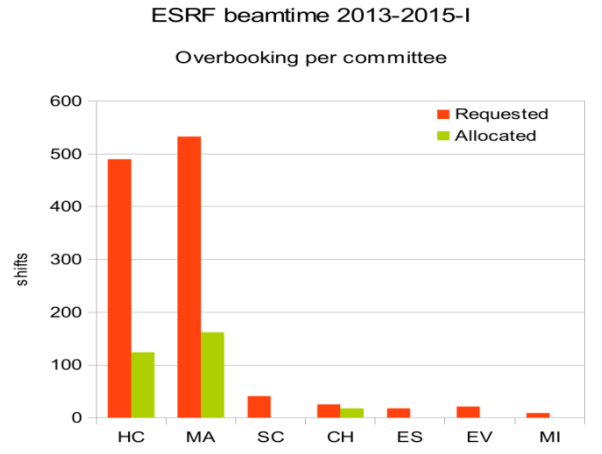

Figure 4: Overbooking per ESRF committee of ESRF beamtime (2013-2015- first semester). Committees: (HC) Hard Condensed Matter Science, (MA) Applied Materials Science, (SC) Soft Condensed Matter Science, (CH) Chemistry, (ES) Earth Sciences, (EV) Environment, and (MI) Methods and Instrumentation

The first half (~45%) of the beamline activities is devoted to the INS instrument and the other half (~55%) is divided between µLaue (35%) and GMT (20%) ones. The mean duration of users experiments is respectively 18, 14 and 15 shifts when performed with INS, µLaue and GMT

instruments. BM32/µLaue were involved in an ESRF Long Term Project 18 shifts within the period 2012-2015.

Scientific Fields and Committees: BM32 has been originally dedicated to interface and surface studies. The distribution of allocated ESRF beamtime by ESRF committee is representative of the scientific fields covered by the beamline with its three instruments (Fig 3 and 4). For the CRG beamtime the distribution is comparable (not shown). More than one experiment over two is devoted to surface and interface studies (former SI ESRF committee during the period 2010-2012), among them a large majority are carried out on the INS instrument. One experiment over three concerns applied materials science (MA ESRF committee). Most of these experiments are performed with the Microdiffraction setup (µLaue). The versatility of the GMT instrument is reflected by the remaining committees mainly SC committee and some MA and Si experiments. For the next period (2013-2015) with a new ESRF committees organisation (figure 4), MA experiments represent one experiment over two (53%). 41% of experiments have been accepted through the new committee HC and 6% through CH one. The beamline is now clearly optimized for physical and physico-chemistry structural investigations at surfaces and interfaces of materials in both applied and fundamental points of view.

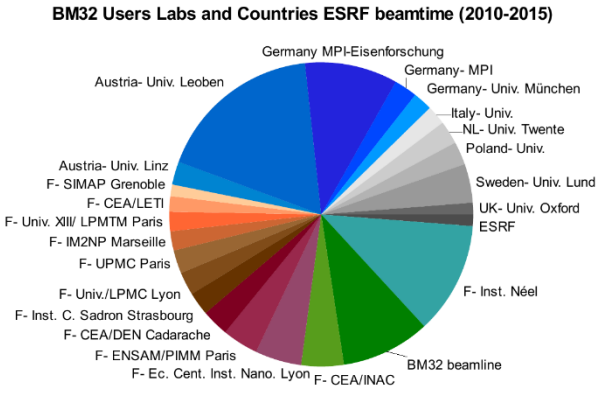

Figure 5 Panel of laboratories of users of BM32 whose experiments have been accepted by ESRF committees (2010-2015)

Users Countries and Laboratories: Figure 5 and 6 present the panel of countries and laboratories from which the main proposer of the experiment originates. Even if proposers of each experiment come from different laboratories, the distribution retrieved from the main proposer or all users data quite the same. Distribution of ESRF beamtime is shown figure 5. This beamtime is shared equally by French and foreign (European) scientists. Some experiments proposed by French teams are submitted in both CRG and ESRF committees and finally obtained by means of ESRF committees. It can be noted the high attraction for BM32 by austria and german teams (one over three allocated experiments by ESRF).

Figure 6 represent the panel of origin of users with beamtime accepted by both CRG and ESRF committees. Close to 25 % beamtime is allocated to other countries, most of the beamtime being used by French community. One half of French users originates from Grenoble, as beamline staff (BM32), external users or strong collaborators from CEA-INAC and Institut Néel.

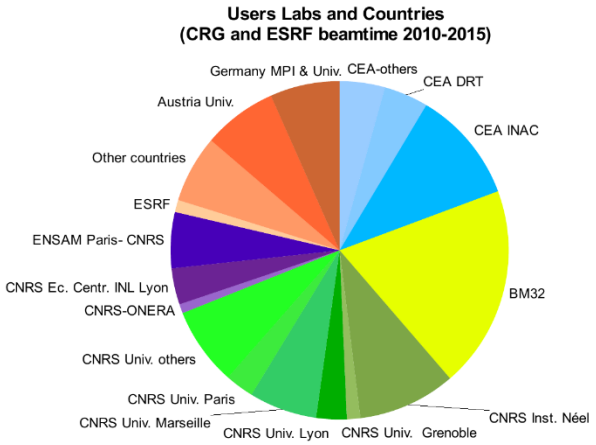

Figure 6 Panel of laboratories of users of BM32 whose experiments have been accepted by both CRG and ESRF committees (2010-2015)

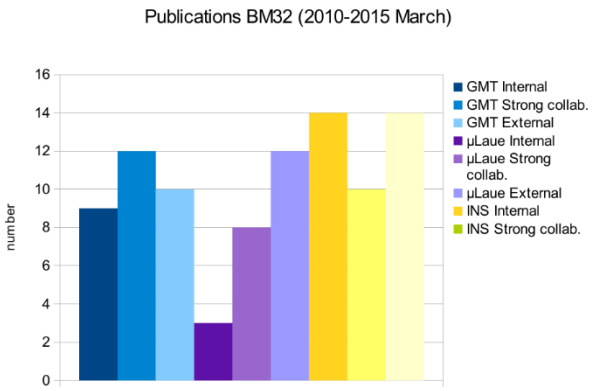

Figure 7 Distribution of scientific articles from BM32 as a function of the instrument (blue or 3 first left bars: GMT; violet or middle 3 bars: µLaue; yellow or 3 right bars: INS) and users type (Internal: beamline BM32 staff, External: external users, Strong Collab.: strong collaboration between BM32 staff and external users).

Publications: Beamline staff of BM32 (internal users) and external users with or without strong collaborations with beamline staff produced 92 articles reviewed by peers over the period 2010-2015 (March). Among them, 7 have been published in journals with an impact factor (5 years) larger than 6 and 3 have been cited more than 30 times (see Annex 3 below). The average rate of production is higher than 15 papers/year. Scientific production is rather well distributed over the three instruments (figure 7). Three modes of production can be considered in this CRG beamline involving first internal scientists using In-House-Research beamtime and allocated one by CRG or ESRF committees, second external users from allocated beamtime only, and third beamline staff and external users within the frame of a strong collaboration (mainly allocated beamtime + casual IHR beamtime). The last mode corresponds to a significant beamline staff investment when valuable instrumental and methodological benefits can be obtained for the general beamline development and higher throughput. In contrast to the last BLRP period (2005-2010), µLaue entered in the maturity age but a lot of resources is still employed to help users towards autonomy at the expense of internal research activities.

Annex 2 : Scientific production 2010-2015

The list of scientific peer-reviewed articles are sorted by year and 5-years-impact factor (in brackets) of the journal. Additional production are listed in the following: ESRF highlight, Book chapter, Awards, Journal covers, selected thesis from internal and external beamline users, proceedings and selected oral communications.

[] 5-years impact factor (march 2015)

() times cited (march 2015)

2015

[14.5] Tensile Strained Germanium Nanowires Measured by Photocurrent Spectroscopy and X-Ray Microdiffraction.
K. Guilloy, N. Pauc, A. Gassenq, P. Gentile, S. Tardif, F. Rieutord, and V. Calvo
Accepted in Nano Letters, 2015

[5.1] "Moiré induced organization of size-selected Pt clusters soft landed on epitaxial graphene"
S. Linas, F. Jean, T. Zhou, C. Albin, G. Renaud, L. Bardotti, and F. Tournus
Scientific Reports, accepted, (2015)

[4.8] In situ bending of an Au nanowire monitored by micro Laue diffraction
C. Leclere, T. W. Cornelius, Z. Ren, A. Davydok, J.-S. Micha, O. Robach, G. Richter, L. Belliard and O. Thomas
J. Appl. Cryst., **48**, 291 (2015)

[4.8] X-ray micro Laue diffraction tomography analysis of a solid oxide fuel cell
D. Ferreira-Sanchez, J. Villanova, J. Laurencin, J.-S. Micha, A. Montani, P. Gergaud, P. Bleuet
J. Appl. Cryst., accepted, (2015)

[3.7] Ordered domain lateral location, symmetry and thermal stability in Ge:Si islands
M.-I. Richard, A. Malachias, T. U. Schulli, V. Favre-Nicolin, Z. Zhong,T. H. Metzger, and G. Renaud,
Applied Physics Letters 106, 012108 (2015)

[3.6] "Formation, stability and atomic structure of the Si(111)-(6x6)Au surface reconstruction: a quantitative study using synchrotron radiation"
R. Daudin, T. Nogaret, A. Vaysset, T.-U. Schülli, A. Pasturel, and G. Renaud
Phys. Rev. B, **91**, 165426 (2015)

[3.6] "Effect of CoO/Ni orthogonal exchange coupling on perpendicular anisotropy of Ni films on Pd(001)"
P. Kuświk, P. L. Gastelois, M. M. Soares, H. C. N. Tolentino, M. De Santis, A. Y. Ramos, A. D. Lamirand, M. Przybylski, and J. Kirschner
Phys. Rev. B **91**, 134413 (2015)

[3.6] "Topography of the graphene/Ir(111) moire studied by surface x-ray diffraction"
F. Jean, N. Blanc, J. Coraux, and G. Renaud
Phys. Rev. B, accepted, 2015

[2.7] The In situ growth of Nanostructures on Surfaces (INS) end station of the ESRF BM32 beamline: a combined UHV-CVD and MBE reactor for in situ x-ray scattering investigations of growing nanoparticles and semiconductor nanowires
V. Cantelli, O. Geaymond, O. Ulrich, T. Zhou, N. Blanc, and G. Renaud
J. Sync. Rad., 22 (2015).

[2.3] Strain driven monoclinic distortion of ultrathin CoO films in the exchange-coupled CoO/FePt/Pt(0 0 1) system

A. D. Lamirand, M. M. Soares, M. De Santis, A.Y. Ramos, S. Grenier and H. C. N. Tolentino
J. Phys.: Condens. Matter **27** 085001 (2015)

[1.9] Spin orientation in an ultrathin CoO/PtFe double-layer with perpendicular exchange coupling
A. D. Lamirand, M. M. Soares, A.Y. Ramos, H.C.N. Tolentino,
M. De Santis, J. C. Cezar, A. de Siervo
J. Magn. Magn. Mater. **373** (2015) 6–9

[1.0] Mechanism Involved in Direct Hydrophobic Si(100)-2x1:H Bonding
Rauer, C., H. Moriceau, F. Rieutord, J.M. Hartmann, F. Fournel, A.-M. Charvet, N. Bernier, H. Dansas, and C. Morales.
accepted in Microsystem Technologies, 2015

"Moiré induced organization of size-selected Pt clusters soft landed on epitaxial graphene"
S. Linas, F. Jean, T. Zhou, C. Albin, G. Renaud, L. Bardotti, and F. Tournus
Scientific Reports, submitted

Laue-DIC: a new method for improved stress field measurements at the micron scale
J. Petit, O. Castelnau, M. Bornert, F. Zhang, F. Hofmann,d A.M. Korsunsky, D. Faurie, C. Le Bourlot, J.-S. Micha, O. Robach and O. Ulrich
submitted to J. Synchr. Rad.

On the reversibility of dislocation slip during small scale low cycle fatigue
C. Kirchlechner, P. J. Imrich, W. Liegl, J. Pörnbacher, J.-S. Micha, O. Ulrich and C. Motz
submitted to Acta Materialia

Elastic strain measurements by Laue microdiffraction and HR-EBSD in a deformed stainless steel single crystal.
E. Plancher, J. Petit, C. Maurice, V. Favier, L. Saintoyant, D. Loisnard, N. Rupin, J.-B. Marijon, O. Ulrich, J.-S. Micha, O. Robach, O. Castelnau
submitted to Scripta Materialia

Laue pattern analysis for 2D strain mapping in light ion implanted polycrystals
M. Ibrahim, E. Castelier, H. Palancher, M. Bornert, S. Caré, J.-S. Micha
submitted to J. Appl. Cryst.

The nature and origin of "double expanded austenite" in Ni-based Ni-Ti alloys developing upon low temperature gaseous nitriding
Fonović, M., Leineweber, A., Robach, O. Jägle, E. A., Mittemeijer, E. J.
submitted to Metall. Mater. Trans. A

2014

[4.8] (2) Integration techniques for SXRD data obtained with a 2D detector
J. Drnec, T. Zhou, S. Pintea, W. Onderwaater, E. Vlieg, G. Renaud and R. Felici,
J. Appl. Cryst. **47**, 365 (2014)

[3.6] (1) Local band bending and grain-to-grain interaction induced strain nonuniformity in polycrystalline CdTe films
V. Consonni, N. Baier, O. Robach, C. Cayron, F. Donatini, and G. Feuillet
Phys. Rev. B **89**, 035310 (2014)

[2.3] X-ray μ-Laue diffraction analysis of Cu through-silicon vias: a 2D and 3D study
D. Ferreira Sanchez, D. Laloum, M. Larissa Djomeni Weleguela, O. Ulrich, G. Audoit, A. Grenier, J.-S. Micha, O. Robach, F. Lorut, P. Gergaud and P. Bleuet
J. Appl. Phys. **116** 163509 (2014)

[2.1] Interfacial Closure of Contacting Surfaces
Rieutord, F., C. Rauer, and H. Moriceau
Europhysics Letters **107** 34003 (2014)

[1.9] Growth of Ge islands on SrTiO3 (001)-2×1 reconstructed surface: Epitaxial relationship and effect of the temperature
B. Gobaut, J. Penuelas, A. Benamrouche, Y. Robach, N. Blanc, V. Favre-Nicolin, G. Renaud, L. Largea, G. St-Girons
Surf. Sci. **624**, 130 (2014)

[1.6] A new method for polychromatic X-ray μLaue diffraction on a Cu pillar using an energy-dispersive pn-junction charge-coupled device
A. Abboud, C. Kirchlechner, S. Send, J.-S. Micha, O. Ulrich, N. Pashniak, L. Struder, J. Keckes and U. Pietsch
Rev. Sci. Instr. **85** 113901 (2014)

2013

[17.2] (2) *A tunable multicolour 'rainbow' filter for improved stress and dislocation density field mapping in polycrystals using X-ray Laue microdiffraction*
O. Robach, J.-S. Micha, O. Ulrich, O. Geaymond, O. sicardy, J. Haertwig, F. Rieutord
Acta Cryst. **A 69**, 164-170 (2013)

[7.4] *(8) Strains induced by Point Defects in Grapheneon a Metal*
N. Blanc, F. Jean, A. V. Krasheninnikov, G. Renaud, and J. Coraux
Phys. Rev. Lett., **111**, 085501 (2013).

[4.2] (1) *Operando atomic structure and active sites of TiO_2(110)-supported gold nanoparticles during carbon monoxide oxidation*
M.C. Saint-Lager, I. Laoufi and A. Bailly
Faraday Discussions **162**, 179-190 (2013)

[3.7] *(3) In-situ observation of stress-induced stochastic twin boundary motion in off stoichiometric NiMnGa single crystals*
R.I. Barabash, C. Kirchlechner, O. Robach, O. Ulrich, J.-S. Micha, A. Sozinov and O.M. Barabash
Appl. Phys. Lett. **103** (2), 021909 (2013)

[3.7] *(1) Interface Accommodation Mechanism for Weakly Interacting Epitaxial Systems*
A. Danescu, B. Gobaut, J. Penuelas, G. Grenet, V. Favre-Nicolin, N. Blanc, T. Zhou, G. Renaud, and G. Saint-Girons
Appl. Phys. Lett. **103**, 021602 (2013).

[3.7] (0) *Effect of H-implantation in the local elastic properties of silicon crystals*
S. Reboh, F. Rieutord, L. Vignoud, F. Mazen, D. Landru, M. Zussy, and C. Deguet
Appl. Phys. Lett. **103**, 181911 (2013)

[3.7] (3) *Agglomeration dynamics of germanium islands on a silicon oxide substrate: A grazing incidence small-angle x-ray scattering study*
F. Cheynis, F. Leroy, T. Passanante *et al.*
Appl. Phys. Lett. **102** (16), 161603 (2013)

[3.6] *(6) Robust perpendicular exchange coupling in an ultrathin CoO/PtFe double layer: Strain and spin orientation*
A. D. Lamirand, M. M. Soares, A.Y. Ramos, H.C.N. Tolentino, M. De Santis, J. C. Cezar, A. de Siervo and M. Jamet
Phys. Rev. **B 88**, 140401 (2013)

[3.6] (5) *Effect of preparation on the commensurabilities and thermal expansion of graphene on Ir(111) between 10 and 1300 K*
F. Jean, T. Zhou, N. Blanc, J. Coraux and G. Renaud,
Phys. Rev. **B 88**, 165406 (2013)

[2.9] (0) *Treatments of deposited SiOx surfaces enabling low temperature direct bonding*
C. Rauer, H. Moriceau, F. Fournel, A.-M. Charvet, C. Morales, N. Rochat, L. Vandroux, F. Rieutord, T. Mc Cormick, and I. Radu
J. Electrochem. Soc., (2013)

[2.8] (5) *Metal organic vapour-phase epitaxy growth of GaN wires on Si (111) for light-emitting diode applications*
D. Salomon, A. Dussaigne, M. Lafossas, C. Durand, C. Bougerol, P. and J. Eymery
Nanoscale Res. Lett. **8**, 61-1 (2013)

[2.3] (6) *Lattice strain of hydrogen-implanted silicon: correlation between X-ray scattering analysis and ab-initio simulations.*
F. Rieutord, F. Mazen, S. Reboh, J. D. Penot, L. Bilteanu, J. P. Crocombette, V. Vales, V. Holy, and L. Capello
J. Appl. Phys. **113**, 153511, (2013)

[2.3] (4) *Nanoscale organization by elastic interactions between H and He platelets in Si*
S. Reboh, F. Rieutord, F. Mazen, N. Cherkashin, M. F. Beaufort, J.-F. Barbot, M. Vallet, P. F. P. Fichtner, and J. Grilhé
J. Appl. Phys. **114**, 073517 (2013)

[2.3] (3) *Development of microcracks in hydrogen-implanted silicon substrates*
J. D. Penot, D. Massy, F. Rieutord, F. Mazen, S. Reboh, F. Madeira, L. Capello, D. Landru, and O. Kononchuk
J. Appl. Phys. **114**, 123513, (2013)

[2.1] (0) *Mechanism of Edge Bonding Void Formation in Hydrophilic Direct Wafer Bonding*
A. Castex, F. Rieutord, K. Landry, and C. Lagahe-Blanchard
Electrochem. Sol. State Lett. **2**, 47-50, (2013)

[1.8] (0) Quantitative study of microtwins in GaP/Si thin film and GaAsPN quantum wells grown on silicon substrates
T. Nguyen Thanh, C. Robert, E. Giudicelli, A. Létoublon, C. Cornet, A. Ponchet, T. Rohel, A. Balocchi, J.-S. Micha, M. Perrin, S. Loualiche, X. Marie, N. Bertru, O. Durand, A. Le Corre
J. Crystal Growth **378**, 25-28 (2013)

[1.4] (1) *Structural investigation of nanoporous alumina film with grazing incidence small angle X-ray scattering*
D. Buttard, T. Schülli and R. Lazzari
Phys. Stat. Solid. **A** 210, 2521-2525 (2013)

[1.0] (2) *Hydrophobic direct bonding of silicon reconstructed surfaces*
C. Rauer, F. Rieutord, J. M. Hartmann, A.-M. Charvet, F. Fournel, D. Mariolle, C. Morales, and H. Moriceau
Microsystem Technologies, **19**, 675 (2013)

2012

[10.7] (6) *Controlling Interactions in supported bilayers from weak electrostatic repulsion to high osmotic pressure*
A. Hemmerle, L. Malaquin , T. Charitat,, S. Lecuyer, G. Fragneto and J. Daillant
Proc. Nat. Acad. Sciences USA **109** (49) 19938-19942 (2012)

[6.5] (5) *From metastable to stable modifications—in situ Laue diffraction investigation of diffusion processes during the phase transitions of (GeTe)nSb2Te3 (6 <= n <= 15) crystals*
M. N. Schneider, X. Biquard, C. Stiewe, T. Schröder, P. Urban and O. Oeckler
Chemical Communications **48** (16) 2192-2194 (2012)

[5.2] (7) *CO-Induced Scavenging of Supported Pt Nanoclusters: A GISAXS Study*
N. Chaabane, R. Lazzari, J. Jupille, G. Renaud, and E. A. Soares
J. Phys. Chem. **C, 116** (44), 23361-23370 (2012)

[4.8] (3) *Strains in light ion implanted polycrystals: influence of grain orientation*
A. Richard, H. Palancher, E. Castelier, J. S. Micha, M. Gamaleri, G. Carlot, H. Rouquette, P. Goudeau, G. Martin, F. Rieutord, J. P. Piron and P. Garcia
J. Appl. Cryst. **45** (4) 826-833 (2012)

[4.8] (3) *Multi scale measurements of residual strains in stabilized zirconia layer*
J. Villanova, C. Maurice, J.-S. Micha, P. Bleuet, O. Sicardy and R. Fortunier
J. Appl. Cryst. **45** (5) p 926-935. (2012)

[4.3] (6) *Expected and unexpected plastic behavior at the micron scale: An in situ Laue tensile study*
C. Kirchlechner , P.J. Imrich, W. Grosinger, M.W. Kapp, J. Keckes, J.S. Micha, O. Ulrich, O. Thomas, S. Labat, C. Motz, and G. Dehm
Acta Mater. **60** (3) 1252-1258 (2012)

[3.8] (12) *In situ study of self-assembled GaN nanowires nucleation on Si(111) by plasma-assisted molecular beam epitaxy*
K. Hestroffer, C. Leclere, V. Cantelli, C. Bougerol, H. Renevier and B. Daudin
Appl. Phys. Lett. **100** (21) 212107 (2012)

[3.6] (10) *Interface-driven phase separation in multifunctional materials: The case of the ferromagnetic semiconductor GeMn*
E. Arras, F. Lançon, I. Slipukhina, É. Prestat, M. Rovezzi, S. Tardif, A. Titov, P. Bayle-Guillemaud, F. d'Acapito, A. Barski, V. Favre-Nicolin, M. Jamet, J. Cibert, and P. Pochet
Phys. Rev. **B 85,** 115204 (2012)

[3.6] (5) *Chemically ordered MnPt ultrathin films on Pt(001) substrate: Growth, atomic structure, and magnetic properties*
M. M. Soares, M. De Santis, H. C. N. Tolentino, A. Y. Ramos, M. El Jawad and Y. Gauthier
Phys. Rev. **B 85**, 205417 (2012)

[3.6] (3) *Epitaxial orientation changes in a dewetting gold film on Si(111)*
R. Daudin, T. Nogaret, T.-U. Schülli, N. Jakse, A. Pasturel and G. Renaud
Phys. Rev. **B 86**, 094103 (2012)

[3.6] (15) *Dynamics, anisotropy, and stability of silicon-on-insulator dewetting fronts*
F. Leroy, F. Cheynis, T. Passanante, and P. Müller
Phys. Rev. **B 85**, 195414 (2012) and erratum **85** 239901 (2012)

[3.6] (5) *Local deformations and incommensurability of high quality epitaxial graphene on a weakly interacting transition metal*
N. Blanc, J. Coraux, C. Vo-Van, A. T. N'Diaye, O. Geaymond, and G. Renaud
Phys. Rev. **B 86**, 235439 (2012)

[2.5] (13) *Floating lipid bilayers: Models for physics and biology*
Fragneto G. Charitat T. Daillant J. -
European Biophysics Journal **41**, pp 863-874 (2012)

[2.3] (5) *Measurement of bonding energy in an anhydrous nitrogen atmosphere and its application to silicon direct bonding technology*
F. Fournel, L. Contini, C. Morales, J. Da Fonseca, H. Moriceau, F. Rieutord, A. Barthelemy and I. Radu
J. Appl. Phys. **111** (10) 104907 (2012)

[2.3] (14) *Structural and optical analyses of GaP/Si and (GaAsPN/GaPN)/GaP/Si nanolayers for integrated photonics on silicon*
T. Nguyen Thanh, C. Robert, W. Guo, A. Letoublon, C. Cornet, G. Elias, A. Ponchet, T. Rohel, N. Bertru, A. Balocchi, O. Durand, J.-S. Micha, M. Perrin, S. Loualiche, X. Marie and A. Le Corre
J. Appl. Phys. **112**, 053521 (2012)
Publisher erratum: J. Appl. Phys. **112**, 079904 (2012)

[2.3] (2) *Low temperature direct bonding mechanisms of tetraethyl orthosilicate based silicon oxide films deposited by plasma enhanced chemical vapor deposition*
C. Sabbione, L. Di Cioccio, L. Vandroux, J.-P. Nieto, and F. Rieutord
J. Appl. Phys. **112**, 063501 (2012)

[1.6] (4) *Advances in martensitic transformations in Cu-based shape memory alloys achieved by in situ neutron and synchrotron X-ray diffraction methods*
B. Malard, P. Sittner, S. Berveiller, E. Patoor
Compt. Rend. Physique **13** (2012) 280–292

[1.5] (3) *Investigation of reversible plasticity in a micron-sized, single crystalline copper bending beam by X-ray μLaue diffraction*
C. Kirchlechner, W. Grosinger, M.W. Kapp, P.J. Imrich, J.-S. Micha, O. Ulrich, J. Keckes, G. Dehm and C. Motz
Philosophical Magazine **92** (25-27), 3231-3242 (2012)

[1.4] (5) *Growth and dewetting of gold on Si(111) investigated in situ by grazing incidence small angle x-ray scattering*
R. Daudin, C. Revenant, G. Davi and G. Renaud
Physica **E 44**, 1905 (2012)

[1.2] (2) *Low temperature direct bonding: an attractive technique for heterostructures build-up*
H. Moriceau, F. Rieutord, F. Fournel, C. Moulet, L. Libralesso, P. Gueguen, R. Taibi and C. Deguet
Microelectronics Reliability **52** (2) p 331-341 (2012)

[1.3] (3) *Si exfoliation by MeV proton implantation*
C. Braley, F. Mazen, A. Tauzin, F. Rieutord, C. Deguet and E. Ntsoenzok
*Nucl. Instr. Methods **B 277**, 93-97 (2012)*

[1.1] (2) *Smart Cut™: review on an attractive process for innovative substrate elaboration*
H. Moriceau, F. Mazen, C. Braley, F. Rieutord, A. Tauzin, and C. Deguet,
Nucl. Instrum. Meth. **B 277**, p 84-92 (2012)

[1.0] (1) *Regular arrays of palladium and palladium-gold clusters supported on ultrathin alumina films: stability under oxygen*
G. Sitja, M. Marsault, F. Leroy, S Le Moal, C.R. Henry
Int. J. Nanotech. **9** (3-7) 567-575 (2012)

2011

[14.5] (53) *M-plane core-shell InGaN/GaN multiple-quantum-well on GaN wires for electroluminescent device*
R. Koester, J. S. Hwang, D. Salomon, X. Chen, C. Bougerol, J.-P. Barnes, D. Le Si Dang, L. Rigutti, M. Tchernycheva, C. Durand and J. Eymery
Nano Letters **11**, p 4839-4845 (2011)

[5.2] (34) *Size and Catalytic Activity of Supported Gold Nanoparticles: An in operando Study during CO Oxidation*
I. Laoufi, M.-C. Saint-Lager, R. Lazzari, J. Jupille, O. Robach, S. Garaudee, G. Cabailh, P. Dolle, H. Cruguel, A. Bailly
J. Phys. Chem. **C 115** (11) pp 4673-4679 (2011)

[5.2] (12) *Competition between polar and non-polar growth of MgO films on Au(111)*
S. Benedetti , N. Nilius, P. Myrach, P. Torelli, G. Renaud, H.-J. Freund, S. Valeri
J. Phys. Chem. **C 115,** 23043 (2011)

[4.9] (4) *In situ grazing-incidence X-ray diffraction during electrodeposition of birnessite thin films: Identification of solid precursors*
M. Ndjeri, S. Peulon, M.L. Schlegel, A. Chaussé
Electrochem. Commun. **13**, (5) p 491-494 (2011)

[4.8] (9) *Full local elastic strain tensor from Laue microdiffraction: simultaneous Laue pattern and spot energy measurement*
O. Robach, J.-S. Micha, O. Ulrich and P. Gergaud
J. Appl. Cryst.. **44** p 688–696 (2011)

[4.3] (5) *In situ synchrotron analysis of lattice rotations in individual grains during stress-induced martensitic transformations in a polycrystalline CuAlBe shape memory alloy*
Berveiller S., Malard B., Wright J., et al.
Acta Mater. **59** (9) p 3636-3645 (2011)

[4.3] (8) *Impact of instrumental constraints and imperfections on the dislocation structure in micron-sized Cu compression pillars*
Kirchlechner C., Keckes J., Motz C., Grosinger W., Kapp M.W., Micha J.S., Ulrich O. and Dehm G.
Acta Mater. **59** (14) p 5618-5626 (2011)

[4.2] (10) *Catalytic properties of supported gold nanoparticles: new insights into the size-activity relationship gained from in operando measurements*
M.-C. Saint-Lager, I. Laoufi, A. Bailly, O. Robach, S. Garaudée and P. Dolle
Faraday Discuss., **152**, p 253–265 (2011)

[3.9] (0) *Metal positioning using dislocation arrays.*
A. Bavard, F. Fournel and J. Eymery
Nanotechnology **22**, 215301(2011)

[3.7] (6) *Effect of doping on global and local order in crystalline GeTe*
Biquard X., Krbal M., Kolobov A. V. *et al*
Appl. Phys. Lett. **98** (23) 231907 (2011)

[3.7] (2) *In situ x-ray study of the formation of defects in Ge islands on Si(001)*
M.-I. Richard, T. U. Schülli, and G. Renaud
Appl. Phys. Lett. **99** 161905 (2011)

[3.7] (12) *Catalyst-free growth of high-optical quality GaN nanowires by metal-organic vapor phase epitaxy*
X.J. Chen, B. Gayral, D. Sam-Giao, C. Bougerol, C. Durand and J. Eymery
Appl. Phys. Lett. **99** (25) 251910 (2011)

[3.6] (2) *Twins and their boundaries during homoepitaxy on Ir(111)*
S. Bleikamp, J. Coraux, O. Robach, G. Renaud and T. Michely,
Phys. Rev. **B 83** 064103 (2011)

[3.6] (6) *Tracking defect type and strain relaxation in patterned Ge/Si(001) islands by X-ray forbidden reflection analysi*s
M.I. Richard, A. Malachias, J.-L. Rouvière, T.-S. Yoon, E. Holmström, Y.-H. Xie, V. Favre-Nicolin, V. Holy, K. Nordlund, G. Renaud, T.-H. Metzger
Phys. Rev. **B 84**, 075314 (2011)

[3.6] (8) *Atomic structure and composition of the 2 × N reconstruction of the Ge wetting layer on Si(001) investigated by surface x-ray diffraction*
T. Zhou, G. Renaud, J. Issartel, C. Revenant, T.U. Schülli, R. Felici and A. Malachias,
Phys. Rev. **B 83**, 195426 (2011)

[2.9] (0) *H_2O diffusion barriers at Si-Si Direct bonding interfaces for low temperature anneals*
H. Moriceau, F. Rieutord, L. Libralesso, C. Ventosa, F. Fournel, C. Morales, T. Mc Cormick, T. Chevolleau and I. Radu
J. Electrochem. Soc. **158** (9) H919 (2011)

[2.9] (4) *An overview of patterned metal/dielectric surface bonding: mechanism, alignment and characterization*
L. Di Cioccio, P. Gueguen, R. Taibi, D. Landru, G. Gaudin, C. Chappaz, F. Rieutord, F. de Crecy, I.

Radu, L.-L. Chapelon, and L. Clavelier
J. Electrochemical Soc. 158 (6) P81-86 (2011)

[2.3] (5) *Highly anisotropic epitaxial (L1)0 FePt on Pt(001)*
Soares M.M., Tolentino H.C.N., De Santis M., Ramos A.Y., Cezar J.C.
J. Appl. Phys. **109** p.07D725-1-07D725-3 (2011)

[2.3] (7) *Structure and magnetism of Ge_3Mn_5 clusters*
A. Jain, M. Jamet, A. Barski, T. Devillers, I.-S. Yu, C. Porret, P. Bayle-Guillemaud, V. Favre-Nicolin, S. Gambarelli, V. Maurel, G. Desfonds, J. F. Jacquot, and S. Tardif
J. Appl. Phys. **109**, 013911 (2011)

[1.8] (7) *In Situ µLaue: Instrumental Setup for the Deformation of Micron Sized Samples*
C. Kirchlechner, J. Keckes, J.-S.Micha and G. Dehm
Advanced Engineering Materials **13** (8) p 837-844 (2011)

[1.6] (17) *A new white beam x-ray microdiffraction setup on the BM32 beamline at the European Synchrotron Radiation Facility*
O. Ulrich, X. Biquard, P. Bleuet, O. Geaymond, P. Gergaud, J. S. Micha, O. Robach, and F. Rieutord
Rev. Sci. Instrum. **82**, 033908 (2011)

[1.5] (16) *Dislocation storage in single slip-oriented Cu micro-tensile samples: New insights via X-ray microdiffraction*
C. Kirchlechner, D. Kiener, C. Motz, S. Labat, N. Vaxelaire, O. Perroud, J. -S. Micha, O. Ulrich, O. Thomas, G. Dehm, and J. Keckes
Phil. Mag. **91** (7-9) Special Issue p 1256-1264 (2011)

[1.4] (0) *Water management on semiconductor surfaces*
Y. Le Tiec, C. Ventosa, N. Rochat, F. Fournel, H. Moriceau, L. Clavelier, F. Rieutord, J. Butterbaugh, and I. Radu
Microelectronic Engineering **88**, p3432-3436 (2011)

[1.3] (5) *Analysis of strain error sources in micro-beam Laue diffraction*
F. Hofmann, S. Eve, J. Belnoue, J.-S. Micha, and A.M. Korsunsky
Nucl. Instrum. Meth. A **660** (1) p 130-137 (2011)

[1.2] (2) *Combined In Situ Grazing Incidence Small Angle X-Ray Scattering and Grazing Incidence X-Ray Diffraction Study of the Growth of Ge Islands on Pit-Patterned Si(001) Substrates*
M.-I. Richard, T. Schülli, G. Renaud, Z.-Z. Zhong and G. Bauer
J. Nanoscience & Nanotechnology **11**, 9123 (2011)

2010

[40.8] (33) *Substrate-enhanced supercooling in AuSi eutectic droplets*
T.U. Schülli, R. Daudin, G. Renaud, A. Vaysset, O. Geaymond and A. Pasturel,
Nature **464**, 1174 (2010)

[5.2] (10) *Nanoscale Patterning by C60 Ordering on Pt(110)*
Torrelles X, Langlais V, De Santis M, Tolentino HCN and Gauthier Y.
J. Phys. Chem. **C 114** p 15645 (2010)

[3.9] (6) *Growth, structure and magnetic properties of FePt nanostructures on NaCl(001) and MgO(001)*
Liscio F., Makarov D., Maret M., Doisneau-au-cottignies B., Roussel H., Albrecht M.
Nanotechnology **21** (6) 065602 (2010)

[3.6] (8) *Strain and correlation of self-organized Ge(1-x)Mn(x) nanocolumns embedded in Ge (001)*
Tardif S., Favre-Nicolin V., Lancon F., Arras E., Jamet M., Barski A., Porret C., Bayle-Guillemaud P., Pochet P., Devillers T. and Rovezzi M.
Phys. Rev. **B 82** (10) 104101 (2010)

[3.6] (13) *Elastic strain relaxation in GaN/AlN nanowire superlattice*
O. Landré, D. Camacho, C. Bougerol, Y.M. Niquet, V. Favre-Nicolin, G. Renaud, H. Renevier and B. Daudin
Phys. Rev. **B 81** 153306 (2010)

[3.6] (21) *Probing nanoscale structural and order/disorder phase transitions of supported Co-Pt clusters under annealing*
P. Andreazza, C. Mottet, C. Andreazza-Vignolle, J. Penuelas, H. C. N. Tolentino, M. De Santis, R. Felici and N. Bouet
Phys. Rev. **B 82** (15) 155453 (2010)

[3.6] (20) *Highly ordered growth of Fe and Co clusters on alumina on $Ni_3Al(111)$*
A. Buchsbaum, M. De Santis, H.C.N. Tolentino, M. Schmid and P. Varga
Phys. Rev. **B 81** (11) 115420 (2010)

[3.6] (13) *Nanostructuring surfaces: Deconstruction of the Pt(110)-(1 X 2) surface by C-60*
X. Torrelles, V. Langlais, M. De Santis, H.C.N. Tolentino and Y. Gauthier
Phys. Rev. **B 81** 041404(R) (2010)

[2.1] (5) *Confinement induced phase transition in a DNA-lipid hydrated complex*
E. Andreoli de Oliveira, E. R. Teixeira da Silva, A. Fevrier, E. Grelet, F. Nallet and L. Navailles
Europhysics Letters **91** (2) 28001 (2010)

[2.2] (10) *Supported bilayers: Combined specular and diffuse X-ray scattering*
Malaquin L, Charitat T and Daillant J
Euro. Phys. J. **E 31** p 285 (2010)

[2.3] (10) *Study of the formation, evolution and dissolution of interfacial defects in silicon wafer bonding*
S. Vincent, J. D. Penot, I. Radu, F. Letertre, and F. Rieutord,
J. Appl. Phys. **107** 093513 (2010)

[2.1] (5) *Influence of the U_3O_7 domain structure on cracking during the oxidation of UO_2*
Desgranges L., Palancher H., Gamaleri M., Micha J.-S., Optasanu V., Raceanu L., Montesin T., Creton N.
J. Nucl. Mat. **402** p 167 (2010)

[1.3] (16) *Determination of global and local residual stresses in SOFC by X-ray diffraction*
Villanova J., Sicardy O., Fortunier R., Micha J.-S., Bleuet P.
Nucl. Inst. Meth. Phys. **B 268** p 282 (2010)

[1.4] (5) *X-ray microbeam strain investigation on Cu-MEMS structures*
Perroud O., Vayrette R., Rivero C., Thomas O., Micha J.-S., Ulrich O.
Microelectronic Engineering **87** p 394 (2010)

ESRF Highlight

An alternative pathway for understanding plasticity at the micron scale
C. Kirchlechner et al
ESRF Highlight 2012

Positive thermal expansion of graphene on its substrate
F. Jean et al
ESRF Highlight 2014, p 109

Book Chapter

Chapitre 4 : Analyse avancée des gradients d'orientation et des contraintes par microdiffraction Laue des rayons X,

O. Robach, J.S. Micha, O. Ulrich, G. Daveau, B. Devincre, T. Hoc, V. Consonni, G. Feuillet, J. Petit, submitted to *Rayons X et Matière, RX2013*, Hermès, Eds : P. Goudeau, R. Guinebretière

Materials and Manufacturing of SOI Wafers.
Moriceau, H., F. Fournel, and F. Rieutord
in *Silicon-on-Insulmator (SOI) Technology Manufacture end Applications*
edited by O. Kononchuk and B;-Y. Nguyen, Woodhead Publishing. Cambridge, 2014.

Laue microdiffraction at ESRF
O. Robach, C. Kirchlechner, J.S. Micha, O. Ulrich, X. Biquard, O. Geaymond, O. Castelnau, M. Bornert, J. Petit, S. Berveiller, O. Sicardy, J. Villanova, F. Rieutord,
Chapter 5 : p 156 in « Strain and dislocation gradients from diffraction »
Editors: Barabash R.I., Ice G.E. ,"Imperial College Press" / "World Scientific Publishing" (2014)

Nanostructures observed by surface sensitive x-ray scattering and highly focused beams
T. Schulli, V. Favre-Nicolin M.-I. Richard and G. Renaud,
in „Characterization of Semiconductor Heterostructures and Nanostructures", C. Lamberti ed.; second edition, 2013, pp 113-173., Elsevier.

Grazing incidence diffraction anomalous fine structure in the study of structural properties of nanostructures
H. Renevier and M.G. Proietti
In: "Characterization of Semiconductor Heterostructures and Nanostructures. 2. Edition", Lamberti C. (Eds.)Agostini G. (Eds.) (Elsevier, 2013) pp.311-359

-« *Propriétés structurales de surfaces, interfaces et nanostructures étudiées à l'aide des rayons X* »
G. Renaud,
Reflets de la Physique n°34-35 et Le BUP, Hors Série N°1, pp 65-69, 2013

X-ray Diffraction analysis of elastic strains at the nanoscale
O. Thomas, O. Robach, S. Escoubas, J.S. Micha, N. Vaxelaire, O. Perroud
Chapter in "Mechanical stress on the nanoscale : simulation, material systems and characterization techniques"
Ed. : M. Hanbücken, P. Müller, U. Gösele, R. B. Wehrspohn, Wiley-VCH Books, 2011

Awards and Covers

Tao Zhou: *best presentation Science Students Days ESRF Oct 2013*
Anne Lamirand et al: *best student poster award Science Students Days ESRF Oct 2013*

In situ micro compression test studied by Laue microdiffraction
Marlene. Kapp *et al*
Best poster award, 7th Winter School on Neutrons and Synchrotron Radiation, Planneralm (Austria), March 6-12, 2011

Cover of Advanced Engineering Materials with Laue Patterns recorded on BM32 (C.Kirchlechner)

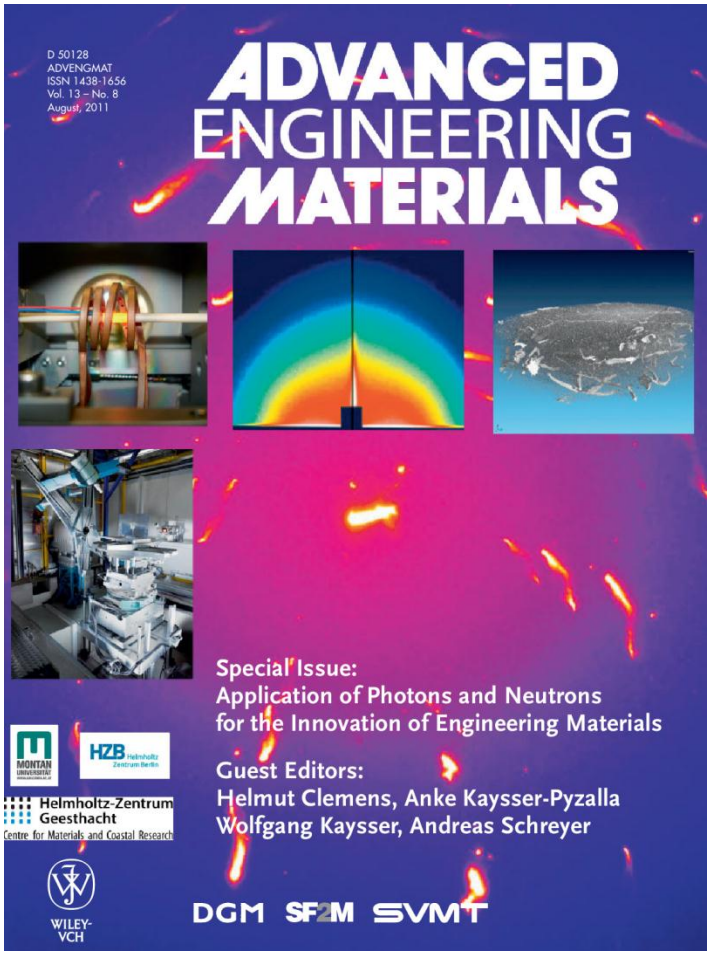
D 50128
ADVENGMAT
ISSN 1438-1656
Vol. 13 – No. 8
August, 2011
ADVANCED
ENGINEERING
MATERIALS
Special Issue:
Application of Photons and Neutrons
for the Innovation of Engineering Materials
Guest Editors:
Helmut Clemens, Anke Kaysser-Pyzalla
Wolfgang Kaysser, Andreas Schreyer
MONTAN UNIVERSITÄT
HZB Helmholtz Zentrum Berlin
Helmholtz-Zentrum Geesthacht
Centre for Materials and Coastal Research
WILEY-VCH
DGM SF2M SVMT

Cover of Chemical Communications with Laue Patterns recorded on BM32 (M. Schneider et al)

Cover of the French physical society bulletin with INS instrument (Responsible G. Renaud) and N. Blanc (now on CRG-D2AM)

Collages directs de silicium et d'oxydes de silicium : mécanisme mis en jeu
Université de Grenoble, 9th july 2014
Caroline Rauer

Croissance épitaxiale, structure atomique et couplage d'échange de bicouches ultra-minces d'oxydes sur métaux
Université de Grenoble, 16th october 2014
Anne Lamirand

Croissance et caractérisation de nanofils de GaN et d'hétérostructures - Growth and characterization of GaN nanowires and GaN/AlN heterostructure nanowires
Université de Grenoble, 2013
Karine Hestroffer

Spectroscopies X et diffraction anomale de boîtes quantiques GaN et d'hétéro-structures III-N : inter-diffusion et ordre à courte distance
Université de Grenoble, 2013
Cédric Leclère

Diffusion de rayons X sur une membrane unique : potentiel d'interaction et effets du champ électrique
Université de Strasbourg, 2013
Arnaud Hemmerle

Contribution à l'étude des mécanismes de relaxation de contraintes dans les films de chromine formés sur Ni-30Cr et Fe-47Cr : approche multi-échelle par spectroscopie Raman et microdiffraction Synchrotron
Université de La Rochelle , 5th October 2012, Sciences des Matériaux
Mathieu Guerain

Interaction dislocations - joints de grains en déformation plastique monotone : étude expérimentale et modélisations numériques
Ecole Centrale Paris, 19th september 2012, Mécanique et Matériaux
Gael Daveau

Etude par diffraction des rayons X des déformations induites par irradiation/implantation d'ions dans le dioxyde d'uranium
Université de Poitiers, 22nd November 2012
Axel Richard

Analyse théorique et physique de matériaux pour application aux Mémoires à Changement de Phases
Université Grenoble, 5th september 2012
Audrey Bastard

Formation and supercooling of AuSi eutectic droplets on Si substrates: an in-situ study using synchrotron radiation
Université Grenoble, Février 2012
Rémi Daudin

Étude des matériaux à changement de phase pour application dans le domaine des PCRAM : verres infrarouges pour l'optique spatiale
Université de Rennes, 2011
Jean-Claude Bastien

Plasticity at the Micron Scale: a µLaue Study
PhD Thesis, University Leoben, Austria, 2011
Christoph Kirchlechner

Grain level deformation studied by micro diffraction techniques
PhD Thesis, Oxford University, United-Kingdom, 2011
Felix Hofmann

Croissance, structure et magnétisme dans les systèmes à décalage d'échange FM/AFM : approche fondamentale par la physique des surfaces
Université Joseph Fourier Grenoble, France, 2011
Marcio M. Soares

Nanocolonnes de GeMn : propriétés magnétiques et structurales à la lumière du synchrotron
Université de Grenoble, 2011.
Samuel Tardif

Proceedings

Synchrotron radiation-based characterization of interconnections in microelectronics: recent 3D results
P. Bleuet, G. Audoit, J. Bertheau, J. Charbonnier, P. Cloetens, M. Weleguela, D. Sanchez, D. Sanchez, F. Hodaj, P. Gergaud, F. Lorut, J.-S. Micha, A. Thuaire, O. Ulric
Book Series: Conference: Location: San Diego, CA Date: AUG 18-20, 2014 Sponsor(s): SPIE Developments In X-Ray Tomography TOMOGRAPHY IX Book Series: Proceedings of SPIE Volume: 9212 Article Number: 92120D Published: 2014

[1.3] Multi-scale X-ray diffraction study of strains induced by He implantation in UO_2 polycrystals
A. Richard, E. Castelier, H. Palancher, J.S. Micha, H. Rouquette, A. Ambard, Ph. Garcia, Ph. Goudeau
Nucl. Instr. Meth. **B 326** 251-255 (2014)
Conference REI -2014

[1.3] *(1) Thermal bump removal of a Crystal Monochromator by designing an optimal shape*
J.-S. Micha, O. Geaymond, F. Rieutord
4th international workshop on Metrology for X-ray Optics, Mirror Design, and Fabrication Barcelona, 4th to 6th July 2012
Nucl. Instr. Methods **A 710**, 155-160 (2013)

Bio-materials characterization across multiple scales at Oxford HEX-lab
Sui T. Hofmann F. Song X. Tao L. Zeng K. Korsunsky A.M.
Lecture Notes in Engineering and Computer Sciences 2199, 1657-1662 (2012)
In: "Proceedings of the World Congress on Engineering, International Association of Engineers", 2012) pp.1657-1662

Combining Laue microdiffraction and digital image correlation for improved measurements of the elastic strain field with micrometer spatial resolution
J. Petit, M. Bornert, F. Hofmann, O. Robach, J.-S. Micha, O. Ulrich, C. Le Bourlot, D. Faurie, A.M. Korsunsky and O. Castelnau
Procedia IUTAM 4 (2012) 133 – 143

Daudin B. Bougerol C. Camacho D. Cros A. Gayral B. Hestroffer K. Leclere C. Mata R. Niquet Y.M. Renevier H. Sam-Giao D. Tourbot G. - Growth, structural and optical properties of GaN/AlN and GaN/GaInN nanowire heterostructures
Physics Procedia 28, 5-16 (2012)
15th Brazilian Workshop On Semiconductors

Coherent integration of photonics on silicon through the growth of nanostructures on GaP/Si
Thanh, TN ; Robert, C ; Cornet, C; Guo, W ; Letoublon, A ; Perrin, M ; Bertru, N ; Even, J ; Chevalier, N ; Folliot, H; Loualiche, S ; Ponchet, A ; Elias, G; Micha, JS; Durand, O ; Le Corre, A
Quantum Sensing and Nanophotonic devices IX Book Series: Proceedings of SPIE 8268 , 82681H (2012)

Fracture in (100) Si after high energy protons implantation

Braley C. Mazen F. Papon A.M. Charvet A.M. Rieutord F. Ntsoenzok E.
Special Issue: E-MRS 2012 Spring Meeting – Symposium A
Physica Status Solidi (c) 9, 2023-2026 (2012)

(1) *X-Ray diffraction determination of macro and micro stresses in SOFC electrolyte and evolution with redox cycling of the anode*
Villanova J., Sicardy O., Fortunier R., Micha J.S., Bleuet P.
Residual Stresses VIII
Materials Science Forum, vol. **681**, p.25-30 (2011)

Stress field in deformed polycrystals at the micron scale
Castelnau O., Bornert M., Robach O., Micha, J.-S., Ulrich O., Chiron R., Le Bourlot C.
ICEM 14: 14th International Conference on experimental mechanics
Book Series: EPJ Web of Conferences **6** 35005 (2010)

Defect formation at hydrophilic silicon bonding interfaces
F. Rieutord, S. Vincent, J. D. Penot, H. Moriceau, and I. Radu,
ECS Transactions, **33** p 451(2010)

Efficiency of H_2O diffusion barriers at Si-Si direct bonding interfaces
H. Moriceau, F. Rieutord, L. Libralesso, C. Ventosa, F. Fournel, C. Morales, T. Mc Cormick, T. Chevolleau, and I. Radu
ECS Transactions **33** p 467 (2010)

An overview of patterned metal/dielectric surface bonding: mechanism, alignment and characterization
L. Di Cioccio, P. Gueguen, R. Taibi, D. Landru, G. Gaudin, C. Chappaz, F. Rieutord, F. de Crecy, I. Radu, L.-L. Chapelon, and L. Clavelier
ECS Transactions **33** p 3 (2010)

Single Crystal Silicon Film Transfer onto polymer
M. Argoud, H. Moriceau, C. Fretigny, F. Rieutord, C. Morales, and L. Clavelier
ECS Transactions **33** p 217 (2010)

Overview on recent direct wafer bonding advances and applications
H. Moriceau, F. Rieutord, F. Fournel, Y. Le Tiec, and L. Di Cioccio
in The 5th International Workshop on Advanced Materials Science and Nanotechnology (IWAMSN2010) Hanoi (2010)

Oral communications:

In situ micromechanics: An overview on µLaue based experiments to study GND accumulation in various loading geometries
C. Kirchlechner, C. Motz, PJ. Imrich, N. Malyar, JS. Micha, O. Ulrich, G. Dehm
International Symposium on Plasticity, Montego Bay, 04.01.2015, **KeyNote Lecture**

Laue Diffraction Microscopy on French CRG-IF BM32 at ESRF
J.-S. Micha, O. robach, O. Ulrich, O. Geaymond, F. Rieutord
SOLEIL users Meeting 22-23 January 2015

In situ micromechanics: An overview on synchrotron based µLaue experiments
C. Kirchlechner
XTOP 2014, Villard de Lans, 17.09.2014, **Invited** Talk

From Idealized Single Crystals Towards Applied Polycrystals: Insights by X-Ray µLaue Diffraction
C. Kirchlechner
Gordon Research Conference
Thin Film and Small Scale Behavior, Boston, 16.07.2014, **Invited** Talk

In Situ Electron Microscopy and Micro-Laue Study of Plasticity in Miniaturized Cu Bicrystals

P.J. Imrich, C. Kirchlechner, C. Motz, J.B. Jeon, G. Dehm,
CAMTEC III, Symposium on Fine-Scale Mechanical Characterisation and Behaviour. Cambridge, UK, 07.04.2014

Why we want to have energy dispersive in situ Laue data and how we will get them one day…
C. Kirchlechner, C. Motz, G.Dehm, A. Abboud, J. Keckes, U.Pietsch, J.S.-Micha, O.Ulrich, O. Robach
TMS 2014, San Diego, CA, USA, 18.02.2014, **Invited** Talk

From idealized bi-crystals towards applied polycrystals: Plastic deformation in small dimensions
G. Dehm, P.J. Imrich, A. Wimmer, C. Kirchlechner,
TMS2014, San Diego, CA, USA, 16.02.2014

Reversible dislocation motion in micron sized bending beams during monotone and cyclic loading
C. Kirchlechner, C. Motz, M.W. Kapp, G. Dehm
International Symposium on Plasticity, Freeport Bahamas, 08.01.2014, **Invited** Talk

Strain-stress determination in copper filled TSVs using X-Rays diffraction : average and local approach
C. Krauss, S. Labat , S. Escoubas, O. Thomas, A. Farcy, J.-S. Micha, O. Robach
Materials for Advanced Metallization 10-13 March 2013, Leuven

La Microdiffraction Laue des rayons X : un outil de métrologie locale
O. Robach et al
RX et matière 2013, Nantes 12-15 Novembre 2013 **Invited** Talk

X-ray Laue Microdiffraction : a local metrology tool
O. Robach et al
Small Scale Plasticity, Cargese, Octobre 2013, **Invited** Talk

Mesures 3D micrométriques de la microstructure et du champ des déformations élastiques par DAXM à BM32 (ESRF)
J.-B. Marijon, F. Grennerat, O. Robach, O. Castelnau, J.-S. Micha
RX et matière 2013, Nantes 12-15 Novembre 2013 , **Invited** Talk

Laue micro-beam tomography on Through-Silicon-Via
D. Ferreira Sanchez et al
RX et matière 2013, Nantes 12-15 Novembre 2013

Analyse quantitative de la perfection cristalline de nanocouches épitaxiales GaP/Si
A. Létoublon et al
RX et matière 2013, Nantes 12-15 Novembre 2013

Influence of dislocation pile-ups on mechanical properties of microcantilevers: New insights via in situ µLaue and in situ SEM bending experiments.
M. Kapp et al
EUROMAT 2013, Seville, 8-13 september 2013

Gallium nitride single-wires studied by X-ray diffraction: homogeneous wires and core-shell heterostructures
J. Eymery, C. Durand, D. Salomon, V. Favre-Nicolin, F. Rieutord, O. Robach, J.S. Micha, M. Burghammer, E. Di Cola, M. Reynolds
E-MRS, strasbourg, May 2013

A tunable multi-color "rainbow" filter for improved stress and dislocation field mapping in polycrystals using x-ray Laue microdiffraction
O. Robach, J.-S. Micha, O. Ulrich, O. Geaymond, O. Sicardy, J. Härtwig, F. Rieutord
TMS 2013, San Antonio (US/TX), 3rd – 7th march 2013

Insights into plastic deformation via X-ray µLaue diffraction
C. Kirchlechner

Summer School on: “Plasticity in small dimensions”, Cargese, France, 14.10.2013

In situ micromechanics: An overview on synchrotron-based experiments
C. Kirchlechner
Max-Planck-Institut für Eisenforschung, Seminar, Düsseldorf, Germany 22.01.2013

µ-XRD study of strains in light ion implanted polycrystals: influence of grain orientation
H. Palancher, A. Richard, E. Castelier, J.S Micha, Ph. Goudeau, Ph. Garcia
Journées de la Matière Condensée 13 2013

In situ micro- and nanomechanical electron microscopy studies of grain boundaries in Cu”
G. Dehm, P.J. Imrich, C. Kirchlechner, M. Smolka, B. Yang, C. Motz
MRS Fall Meeting 2012, Boston, MA, USA, 25.11.2012

Relations contraintes résiduelles – endommagement dans des systèmes oxydes thermiques sur métal : apports de la spectroscopie Raman et de la micro-diffraction Synchrotron
M. Guerain, J.L. Grosseau-Pouyssard, P. Goudeau, B. Panucaud, N. Tamura, M. Kunz, J.-S. Micha.,
Colloque GFAC-SF2M, St Nazaire, 3-4/04/2012
and
8th International Symposium on High-Temperature Corrosion and Protection of Materials 2012, 20-25 May 2012, Les Embiez

Use of Raman Spectroscopy and Synchrotron micro-Diffraction to investigate stress in thermal oxide films : a multiscale approach
FAC: Déformations élastiques dans des échantillons polycristallins d’UO_2 implantés en hélium : mesures par micro diffraction Laue et modélisation élastique
É. Castelier, H. Palancher, A. Richard, J.-S. Micha, P. Goudeau

Combining Laue microdiffraction and digital image correlation for improved stress field measurements with micrometer spatial resolution
F. Zhang, O. Castelnau, M. Bornert, J. Petit, O. Robach, J.S. Micha, F. Hofmann, A. Korsunsky
Int. Conf. of Residual Stresses (oct 2012)

Strain-stress determination in silicon around copper filled TSVs using Laue microdiffraction
C. Krauss, S. Labat, S. Escoubas, O. Thomas, M. Bouchoucha, L.-L. Chapelon, P. Chausse, J.-S. Micha and O. Ulrich
12th Workshop on Stress-Induced Phenomena in Microelectronics.
Kyoto du 28 - 30 May 2012

Measuring energy profiles of Laue spots: a third method
O. Robach et al
Synchrotron Radiation Instrumentation 9-13 July Lyon 2012

Combined Analysis of Delamination Process at the Surface of Cr_2O_3 Thermal Oxide Films
P. Goudeau , M. Guerain , J.-L. Grosseau- Poussard, N. Tamura , M. Kunz , J.-S. Micha ,
MRS Fall 2012

Influence of Grain Orientation on Radiation Induced Strains in UO2 Polycrystals
P. Goudeau , E. Castelier , H. Palancher , A. Richard, J.-S. Micha ,
MRS Fall 2012

Growth and structure of cobalt oxide on an ultrathin PtFe epitaxial ferromagnetic layer by GIXRD
A. Lamirand, M. De Santis, H.C.N. Tolentino, M.M. Soares, A.Y. Ramos,
ECOSS-28, 28 Aug.-2 Sep., 2011, Wroclaw.

µLaue diffraction: A tool to probe imperfect crystals at the micron scale
C. Kirchlechner
NESY Winterschool, Institut für Physik, Montanuniversität Leoben, Donnersbach Planneralm, 06.03.2011

Annex 3 selected publications

Publications in journals with impact factor higher than 3 (since 2010)

The following list is sorted by decreasing impact factor (5 years impact factor in march 2015).
User type codes:

E for external users,
I for beamline staff,
E+I for strong collaboration between beamline staff and external users

Journal	Impact factor	#	Instrument	User type
Nature	40.8	1	INS	I
Acta Cryst. A	17.2	1	µLaue	I
Nano Letters	14.5	2	µLaue + GMT	E, E+I
Proc. Nat. Acad. Sc. USA	10.7	1	GMT	E
Phys. Rev. Lett.	7.4	1	INS	I
Chem. Commun.	6.5	1	µLaue	E
---	---	---	---	---
J. Phys. Chem. C	5.2	4	INS + GMT	
Electrochem. Comm.	4.9	1	GMT	
J. Appl. Cryst.	4.8	6	µLaue+INS	
Acta Mater.	4.3	3	µLaue	
Faraday disc.	4.2	2	GMT	
Nanotechnology	3.9	2	INS	
Appl. Phys. Lett.	3.7	9	INS + GMT + µLaue	
Phys. Rev. B	3.6	16	INS + GMT + µLaue	

Most cited articles (published since 2010)

The following list is sorted by decreasing number of citations.
User type codes:

E for external users,
I for beamline staff,
E+I for strong collaboration between beamline staff and external users

First author, Journal, year	Instrument	#cited	Scientific Field	User type
R. Koester et al., Nano Letters, 2011	GMT	53	Semiconductor, photonics	E
I. Laoufi et al., J. Phys. Chem. C, 2011	GMT	34	Fund. Catalysis	E+I
T.U. Schülli et al., Nature, 2010	INS	33	Fund. Surface science	I
P. Andreazza et al ., Phys. Rev. B, 2010	INS	21	Fund. Surface science	E
A. Buchsbaum et al., Phys. Rev. B, 2010	INS	20	Fund. Surface science	E
O. Ulrich et al., Rev. Sci. Instrum., 2011	µLaue	17	Instrumentation I	
J. Villanova et al., Nucl. Instr. Meth. B, 2010	µLaue	16	Applied Materials & Energy	E+I
C. Kirchlechner et al., Phil. Mag, 2011	µLaue	16	Fund. Materials Mechanics	E
F. Leroy et al., Phys. Rev. B, 2012	INS	15	Fund. Surface science	E
T. Nguyen Thanh et al., J. Appl. Phys., 2012	GMT	14	Semiconductor, photonics	E
G. Fragneto et al., Euro. BioPhys. J., 2012	GMT	13	Fund. Soft Matter	E
O. Landré et al., Phys. Rev. B, 2010	INS	13	Fund. Surface science	E
X. Torrelles et al., Phys. Rev. B, 2010	INS	13	Fund. Surface science	E
K. Hestroffer et al., Appl. Phys. Lett., 2012	INS	12	Fund. Surface science	E
S. Benedetti et al., J. Phys. Chem C, 2011	INS	12	Fund. Surface science	E
X.J. Chen et al.,Appl. Phys. Lett., 2011	GMT	12	Semiconductor, photonics	E

Selected publications: 5 reprints / publications of work accomplished on the beamline

SL 1: T.U. Schülli et al, Nature, 2010	INS
SL 2: A.D. Lamirand et al, Phys. Rev B, 2013	INS
SL 3: M. Ndjeri et al, Electrochemistry Communications, 2011	GMT
SL 4: I. Laoufi et al, J. Phys. Chem. C, 2011	GMT
SL 5: C. Kirchlechner et al, Acta Materialia, 2012	µLaue